

ANL-7553

RETURN TO ANL (IDAHO) LIBRARY

Argonne National Laboratory

REACTOR DEVELOPMENT PROGRAM PROGRESS REPORT

February 1969

The facilities of Argonne National Laboratory are owned by the United States Government. Under the terms of a contract (W-31-109-Eng-38) between the U. S. Atomic Energy Commission, Argonne Universities Association and The University of Chicago, the University employs the staff and operates the Laboratory in accordance with policies and programs formulated, approved and reviewed by the Association.

MEMBERS OF ARGONNE UNIVERSITIES ASSOCIATION

The University of Arizona
Carnegie-Mellon University
Case Western Reserve University
The University of Chicago
University of Cincinnati
Illinois Institute of Technology
University of Illinois
Indiana University
Iowa State University
The University of Iowa

Kansas State University
The University of Kansas
Loyola University
Marquette University
Michigan State University
The University of Michigan
University of Minnesota
University of Missouri
Northwestern University
University of Notre Dame

The Ohio State University
Ohio University
The Pennsylvania State University
Purdue University
Saint Louis University
Southern Illinois University
University of Texas
Washington University
Wayne State University
The University of Wisconsin

LEGAL NOTICE

This report was prepared as an account of Government sponsored work. Neither the United States, nor the Commission, nor any person acting on behalf of the Commission:

A. Makes any warranty or representation, expressed or implied, with respect to the accuracy, completeness, or usefulness of the information contained in this report, or that the use of any information, apparatus, method, or process disclosed in this report may not infringe privately owned rights; or

B. Assumes any liabilities with respect to the use of, or for damages resulting from the use of any information, apparatus, method, or process disclosed in this report.

As used in the above, "person acting on behalf of the Commission" includes any employee or contractor of the Commission, or employee of such contractor, to the extent that such employee or contractor of the Commission, or employee of such contractor prepares, disseminates, or provides access to, any information pursuant to his employment or contract with the Commission, or his employment with such contractor.

Printed in the United States of America
Available from

Clearinghouse for Federal Scientific and Technical Information
National Bureau of Standards, U. S. Department of Commerce
Springfield, Virginia 22151

Price: Printed Copy \$3.00; Microfiche \$0.65

ARGONNE NATIONAL LABORATORY
9700 South Cass Avenue
Argonne, Illinois 60439

REACTOR DEVELOPMENT PROGRAM
PROGRESS REPORT

February 1969

Robert B. Duffield, Laboratory Director
Stephen Lawroski, Associate Laboratory Director

<u>Division</u>	<u>Director</u>
Chemical Engineering	R. C. Vogel
EBR-II Project	M. Levenson
Metallurgy	M. V. Nevitt
Reactor Engineering	L. J. Koch
Reactor Physics	R. Avery

Report coordinated by
A. D. Rossin and A. Glassner

Issued March 25, 1969

FOREWORD

The Reactor Development Program Progress Report, issued monthly, is intended to be a means of reporting those items of significant technical progress which have occurred in both the specific reactor projects and the general engineering research and development programs. The report is organized in accordance with budget activities in a way which, it is hoped, gives the clearest, most logical overall view of progress. Since the intent is to report only items of significant progress, not all activities are reported each month. In order to issue this report as soon as possible after the end of the month editorial work must necessarily be limited. Also, since this is an informal progress report, the results and data presented should be understood to be preliminary and subject to change unless otherwise stated.

The issuance of these reports is not intended to constitute publication in any sense of the word. Final results either will be submitted for publication in regular professional journals or will be published in the form of ANL topical reports.

The last six reports issued
in this series are:

August 1968	ANL-7487
September 1968	ANL-7500
October 1968	ANL-7513
November 1968	ANL-7518
December 1968	ANL-7527
January 1969	ANL-7548

REACTOR DEVELOPMENT PROGRAM

Highlights of Project Activities for February 1969

EBR-II

All modification and maintenance work scheduled for the reactor shutdown was completed by February 15. The plant was heated to standby conditions, preoperational tests and calibrations were made, and fuel handling for Run 33A was started.

Phasing out of remote processing and fabrication of fuel in the FCF hot line is complete through the injection-casting step. Equipment in the cold line is being modified to produce sufficient experimental Mark-II fuel elements for five subassemblies to be irradiated in EBR-II.

The ANL acceptance rate for vendor-produced Mark-IA driver-fuel elements continues to be higher than 95%. A total of 9763 of these elements had been received through February 14.

ZPR-3

Preliminary modifications of safety-rod drawers were made and a larger cooling manifold installed. Subsequently the reference core for Assembly I of the Resumed Phase-B Critical Experiment (Assembly 56B, 374.2 kg total plutonium) was loaded into ZPR-3. After correcting for the inherent spontaneous-fission neutron source, calibrations of control and safety rods were made using delayed-neutron fractions appropriate to the four fissioning isotopes in the assembly. The temperature coefficient of reactivity and edge worth of core drawers were measured. Radial traverses are now in progress.

ZPR-6 and -9

The contractor has virtually completed the plutonium conversion modifications for the ZPR-6 and -9 facilities. Acceptance testing of the new components is in progress.

Answers to Commission questions on the Final Safety Analysis Report on the use of plutonium in these facilities have been prepared and are in the process of being submitted to the AEC.

ZPPR

An unreflected core, exclusive of fissionable material, has been pre-loaded into the matrix, and the facility remains in a state of readiness awaiting approval for operation.

Equipment and analytic techniques for measurements of the Doppler reactivity effect are being developed, and parts of the on-line computer system have been installed. The Autorod System has had final operational testing, and the drive system for the axial sample drawer has been tested in the reactor assembly.

TABLE OF CONTENTS

	<u>Page</u>
I. LIQUID METAL FAST BREEDER REACTORS--CIVILIAN	1
A. Fuel Development--LMFBR	1
1. Oxide	1
2. Carbide	5
B. Physics Development--LMFBR	6
1. Theoretical Reactor Physics	6
2. Experimental Reactor Physics	8
3. ZPR-3 Operations and Analysis	11
4. ZPPR Operations and Analysis	13
5. ZPPR Materials	15
C. Component Development--LMFBR	24
1. Reactor Mechanism and Instrumentation	24
2. Fuel Handling, Vessels, and Internals--Core Component Test Loop	27
D. Systems and Plant--LMFBR	28
1. 1000-MWe Plant	28
E. EBR-II	29
1. Research and Development	29
a. Reactor Experimental Support--Reactor Analysis and Testing	29
b. Nuclear Analysis Methods Development	32
c. Fuel Performance Studies--Mark I Series	37
d. Mark II Driver Fuel Element Development	40
e. Equipment--Fuel Related	41
f. New Subassemblies Design and Experimental Support	43
g. Instrumented Subassembly	46
h. Experimental Irradiation and Testing	47
i. Feasibility Study of Fuel Failure Detection--Chemical and Mechanical Methods	48
j. Materials-Coolant Compatibility	49
k. Study of Operation with Failed Fuel	50
l. Driver Fuel Transient Performance Studies--TREAT Experiments	53
m. Systems Engineering	53
n. Oxide Driver	57
2. Operations	57
PUBLICATIONS	70

TABLE OF CONTENTS

	<u>Page</u>
II. OTHER FAST REACTORS--CIVILIAN--OTHER FAST BREEDER REACTORS	71
A. Fuel Development	71
1. Corrosion of Fuel Jacket Alloys	71
2. Other Fuel Jacket Alloy Studies	73
III. GENERAL RESEARCH AND DEVELOPMENT--CIVILIAN--STUDIES AND EVALUATIONS	75
A. Evaluation of Fast Reactor Analysis Methods and Data	75
1. Thermal-Hydraulic Analysis	75
IV. GENERAL REACTOR TECHNOLOGY	76
A. Applied and Reactor Physics Development	76
1. Theoretical Reactor Physics--Research and Development	76
2. Nuclear Data--Research and Development	80
B. Reactor Fuels and Materials Development	81
1. Fuels and Cladding	81
2. Coolants, Moderators, and Control Materials--Fundamentals of Corrosion in Liquid Metals	82
3. Radiation Damage on Structural Materials--Research and Development--In-Reactors Creep Studies	85
4. Engineering Properties of Reactor Materials--Research and Development--High Temperature Mechanical Properties of Ceramic Fuels	88
C. Engineering Development	96
1. Research and Development	96
D. Chemistry and Chemical Separations	98
1. Aqueous and Volatility Processes--Research and Development--Fluoride Volatility Process	98
2. Closed Cycle Processes--Research and Development--Compact Pyrochemical Processes	100
3. General Chemistry and Chemical Engineering--Research and Development	103
PUBLICATIONS	105

TABLE OF CONTENTS

	<u>Page</u>
V. NUCLEAR SAFETY	106
A. Reactor Kinetics--Other Reactor Kinetics	106
1. Core Structural Safety	106
2. Fuel Meltdown Studies with TREAT	108
3. Materials Behavior and Energy Transfer	113
4. Fast Reactor Safety Test Facility Study	116
5. 1000-MWe Safety Studies	117
B. TREAT Operations	117
1. Reactor Operations	117
C. Chemical Reaction--Research and Development--Chemical and Associated Energy Problems (Thermal)	118
1. Analysis of Excursion Accidents	118
2. Pressure Generation due to Particle-Water Energy Transfer	118
D. Engineered Safety Features	120
1. Safety Features Technology--Containment	120
PUBLICATIONS	123

I. LIQUID METAL FAST BREEDER REACTORS--CIVILIAN

A. Fuel Development--LMFBR

1. Oxide

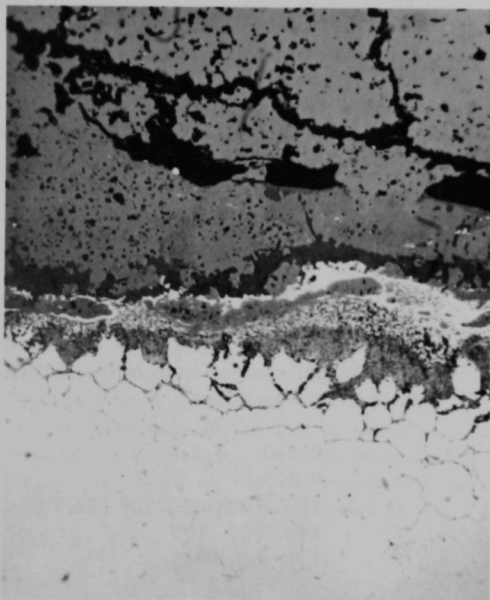
a. Fuel Studies

(i) Fuel Element Performance (L. A. Neimark and R. Natesh)

Last Reported: ANL-7548, pp. 1-2 (Jan 1969).

(a) High-power, Low-burnup Irradiations (Group 0-2).

Large concentrations of the fission product cesium have been identified at the fuel-cladding interface of Element SOV-7 and also as a grain-boundary phase in the Type 304 stainless steel cladding. Cesium had formed a boundary phase of up to 3μ in thickness around the grains of the stainless steel. Thus far, the maximum penetration of cesium into the cladding has



been found to a depth of 0.004 in. Figure I.A.1 is an optical micrograph of an unetched cross section obtained from near the top of the element, where the calculated interface temperature was about 600°C . Shown from top to bottom are the fuel, a number of fuel-cladding interface layers, and the grain-boundary phase in the cladding. An electron-probe scanning image of a typical grain of stainless steel at the fuel-cladding interface (Fig. I.A.2) shows the enrichment of cesium in the grain boundaries.

Iron and chromium were only minimally present in the grain boundaries, but the silicon content was enriched. Nickel appeared in small discrete areas in the grain boundaries, and the concentration of nickel within the grains was nonuniform.

Fig. I.A.1. Fuel-Cladding Interaction at the Upper End of Element SOV-7 Showing the Penetration of Stainless Steel Grain Boundaries by Cesium (250X)

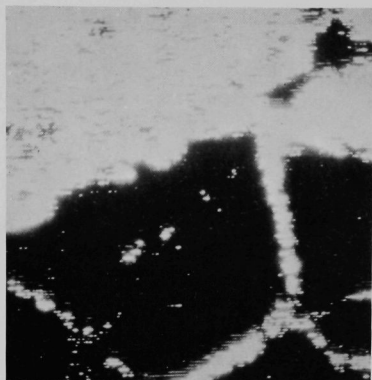


Fig. I.A.2. Electron-probe Scanning Image (Cs-La X ray) Showing Cesium (white) at the Fuel-Cladding Interface (top) and within the Grain Boundaries of the Stainless Steel Cladding (950X)

EBR-II under conditions applicable to the near-term and the longer-range mixed-oxide-fueled fast reactors. A detailed work plan for these experiments is in preparation and will be submitted to the AEC-RDT for approval.

(ii) Fuel Element Modeling (T. R. Bump)

Last Reported: ANL-7518, pp. 4-6 (Nov 1968).

To aid the planning of EBR-II mixed-oxide fuel-element irradiations for maximum benefit to the FFTF and LMFBR programs, the SWELL-2B mutation of the SWELL-2 fuel-element-lifetime code has been used to predict performance of FFTF driver fuel elements in both EBR-II and FFTF. Predictions were made with the key variables:

Cladding OD, in.	0.230
Cladding wall thickness, in.	0.015
Coolant inlet temp, °F	700 (EBR-II), 900 (FFTF)
Coolant temp rise, °F	200, 300, 400
Ratio of plenum to fuel volume	1.0, 0.5, 0.25
Effective fuel density, %	88, 85, 82
Avg linear heat flux, kW/ft	2 to 20
Fuel length, in.	14 (EBR-II), 36 (FFTF)
Effective neutron flux, n-cm ⁻² -sec ⁻¹	2.3 × 10 ¹⁵ (EBR-II), 2.5 × 10 ¹⁵ (FFTF), and varied with heat flux.

(b) Void Deployment (Group 0-3).

Fabrication of the remaining four vibrationally compacted (U_{0.8}Pu_{0.2})O₂ fuel elements for the Group 0-3 irradiation experiment in EBR-II is in progress (see Progress Report for January 1969, ANL-7548, Table I.A.1, p. 2 for design parameters). The quality-assurance procedures and records of the entire 0-3 group are being reviewed prior to acceptance for irradiation.

(c) Fuel-element Swelling (Groups 0-4 and 0-5).

A series of irradiation experiments has been planned to verify the behavior of mixed-oxide core, stainless steel-clad fuel elements predicted by the SWELL-2 fuel-element design code of ANL and to obtain design data for this fuel-cladding system. The experiments are to be performed in

For each of the fuel-element design variations considered, estimations were made of the following measurable quantities: a/o burnup at failure; cladding diametral strain versus axial position versus a/o burnup; OD of columnar grain region versus axial position versus a/o burnup; and fission-gas release versus a/o burnup. Figures I.A.3 and I.A.4 are typical examples of the results; for both cases in these figures, the coolant temperature rise and effective fuel density were assumed to be 300°F and 88%.

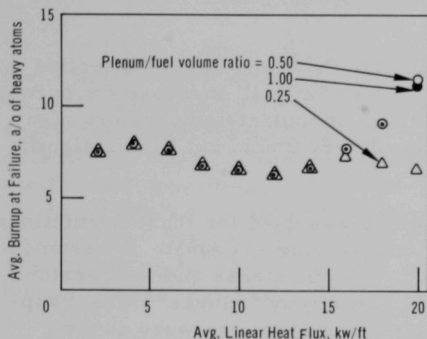


Fig. I.A.3. Predicted Performance of FFTF Fuel Elements in EBR-II

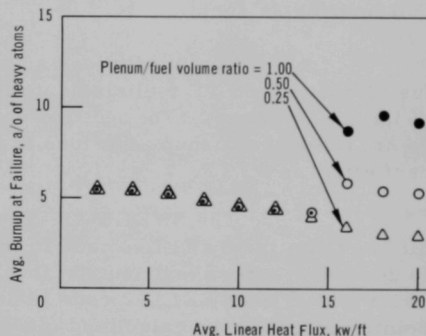


Fig. I.A.4. Predicted Performance of FFTF Fuel Elements in FFTF

The predictions indicate that FFTF fuel elements will fail at about 2 a/o burnup less in FFTF than in EBR-II (due to the higher coolant temperatures in FFTF), and the ratio of plenum to fuel volume of the FFTF fuel elements can be reduced from 1.0 to 0.25 without reducing the element lifetime* at linear heat fluxes up to 14 kW/ft (because failures are due to fuel swelling rather than to plenum gas; however, consequences of failure might be more severe with smaller plenums and higher plenum pressures. At heat fluxes above 14 kW/ft, the larger plenum becomes effective because the fuel temperatures are high enough that most of the fission gas is released from the fuel. Then the predominant internal load on the cladding can be due to pressure of fission gas in the plenum, rather than to fuel swelling. The sudden change in burnup between 14 and 16 kW/ft in Fig. I.A.4 for the large plenum can perhaps best be explained by the following calculated conditions at time and location of failure:

Linear heat flux, kW/ft	Plenum pressure, psi	Fuel-swelling pressure, psi
	(Plenum-to-fuel volume ratio: 1.0)**	
12	265	1538
14	351	1261
16	876	1012
18	992	471

*Possible abnormal conditions, such as overpower or flow coastdown, are not considered.

** Actually (effective height of plenum)/(fuel-column height). Space within the fuel column available to released fission gas is not yet accounted for when calculating the pressure of that gas.

<u>Linear heat flux, kW/ft</u>	<u>Plenum pressure, psi</u>	<u>Fuel-swelling pressure, psi</u>
	(Plenum-to-fuel volume ratio: 0.25)*	
12	1049	1538
14	1246	1120
16	1293	467
18	1210	171

Note that at heat fluxes higher than 14 kW/ft, some fuel melting is calculated to occur; SWELL-2 is not sophisticated enough to account for the effects of that melting as such.

The predictions also indicate that reducing the effective fuel density of FFTF fuel elements from 88 to 82% will increase the burnup at failure by about 2 a/o, and that variations in coolant-temperature rise do not influence burnup at failure in EBR-II very much, but have a significant effect in FFTF.

The SWELL-2B code, which was used for these predictions, differs from the SWELL-2 code in that the cladding creep rate is assumed to depend on stress and neutron flux as well as on stress and temperature. Prior use of the SWELL-2 code to predict Dounreay failures** was disappointing because the calculated cladding strains at failure were several times greater than the measured strains. To force SWELL-2B predictions to agree with Dounreay results (failures at 6 a/o burnup with about 1% cladding diametral strain, when the effective fuel density is 85% and the linear heat flux is 5-10 kW/ft), two key constants had to be changed as follows:

	<u>Earlier work</u>	<u>Present work</u>
A ₁₅	-0.01085	-0.018
A ₃₅	0.67	0.85

The physical significance of these constants is that an A₁₅ of -0.01085 causes the cladding strain associated with failure to be reduced, logarithmically, to 50% of its unirradiated value at a fluence of 10²⁰; an A₁₅ of -0.018 further reduces the failure strain at 10²⁰ fluence to only 17% of its unirradiated value. An A₃₅ of 0.67 causes only 23% of the pressure of the fission gas retained in the fuel to be exerted on the cladding; an A₃₅ of 0.85 reduces the percentage further to 15%.

The estimated values of effective neutron flux used in the calculations were

	<u>Dounreay</u>	<u>EBR-II</u>	<u>FFTF</u>
ϕ_{total}	2.5×10^{15}	3.0×10^{15}	5.2×10^{15}
Effective fraction	-	0.77	-
Relative value of $\phi_{\text{total}}^{\dagger}$	0.91	1.0	0.625
$\phi_{\text{effective}}$	1.75×10^{15}	2.3×10^{15}	2.5×10^{15}

* See 2nd footnote, previous page.

** Lawton, H., et al., The Irradiation Behavior of Plutonium-bearing Ceramic Fuel Pins, Paper 4B/4, British Nuclear Soc., London Conf. on Fast Breeder Reactors, May 17-19, 1966.

[†] Russcher, G. E., and Dahl, R. E., Fast Reactor Irradiations, Trans. Am. Nucl. Soc. 11(2), 499 (Nov 1968).

2. Carbide

a. Fabrication and Evaluation

- (i) Fuel Element Performance (L. A. Neimark and T. W. Latimer)

Last Reported: ANL-7548, p. 3 (Jan 1969).

After irradiation, the gas plenum of Element NMV-11 was found to be sealed off from the fuel section. The cause of this blockage has been identified as a small amount of sodium at the upper surface of the restrainer plug located at the top of the fuel column; sodium formed a fillet between the edge of the plug and the cladding. The sodium (from the sodium bond in the capsule) gained access to the fuel through longitudinal cracks in the Nb-1 w/o Zr cladding. The similarity of the pressures in the capsule and element plenums (see ANL-7548, p. 3) indicates that the sodium did not prevent the fission gas in the element plenum from entering the capsule plenum during irradiation.

(a) Metallographic Examination of Element NMV-11.

Sections were removed from the midplane, from 1 in. below the top, and from 1 in. above the bottom of Element NMV-11 for metallographic examination. These were no changes in the microstructure of the hyperstoichiometric (U,Pu)C because of the ingress of sodium into the element, and particles near the cracks in the cladding showed no depletion of the (U,Pu)₂C₃ phase. No interaction occurred between the fuel and the Nb-1 w/o Zr cladding. In the top and bottom sections, all fission-gas bubbles appeared to be in the (U,Pu)₂C₃ phase and at the (U,Pu)C grain boundaries. In the midplane (hottest) section, fine gas bubbles were also found in (U,Pu)C grains from the midradius inward. The dendritic appearance of the (U,Pu)₂C₃ phase appeared to be unchanged from its original arc-melted structure throughout the element. Densification by sintering occurred in the midplane section for 60% of the radius, but no sintering was evident in the top and bottom sections.

(b) Metallographic Examination of Elements SMV-2 and HMV-5. Similarly located fueled sections were also removed from Elements SMV-2 and HMV-5 for metallographic examination. The PuC fraction (original particle size $\leq 44 \mu$) in the midplane sections sintered into a continuous matrix that conformed to the contours of the UC particles (original particle size ranged from 500 to 1700 μ) and the cladding. In the top and bottom sections, sintering of the PuC fraction was less complete; the original PuC particles were still visible in the outer regions. In general, the original shape of the UC particles were retained. The dicarbide phase in the UC generally was absent from particles in the interior of the element. There was no depletion of dicarbide in UC particles that were

against the Type 304 stainless steel or Hastelloy-X claddings. Inter-diffusion between the UC and PuC fractions may have occurred in the inner 60% of the diameter of the midplane sections. These areas were characterized by a change in the microstructure of the original UC particles and the presence of relatively large ($\sim 6\mu$) fission-gas bubbles. Penetration of PuC along grain boundaries of the UC was also observed. These areas were not observed in the top and bottom sections.

The maximum depths of fuel-cladding interactions found in the midplane sections were 19μ in the Type 304 stainless steel and 50μ in the Hastelloy-X. Variations in the depths of the reactions appeared to correlate with the proximity, but not necessarily the contact, of UC particles with the Hastelloy-X cladding. There was no such correlation with the stainless steel cladding.

B. Physics Development--LMFBR

1. Theoretical Reactor Physics

a. General Fast Reactor Physics

(i) Reactivity Coefficients (H. H. Hummel)

Last Reported: ANL-7457, pp. 11-15 (May 1968).

The analytical aspects of the problems in the theory and application of the multilevel formalism to Doppler-effect studies have been examined by Hwang.* Follow-up studies using direct numerical methods have been completed. The studies that have been made in both the resolved and unresolved regions can be summarized as follows:

(a) Resolved Region. The problem in the resolved region is quite simple. The existing RABBLE Program** has been modified to allow both single-level and multilevel resonance parameters in the Adler-Adler formalism. Hence, the calculations can be made on a rather routine basis. Preliminary results show that multilevel effects are significant when ^{235}U is considered.

(b) Unresolved Region. The problems in the unresolved region are considerably more complicated than those in the resolved region. In order to utilize the "R-matrix statistical models" for the S-matrix or Adler-Adler parameters (see Progress Report for May 1968, ANL-7457, p. 12), a matrix-inversion code capable of treating a large complex matrix is required. Two codes for this purpose have been completed. The MODMAT code, which is essentially the modified version of the MATDIAG code,[†] allows

*Hwang, R. N., Nucl. Soc. Eng., to be published in April 1969.

**Kier, P. H., and Robba, A. A., ANL-7326 (1967).

[†]Moldauer, P. A., Phys. Rev. 136, 947 (1964).

for a maximum of 120 poles for IBM-360. Another code, CHOPSUEY, which is based on the complex eigenvalue and eigenvector routines of Garbow at ANL, is a better alternative to MODMAT. The CHOPSUEY code is more than three times faster than MODMAT. Both these codes not only diagonalize the inverse-level matrix A^{-1} , but also punch out the Adler-Adler parameters in RABBLE format so that Doppler-effect calculations can be carried out readily.

The calculations have been carried out for both ^{239}Pu and ^{235}U under various conditions. It was found that the effect of multilevel interference on the Doppler effect of the fissile isotopes depends on several factors. Specifically, the effect depends strongly on the magnitude of the ratio of the average total width to the average spacing, the number of fission channels assumed, and the energy region under consideration. Under some conditions multilevel effects may not be negligible. A detailed report on these studies is under preparation.

- b. Fast Critical Experiments--Theoretical Support (R.B. Nicholson and R. G. Palmer)

Last Reported: ANL-7548, pp. 8-11 (Jan 1969).

Appropriate formulae have been derived for bilinear averaging of the cross sections of multigroup transport theory for the purpose of simultaneous group collapsing and cell homogenization. The derivation was based upon the variational principle. It is the intent to incorporate this scheme into the TESS one-dimensional transport code[†] developed primarily for studying heterogeneity effects in the ZPR reactors. The coarse-group (G or J) cross sections are expressed in terms of the fine-group (g or j) cross sections averaged over the cell and angle with angular fluxes and adjoints calculated from a cell calculation with periodic boundary conditions. The results are as follows. Define the normalization integral

$$\eta_G \equiv \frac{1}{2\pi V} \sum_g \int \int d\Omega dV N_g(x, \Omega) |\mu| N_g^*(x, \Omega),$$

where μ is the cosine of the angle between the x direction and Ω . We then obtain for the total cross section

$$\Sigma_G = \frac{1}{4\pi V \eta_G} \sum_g \int \int d\Omega dV N_g^*(x, \Omega) \Sigma_g(x) N_g(x, \Omega).$$

The fission matrix is

$$\langle \chi \nu \Sigma_f \rangle_{JG} = \frac{1}{16\pi^2 V \eta_G} \sum_g \int \int d\Omega dV \sum_j \int \int d\Omega' dV' N_g^*(x, \Omega) \chi_{g\Sigma_{fj}}(x) N_j(x, \Omega).$$

[†]Goin, R. W., TESS--A One-dimensional S_N Transport Theory Code for the CDC-3600, report in preparation.

The ℓ^{th} legendre component of the scattering transfer matrix is

$$\Sigma_{JG}^{(\ell)} = \frac{1}{v\eta_G} \sum_g \sum_{\text{in } G} \sum_j \sum_{\text{in } J} \int dV \Sigma_{Jg}^{(\ell)}(\mathbf{x}) \int d\Omega |P_\ell(\mu)| N_g^*(\mathbf{x}, \Omega) \int d\Omega' |P_\ell(\mu')| N_j(\mathbf{x}, \Omega') \bigg/ \left[\int |P_\ell(\mu)| d\Omega \right]^2$$

This formulation has not yet been tested by numerical calculations.

2. Experimental Reactor Physics

a. Fast Critical Experiments--Experimental Support (Idaho)

(i) Integral Studies of Cross Sections (W. G. Davey)

Last Reported: ANL-7548, p. 12 (Jan 1969).

Participation in the efforts of the Data Testing Subcommittee of the Cross Section Evaluation Working Group (CSEWG) for the testing of ENDF/B with fast-reactor integral data continued in two areas: 1) the establishment of "benchmark" cases, and 2) the review of analyses of benchmarks reported by CSEWG agencies.

In the first area, a total of ten fast-reactor benchmark prescriptions were submitted to CSEWG for analyses by participating agencies. The systems to be studied are all based on simple "physics" core studies in various fast-critical facilities and emphasize the primary fuel materials U-235, U-238, and Pu-239, containing also a limited number of diluents (principally carbon and sodium). The bases for these ten cases are the following:

- | | |
|-----------------|----------------------|
| 1. Jezebel | 6. Vera 1-B |
| 2. Vera 11-A | 7. ZPR-3 Assembly 6F |
| 3. ZPR-3 | 8. ZPR-3 Assembly 12 |
| 4. Zebra Core 3 | 9. ZPR-3 Assembly 11 |
| 5. Godiva | 10. Zebra Core 2 |

In the second area, the results of analyses of the original benchmarks, ZPR-3 Assemblies Nos. 48 and 11, are still being received from a few agencies and are under study. The consistency between results from different laboratories is encouraging; for Assembly 48, the eigenvalues from S_4 transport calculations (or adjusted diffusion-theory results) average about 0.985. For Assembly 11, although there is more divergence in results, the average k from S_4 transport calculations (or diffusion theory with adjustment) appears to be about 0.979.

b. Fast Critical Experiments--Experimental Support (Illinois)

(i) Fission Process and Cross Section Data Related to Fast Reactors (R. Gold)

Last Reported: ANL-7487, pp. 10-11 (Aug 1968).

(a) Precise Cross-section Measurements Using the Manganese Bath. The manganese-bath technique has, in the past, been primarily used to determine the emission rate of neutron sources. By virtue of improvements in the assay of ^{56}Mn activity, certain other experiments have become feasible.* One, which was already established, is that of determining the hydrogen-to-manganese 2200-m/sec cross-section ratio. We have extended the range of this experiment with data taken over a five-year period so that a standard error (combined precision and accuracy) of 0.2% is available. Other neutron cross sections which have resulted from these same experiments are that of sulfur (at 2200 m/sec) and the relative fast-neutron-absorption cross-section ratios for sulfur and oxygen. By poisoning the bath with boric acid, both the boron-to-manganese and hydrogen-to-manganese cross-section ratios emerge; so far these numbers have been determined with errors of about 0.6% by this latter method. Values at 2200 m/sec obtained to date are $\sigma_{\text{H}}/\sigma_{\text{M}} = 0.02506 \pm 0.00005$; $\sigma_{\text{B}}/\sigma_{\text{M}} = 57.33 \pm 0.32$ (natural boron of undetermined isotopic content); $\sigma_{\text{S}} = 0.520 \pm 0.010$ b.

c. Planning and Evaluation of FFTF Critical Assembly Experiments (D. Meneghetti)

Last Reported: ANL-7548, pp. 14-15 (Jan 1969).

(i) Calculated Worth of Substitution of Sodium Cans for Axially Central Core Materials in ZPR-3 Assembly 51. The reactivity change due to substitution of sodium contained in stainless steel plate-shaped cans in place of the core material in ZPR-3 Assembly 51 of the two axially central drawers and associated axial reflector materials was calculated by the MACH-1 diffusion-theory code and the 29-group cross-section set. The calculated value of -789 lh may be compared with the experimental value of -763.08 lh (see Progress Report for March 1968, ANL-7438, p. 14).

(ii) Estimation of Flux Depression and Self-shielding in Small ^{10}B Reactivity Sample in ZPR-3 Assembly 51 Using the 1D-SNARG Program. In ANL-7548 the effects of self-shielding in a small, hollow ^{10}B cylindrical sample upon reactivity-worth calculations were estimated

*De Volpi, A., and Porges, K. G., Precise Cross-section Measurements Using the Manganese Bath, Bull. Am. Phys. Soc. 13, 1421 (1968).

using self-shielding factors obtained by application of the method of Dwark et al.* This method assumes that the flux shape external to the sample is flat.

Both the flux depression at the sample surface and the self-shielding have since been estimated using the 1D-SNARG discrete-ordinate transport program. A high-order modified** single Gaussian quadrature was used in order to facilitate calculation of the thin-absorber effects. The sample was approximated by a spherical shell having the identical shell thickness as the cylindrical shell sample and a radius such that the spherical shell mass was identical to the cylindrical sample mass.

The group-wise flux-depression and self-shielding factors are listed in Table I.B.1 for the sample embedded in compositions corresponding to the core and reflector of ZPR-3 Assembly 51. The calculated self-shielding values are also listed. It is interesting to note that these values for self-shielding, assuming flat external flux, give values similar to the respective products of the flux-depression factors and the self-shielding factors obtained by the transport calculation except with the core composition in a few groups.

TABLE I.B.1. Flux Depression and Self-shielding Factors in Small, 10B Reactivity Sample in ZPR-3 Assembly 51 Using 1D-SNARG Program

(a) Energy Group	(b) Lower Energy Limit (eV)	In Core			In Reflector			(e) Self- Shielding by Formula
		(c) Depression	(d) Self- shielding	Product	(c) Depression	(d) Self- shielding	Product	
13	9119	0.94	1.00	0.94	0.93	1.00	0.93	0.95
14	4307	1.00	1.00	1.00	0.96	1.01	0.97	0.93
15	2613	0.99	0.99	0.98	0.95	1.01	0.96	0.92
16	2035	0.91	0.99	0.90	0.89	1.00	0.89	0.91
17	1234	0.91	1.00	0.91	0.89	1.02	0.90	0.89
18	961	0.92	0.91	0.91	0.87	1.01	0.88	0.88
19	583	0.89	1.00	0.89	0.86	1.01	0.87	0.86
20	275	0.87	1.00	0.87	0.83	1.01	0.84	0.83
21	101	0.84	0.99	0.83	0.77	1.00	0.77	0.73
22	29.0	0.84	0.95	0.79	0.68	0.96	0.65	0.70
23	17.6	1.10	0.91	1.01	0.61	0.90	0.55	0.59
24	6.48	0.78	0.84	0.66	0.54	0.83	0.45	0.53
25	3.93	1.02	0.78	0.80	0.49	0.74	0.36	0.40
26	1.44	0.50	0.61	0.31	0.44	0.62	0.28	0.32
27	0.87	0.51	0.48	0.25	0.41	0.48	0.20	0.24
28	0.53	0.52	0.40	0.21	0.40	0.40	0.16	0.19
29	0	0.53	0.28	0.15	0.39	0.28	0.11	0.13

a--Values for higher-energy groups assumed to be unity.

b--Upper energy of Group 13 is 15034 eV.

c--Ratio of flux level at sample surface to flat flux level distant from sample.

d--Ratio of average flux level in sample to flux level at outer surface of sample.

e--Self-shielding ratios obtained by application of formula of Dwark et al.; see text.

*Dwark, J., Hoffman, P. L., Hurwitz, H., Jr., and Clancy, E. F., Self-shielding Factors for Infinitely Long, Hollow Cylinders, KAPL-1262 (1955).

**Meneghetti, D., Discrete Ordinate Quadratures for Thin Slab Cells, Nucl. Sci. Eng. 14, 295 (1962).

The comparisons of calculated and experimental radial worths of the ^{10}B sample in ZPR-3 Assembly 51 are given in Table I.B.2. The calculated worths are by perturbation theory, uncorrected and corrected, respectively, for the flux depression and self-shielding.

TABLE I.B.2. Comparison of Calculated and Experimental Radial Worths of ^{10}B in ZPR-3 Assembly 51

Radial Distance from Reactor Centerline (cm) ^a	Experimental Worth ^b (Ih/kg)		Calculated Worth (Ih/kg)	
			Diffusion-theory Perturbation	Flux Depression and Sample Self-shielding Included
	2-P Row Normal	2-P Row Rotated 90°		
0	-9647	-9695	-10940	-10537
2.54	-9597	-9652	-10859	-10470
6.35	-9193	-9274	-10508	-10117
12.70	-7939	-8091	-9288	-8959
15.24	-7276	-7445	-8718	-8354
17.78	-6574	-6748	-8078	-7701
20.32	-6024	-6112	-7449	-7068
25.40	-4710	-4763	-6475	-5969
30.48	-3988	-4037	-6514	-5614
33.02	-3643	-3907	-7378	-6030
35.56	-3439	-3835	-7773	-5719
38.10	-2733	-3380	-5481	-4075
40.64	-1901	-2540	-3229	-2468
43.18	-1113	-1619	-1902	-1357
45.72	-573	-902	-854	-699
50.80	-112	-189	-179	-157
57.15	129	65	-31	-28.6
63.50	148	144	-	-
76.20	0	0	-	-

^aMean experimental core radius, 33.5 cm. Experimental radial core-reflector interface position at position of traverse, 35.9 cm.

^bSee Progress Report for August 1968, ANL-7487, Table I.B.4, p. 15.

3. ZPR-3 Operations and Analysis

a. Heterogeneity (W. G. Davey and R. L. McVean)

Last Reported: ANL-7527, p. 12 (Dec 1968).

The analysis of the data from the heterogeneity traverses in ZPR-3 Assembly 53 is essentially complete.

b. Mockup Studies (W. G. Davey and R. L. McVean)

Last Reported: ANL-7548, pp. 16-18 (Jan 1969).

(i) FTR Critical Program. The eight safety-rod mechanisms of ZPR-3 were modified to move two safety-rod drawers with each drive and a larger air-cooling manifold was installed.

The entire radial reflector was reloaded so as to give the composition of the FTR radial reflector. Starting from approximately 83% of the critical mass of Assembly 56A, the assembly was then reloaded to critical. This critical configuration, Assembly 56B Loading 56-17 (see Fig. I.B.1), is the reference core for Assembly 1 of the FTR Resumed Phase-B Critical Experiment and contained 374.2 kg total plutonium. Both radial reflectors 1 and 2 contain the FTR nominal composition (see Progress Report for December 1968, ANL-7527, Table I.B.4, p. 12). The difference in the radial reflectors lies in the lengths of the ZPR-3 drawers in which the material is loaded, which changes the location of the spring gap. Calculations are being made for the exact as-loaded composition.

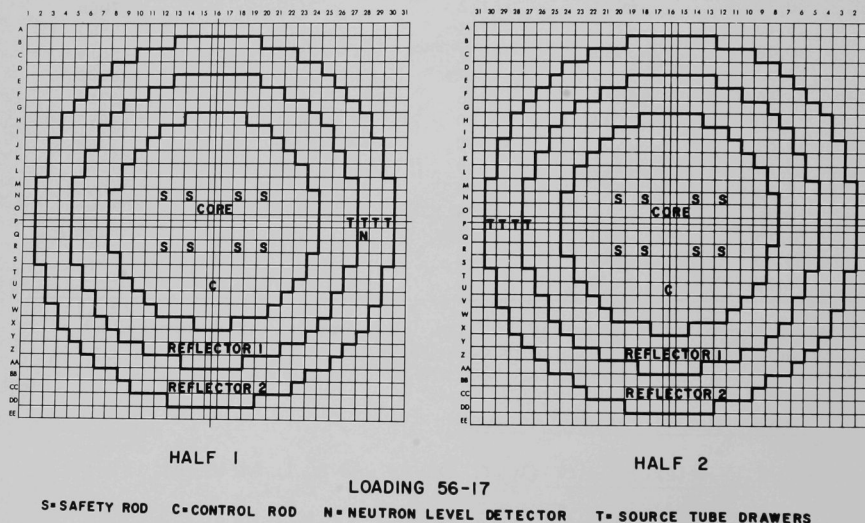


Fig. I.B.1. Critical Loading for Assembly 56B of ZPR-3 (Reference Core of Assembly 1 of FTR Resumed Phase-B Critical Experiment)

The control and safety rods were calibrated by the inverse kinetics method. First, three period-type measurements were performed to evaluate the effective neutron source in the reactor due to the spontaneous fission of Pu-240. Second, the reactor was taken to a high power level (~30 W) and stabilized. The rod being calibrated was then withdrawn and the

resultant flux history recorded. The flux history was analyzed using the delayed-neutron fractions given in Table I.B.3, and the source term measured in the period experiments. The measured worth of a yoked safety rod from the fully in position to 9.5 in. out (each drive moving two of the heavily loaded core drawers) was $-0.189\% \Delta k/k$. Hence, all eight safety rods moving from 0 to 9.5 in. are worth $1.51\% \Delta k/k$. The measured control-rod worth for the same interval is -82 lh.

TABLE I.B.3. Calculated Beta Fractions for
Assembly 56 of ZPR-3

Group	β_i (U-235)	β_i (U-238)	β_i (Pu-239 + 241)	β_i (Pu-240)
1	1.8171 -06	1.7951 -05	5.9505 -05	1.7121 -06
2	1.0185 -05	1.8918 -04	4.3846 -04	1.6693 -05
3	8.9899 -06	2.2370 -04	3.3824 -04	1.1740 -05
4	1.9462 -05	5.3578 -04	5.1363 -04	2.1401 -05
5	6.1208 -06	3.1070 -04	1.6129 -04	7.8267 -06
6	1.2433 -06	1.0357 -04	5.4808 -05	1.7732 -06

Notes: $\beta_{\text{eff}} = 3.0558 -03$; $\ell = 5.4592 -07$; $\text{lh}/\% \rho = 1.0391 +03$.

The delayed-neutron fractions were derived on the basis of four calculations in cylindrical and spherical geometry. They varied in the use of the axial or radial reflector compositions for the reflector of the spherical calculations. A check of reactivity in inhours versus periods from 20 to 200 sec showed no significant deviations for all four calculations. The values given in Table I.B.3 were taken from a spherical calculation with the radial reflector composition as the reflector of the sphere, since the calculated mass of this system was closest to the experimental critical mass.

Upon completion of the control- and safety-rod calibrations, the edge worths of core drawers at U-10, U-23, V-11, V-22, W-12, X-17, and X-18 and the temperature coefficient of reactivity were measured. These data are now being analyzed and will be used to determine the final critical mass. The radial traverses are now in progress, with the U-238, Pu-239 and B-10 reaction rates completed.

4. ZPPR Operations and Analysis (W. G. Davey and P. I. Amundson)

Last Reported: ANL-7548, pp. 26-27 (Jan 1969).

a. Doppler Effect

(i) Reactivity Doppler Equipment. The drive mechanism has been successfully operated in the ZPPR Cell. All motor and vacuum controls function properly in both local (in the cell) and remote (in the control room) modes.

Heater controllers have been received, and one has been tested. Isolation transformers have been ordered to prevent interference with reactor instrumentation.

Construction of the Doppler-rod extension and capsule is proceeding on schedule.

(ii) Reactivity Doppler Analysis. Previous problems with RABBLE calculations in the unresolved resonance region were found to be the result of an insufficient number of fine groups. Some of the cases were rerun, and results appeared consistently good. The type of input data required for two-dimensional diffusion and perturbation runs using the ARC system have been investigated. ARC library-tape procedures were also reviewed in preparation for making a 20-group, 18-material tape for UO₂ Doppler analysis.

b. Reactor Equipment Development

(i) Equipment

(a) ZPPR Computer. Portions of the ZPPR On-line Computer System have been installed. Acceptance tests are in progress. Maintenance schedules and procedures for the computer and peripheral equipment are being written. Construction of the initial remote I/O terminal has been started.

(b) Data-collection System. The Data Logger portion of the Digital Data Collection System has been returned to the manufacturer for correction of discrepancies found during checkout. The Data Collection System signal cabinet has been completed. Installation is in progress.

(c) Experimental Reactor Equipment. The ZPPR Autorod System has undergone the final operational tests in AFSR. During these tests, the ZPPR experimental ion chambers were evaluated for performance characteristics.

The drawer-drive system for the axial sample has been tested in the reactor assembly. Results of these tests are expected to guide design efforts of the associated sample-exchange mechanism.

The reactor bed and tables have been realigned under load. This complies with the manufacturer's recommendation for periodic review of the alignment characteristics of the system under varying static load conditions.

(d) Technique Development. A program to read the incremental magnetic tape from the data-acquisition system of ZPPR is complete.

Output from the data-acquisition system is needed to test input acceptance. A program for control-rod calibration is complete. Testing will begin following acceptance of the ZPPR computer.

The inverse kinetics algorithm, with source and drift correction, has been checked out and run with different weighting functions. The drift rates are very small ($<10^{-8} \Delta k/k$) and may be as much the result of statistical error in the least-squares calculation as reactor drift. Error calculations and similar tests are being incorporated into the program to provide a check on the reliability of the drift calculation.

Program SPECB, which was written to calculate spectrum-averaged delayed-neutron parameters, has been checked out on the CDC-1604.

The fission ratio $\sigma_F(^{239}\text{Pu})/\sigma_F(^{235}\text{U})$ has been measured from several tenths of a keV to 24 keV, using the time-changing neutron spectrum in a lead slowing-down-time spectrometer. Bursts of neutrons at 14 MeV are injected into a lead block (4 x 4 x 4 ft) and very quickly they attain an asymptotic energy distribution given by $\bar{E} = (181/t^2) \text{ keV}$ (t in μsec). The time distribution of the output of ^{235}U and ^{239}Pu fission chambers is recorded with a multichannel time analyzer, and the ratio of the counts in corresponding time channels is formed from the data obtained with each detector to yield the energy variation of the fission ratio. This, in turn, is normalized to a value of the fission ratio obtained by Perkin *et al.*,* using 24-keV neutrons from an Sb-Be source. The results obtained are presently being evaluated.

c. Mockup Studies. The unreflected core preloaded in ZPPR has been maintained in a condition of readiness to accept possible performance of Assembly 2 of FTR Continuing Phase-B experiments.

5. ZPR Materials (A. B. Shuck)

Last Reported: ANL-7513, pp. 27-35 (Oct 1968).

a. Procurement

(i) Process Materials

(a) Metallic Plutonium. Approximately 3700 kg of metallic plutonium of 88% fissile isotopes were required for the fabrication of the basic U-28.3 w/o Pu-2.5 w/o Mo alloy fuel plates for the zero-power reactors. Examination of the isotopic compositions available showed that it

*Perkin, J. L., White, P. H., Fieldhouse, P., Axton, E. J., Cross, P., and Robertson, J. C., J. Nucl. Energy 19, 423 (1965).

would be possible to normalize the composition, by careful blending of high ^{240}Pu with low ^{240}Pu isotopic compositions, to a constant 11.5% ^{240}Pu , and the other plutonium isotopes would fall proportionally into a rather narrow range. Further normalization of the fissile composition of the ZPR fuel could then be achieved by adjusting the calculated melt charge to produce 25 w/o fissile plutonium in the alloy plates.

An order, Contract 2013, was placed for this work to be carried out at AEC plants in Richland, Washington, by Isochem, Inc., and its successor contractor, Atlantic Richfield Hanford Corp. The work, started in February 1967, was completed in December 1968. A total of 3880 kg of plutonium of various isotopic compositions was used to produce 3685 kg of blended ingots in 1218 melts. The specified composition grand average of analyses achieved and 2 σ dispersion of the analysis is shown in Table I.B.4.

TABLE I.B.4. Specified Compositions and Average Isotopic Analyses of ZPR Plutonium

Isotope	Specified Composition (%)			Analysis Average		1218 Melts 2 σ
	Nom	Min	Max			
^{238}Pu	<0.10	-	0.10	0.052	±	0.027
^{239}Pu	86.40	85.60	87.20	86.522	±	0.545
^{240}Pu	11.50	11.00	12.00	11.510	±	0.294
^{241}Pu	1.70	1.00	2.50	1.724	±	0.324
^{242}Pu	<0.40	-	0.50	0.174	±	0.045

A total of 1140 kg of plutonium ingots was shipped to the Dow Chemical Co. and 2496 kg of ingots were shipped to Nuclear Materials and Equipment Corp. (NUMEC) for fabrication into ZPR fuel elements.

A second isotopic composition is required to simulate fast-reactor recycle plutonium. A special batch of plutonium was produced from highly irradiated source materials. Chemical processing of these materials was started at Atlantic Richfield Hanford Corp. in January 1969 under Contract No. 2308. Metallic reduction buttons will be needed to fabricate the fuel by April 1969. Process-stream analysis indicates that there are about 233 kg of plutonium in this lot of the following isotopic composition (%): 66.7 ^{239}Pu , 26.13 ^{240}Pu , 5.67 ^{241}Pu , 1.48 ^{242}Pu . At 90% yield, about 210 kg of plutonium will be available as reduction buttons.

(b) Plutonium Nitrate. An order has been placed with Atlantic Richfield Hanford Corp. for the production of 370 kg of plutonium as aqueous nitrate solution. This solution will be supplied to the fabrication contractor to make coprecipitated (U,Pu) O_2 for pellet-loaded fuel rods. The

aqueous plutonium nitrate is being supplied in accordance with ANL Specification RF-A2a (ZPR). The isotopic plutonium specification is the same as that for the 11.5% ^{240}Pu metallic plutonium. The work is now scheduled for completion in June 1969. Plutonium nitrate solution of 27.0 w/o ^{240}Pu will also be required, but because of the very limited supply of the composition, it will be necessary to recover this from the residues from metal fabrication.

(c) Stainless Steel for Element Jackets. Type 304L stainless steel has been standardized for ZPR core structure and cladding. Because commercial Type 304L stainless steel varies widely in physical characteristics, quality, uniformity, and purity, reactor-grade vacuum-processed Type 304L stainless steel was ordered by ANL for the various types of fuel elements and calandria. Stainless steel as indicated in Table I.B.5 has been ordered for ZPR core components.

TABLE I.B.5. Stainless Steel for ZPR Core Components

Item		Manufacturer	End Use	Mo/Year Delivered	
1. <u>Tubing</u>					
a.	24,000 ft	1.35-in.-OD x 0.015 in.	Pacific Tube Co. P.O. 549-452	Fuel Plates	4-67
b.	41,000 ft	1.35-in.-OD x 0.015 in.	Pacific Tube Co.	Sodium Elements	1-67
c.	50,000 ft	0.3760 x 0.011 in.	Superior Tube Co.	Oxide Rods	4-69
d.	33,000 ft	0.388-in.-ID x 0.011 in.	Superior Tube Co.	Calandria Tubes	4-69
e.	18,700 ft	1.35-in.-OD x 0.015 in.	Wall Tube and	Sodium Na ₂ CO ₃	11-68
	21,000 ft	1.475-in.-OD x 0.015 in.	Metal Products	and B ₄ C Elements	
2. <u>Strip</u>					
a.	1200 lb	0.019 x 15 in.	Wallingford Steel Co. P.O. 630068	Calandria	2-69
b.	3000 lb	0.065 x 15 in.		For Tubing and Structural	2-69
c.	1800 lb	0.120 x 15 in.		For Tubing and Structural	2-69
d.	3000 lb	0.035 x 5.87 in.	Wall Tube Co.	Calandria	2-69
e.	Rerolled	0.019 x 5.87 in.	Wallingford Steel Co.	Calandria	2-69

Items 1b and 1c were originally scheduled for shipment in January 1969, but the first lot of strip shipped from Carpenter Steel Co. to Superior Tube Co. did not meet the specified precipitation and inclusion ratings. The strip was rejected and replaced by Carpenter Steel Co. on February 10, 1969. The new strip met Superior Tube Co., and ANL laboratory evaluation tests and was approved for release to tube production on February 21.

The Superior Tube Co. plant was visited on February 25, 1969, to discuss delivery schedules and quality control of the tubing.

A double ultrasonic test will be done on part of the oxide-fuel tubing to supply 12,000 ft to a transverse and longitudinal defect standard, 0.030 in. long x 10% of the wall thickness. This tubing will be reserved for the jacketing of the (U,Pu)O₂ oxide-fuel rods. The balance of the tubing for uranium oxide and calandria will be tested against a defect standard 0.125 in. long x 10% of wall thickness.

The strip for calandria manufacture was ordered to specifications similar to those for the tubing. The first vacuum-processed billet ruptured in the breakdown rolling operation and the rescheduled strip is to be shipped from Wallingford Steel Co. during the week of February 27, 1969. In order to start calandria fabrication in February, 3000 lb of 0.035 x 5.875 in. of strip were furnished from Wall Tube Co. and re-rolled by Wallingford Steel Co. to 0.019-in. thickness. The minimum order to the hot mill was for 6000 lb of strip. The excess strip will be cold rolled to 0.065- and 0.120-in. thickness by 15-in. width, annealed, and furnished to ANL for future ZPR and LMFBR requirements for reactor-grade Type 304L stainless steel.

The ANL tooling for stretch-forming fuel jackets was furnished to D. K. Aerospace Industries Corp. to make jackets for the sodium-element contract. A supplemental order was placed with this company to manufacture 1750 additional jacket sleeves to be used for manufacture of special isotopic and instrumented fuel elements. The end plugs for these elements are being made in ANL shops.

(ii) Fuel-element Manufacture

(a) Metallic Fuel Elements. Approximately 2900 kg of the 11.5% ²⁴⁰Pu is being fabricated into 16,000 stainless steel-jacketed, alloy-fuel plates. These plates, nominally 0.250 in. thick by 2.0-in. wide, are furnished in lengths of 1, 4, 5, 6, 7, and 8 in. The fuel-element cores are made up to contain 25.0 w/o of the fissile plutonium isotopes ²³⁹Pu and ²⁴⁰Pu. The nominal composition of the core plates is U-28.3 w/o Pu-2.5 w/o Mo, as an alloy.

The first 4168 plates were made by Dow Chemical Co. in the AEC Rocky Flats Plant before a commercial contract could be negotiated. The Dow production was terminated when commercial production of these plates became established at Nuclear Materials and Equipment Corp. The fabrication of these fuel elements is now expected to be completed in March 1969. Table I.B.6 shows the cumulative numbers of fuel elements of each size shipped from Dow and NUMEC.

Eleven fuel elements from NUMEC Melt 989 were rejected on February 28, 1969 as the result of gamma-scan assay evidence that the plutonium content was 10% above specification. A core plate from this heat was sampled and the analysis was 31.41% plutonium.

TABLE I.B.6. Cumulative Shipments and Inventory of
U-28.3 w/o Pu-2.5 w/o Mo Elements, Feb. 14, 1969

Length, in.:	1	4	5	6	7	8	Total All Sizes	Total Pu (kg)
Inventory, Dow Elements	118	739	1085	779	720	727	4,168 ^a	758 ^a
NUMEC Shipments								
Receipts	-	2006	3160	1995	2068	2149	11,378 ^b	2,130.5 ^b
Rejects at ANL	-	16	35	17	15	19	102	18.8
Destructively Tested	-	23	29	20	13	18	103	18.6
Inventory, NUMEC Ele.	-	1967	3096	1958	2040	2112	11,173	2,092.9 ^b
Total Inventory	118	2706	4181	2737	2760	2839	15,341	2,850.9 ^b

^aDow inventory includes 17 inspection rejects, which will be rejacketed as instrumented elements.

^bReceipts from NUMEC are based upon NUMEC shipping documents subject to ANL verification or dispute.

(b) Evaluation of U-28.3 w/o Pu-2.5 w/o Mo Fuel Elements.

The ANL quality-assurance program for the metallic elements has consisted of (1) field surveillance and resident inspection on both operating shifts in the NUMEC plant, (2) receiving inspection of each fuel element, and (3) destructive evaluation sampling and analysis of about one percent of the fuel elements. In addition, each element is assayed nondestructively, by the ANL Special Materials gamma-scan method, which quantitates the ²³⁹Pu characteristic radiation of each production fuel element against that of standardized elements.

The four most important characteristics of the fuel elements:

1. the quantity of fissile isotope;
2. the composition of the core alloy;
3. the integrity and freedom from exterior contamination of the jackets;
4. dimensional conformity with the drawings.

Items 1 and 2 are verified as follows:

The NUMEC charge calculations are monitored and statistically compared with NUMEC analytical results and results of the gamma-scan assay. The NUMEC analytical values are compared with ANL analysis of the destructively evaluated samples. The scatter of individual analytical results confounded individual comparison, and comparisons were made of the averages of each 25 NUMEC melts. These are shown as control charts. The averages of ANL and NUMEC analyses are not significantly different. Both show a grand average of 24.92 w/o fissile plutonium and $\sigma = \pm 0.13$ w/o. However, NUMEC has transferred all fuel elements on the basis of the charge-calculated value of fissile plutonium,

which averages 25.00 w/o of the core weight. ANL has disputed the amount of plutonium transferred on the basis of the difference of the ANL and NUMEC analyses from the charge-calculated transfer values.

One factor of the plutonium "loss" during fabrication of ZPR fuels is the decay of ^{241}Pu during the period between ARHCO ingot analysis, NUMEC analysis of the ternary castings, and ANL analysis of the core plates from the finished fuel elements. This fact was recognized during a calculation of ^{241}Am buildup, but since the ^{241}Am buildup is not the most direct approximation of ^{241}Pu decay, the decay calculations have been made for ^{241}Pu as follows, based on a (13.2 ± 0.2) -yr half-life:

$$\Delta^{241}\text{Pu}_t = {}^{241}\text{Pu}_0(1 - e^{-\lambda t}),$$

where

$$\Delta^{241}\text{Pu}_t = \text{the decay loss of plutonium after time } t;$$

$${}^{241}\text{Pu}_0 = {}^{241}\text{Pu} \text{ content at time of initial analysis};$$

$$\lambda = 0.693/13.2 = 0.0525 \text{ yr}^{-1}, {}^{241}\text{Pu} \text{ decay constant}$$

$$= 0.693/12 \times 13.2 = 0.004375 \text{ mo}^{-1}, {}^{241}\text{Pu} \text{ decay constant.}$$

Examination of the NUMEC charge-data sheets shows that the plutonium ingots were used three to seven months after the ARHCO production date. However, the recycle charge constitutes 15 to 30% of typical furnace charge, which will add additional time before casting analysis. It may, therefore, be assumed that the NUMEC castings are analyzed about six months after the plutonium in them was ingoted and analyzed at ARHCO. The ANL analyses are made six to eight months after. The calculation shows the following decay loss of 1.7% ^{241}Pu :

<u>Time</u> <u>(mo)</u>	<u>Percent of</u> <u>Fissile Plutonium</u>	<u>Percent of</u> <u>Ternary Alloy</u>
3	0.022	0.006
5	0.037	0.009
6	0.044	0.011
8	0.058	0.015

(c) Oxide-fuel Rods. Various ^{235}U enrichments of UO_2 and compositions of $(\text{U,Pu})\text{O}_2$ -loaded fuel rods are required to study the parametric effects of oxide heterogeneity and temperature on reactor physics. The fuel will be in the form of oxide pellets in 3/8-in.-dia x 6-in.-long stainless steel jackets. The quantities of each composition and schedular requirements are shown in Table I.B.7.

TABLE I.B.7. Oxide-loaded Fuel Rods

Quantity	Pellet Composition	^{235}U or ^{239}Pu		Contractor	Required Delivery
		g/rod	kg Total		
a. 14,600	0.22% ^{235}U depleted UO_2			Kerr-McGee Corp.	June 1969
b. 11,500	16.41% ^{235}U enriched UO_2	13.08	150.4	Kerr-McGee Corp.	June 1969
c. 4,500	46.5% ^{235}U enriched UO_2	37.07	166.8	Kerr-McGee Corp.	June 1969
d. 12,700	15% Pu (U,Pu) O_2	10.45	132.7	Under negotiation	April 1970
e. 5,900	30% Pu (U,Pu) O_2	19.68	116.1	Under negotiation	April 1970

The schedules have been set up to better the required delivery dates by incremental deliveries and acceptance of fuel rods as they are completed. Contracts have been signed with Kerr-McGee Corp. to produce the depleted and enriched UO_2 fuel rods in their Cimarron Plant.

Kerr-McGee Corp. processed 1472 kg of 0.204% depleted uranium from UF_6 to UO_2 containing 1395 kg of uranium by analyses. Forty-one preproduction fuel elements were received the week of February 10, 1969. These were not acceptable because of excessive axial clearance in the fuel column and slag inclusions in the welds. Fifty additional fuel elements were received for ANL evaluation on February 18, 1969. These latter elements are now undergoing ANL evaluation.

On the basis of Kerr-McGee preliminary procedures, analyses, and inspection reports, the company was authorized February 7, 1969, to proceed with a process-variability study. Approximately 13,000 pellets were processed, of which 3000 were measured and 54 were analyzed. The data from these were reviewed in a meeting at the Cimarron Plant on February 18 and 19, 1969, and Kerr-McGee was authorized to proceed with depleted UO_2 pellet manufacture. A 175,000 depleted UO_2 pellet run was started on February 24, 1969.

(d) Quality-assurance Program for ZPR Fuels. Simultaneous fabrication at two plants of metallic and oxide fuel required two-shift ANL representation and inspection at each plant. A group of six inspectors have been assigned, three to NUMEC and three to Kerr-McGee. These will be rotated so that each shift is covered, and two men cover receiving inspection and destructive testing at ANL. A resident inspector will also be employed, one shift, at Superior Tube Co. during ultrasonic testing and inspection of the tubing for oxide-fuel jackets. It is hoped by this means to ship tubing with a high degree of quality assurance to the fuel fabricator.

The large numbers of pellets are being subjected to quality control on a statistical basis by Kerr-McGee Corp. Nine pellets are being removed from each firing of about 800 pellets, and these are being plotted on \bar{x} -R control charts. From each process lot of 25,000 pellets about 270 pellets will be measured. Standard deviations and control

limits are being calculated on increments of 70 to 100 measured pellets. A graphic frequency distribution analysis method is being used to determine standard and process control limits.

(iii) Nonfissile Elements

(a) Sodium and Sodium Carbonate Elements. Zero-power reactor experiments utilize sodium and sodium carbonate elements as a source of sodium and oxygen in various assemblies. Most of the elements supplied to date have been manufactured by D. K. Aerospace Industries supplemented by ANL Central Shops. A total of 24,300 sodium carbonate elements has been shipped, which completes the requirement.

D. K. Aerospace has delivered 35,900 sodium elements under its contract with ANL. This contract will be completed in late February. ANL Central Shops has delivered 24,400 sodium elements in the course of demonstrating manufacturing feasibility and satisfying early experimental requirements.

Large FFTF critical assemblies, which are expected to run concurrently with other criticals, has led to an increased requirement for sodium inventory. Both facilities will be used to produce an additional quantity of 34,000 elements, containing approximately 2000 liters of sodium. Manufacture is just getting underway, and delivery is scheduled for completion by the end of June 1969.

(b) Boron Carbide and Tantalum Elements. Boron carbide and tantalum elements have been requested by PNL to study FFTF control concepts in zero-power reactors.

In mid-January 1969, ANL Central Shops completed the jacketing of 1548 boron carbide elements and shipped them to Idaho. These elements are structurally similar to sodium and sodium carbonate elements. The core material was obtained from the Norton Co. in plates measuring $1/2 \times 2$ in. x assorted lengths of 4, 5, 6, 7, and 8 in. Cores contained approximately 77% boron, and ranged in density from about 2.40 to 2.47 g/cc. Core-to-core weights were controlled within one percent of nominal.

The 2200 unclad pieces of B_4C measuring $1/4 \times 1/2 \times 2$ in. have also been delivered by Norton Co. and inspected by ANL Central Shops. These and the above pieces constitute a highly uniform set having all been made from the same lot of molding powder and ground to within $\pm 1\%$ of nominal weight.

The tantalum element requirement can be satisfied with metallurgical-grade materials. For maximum loading flexibility, plates

measuring $1/16 \times 2 \times 2$ in. and $1/16 \times 2 \times 3$ in. are desired. Specifications have been written and commercial suppliers are being contacted for price and delivery.

(c) Iron Oxide Plates. In December 1968, Lake Products, Inc., completed delivery of 20,000 Fe_2O_3 plates measuring $1/8 \times 2 \times 2$ in. and $1/8 \times 2 \times 3$ in. The FFTF requirements have increased the need for iron oxide plates. Accordingly, Lake Products, Inc., has been requested to supply an additional 10,000 plates. Production has been resumed at the rate of 2500 per month and delivery is expected to be complete about June 1, 1969.

(d) Calandria. Four model (shop-made) prototype calandria were produced to test the revised design modifications for calandria. Although the welds on these were not of the quality desired from production calandria, Central Shops was authorized to proceed with the design and manufacture of production tooling and to make 40 calandria. If these prove to be satisfactory, it is expected that the remaining 1400 calandria will be ordered through ANL Central Shops, with much of the work subcontracted.

Sodium filling and welding have been determined to be very critical operations in calandria manufacture. Sodium filling must be very carefully controlled so that the expansion of the sodium does not cause the calandria to burst when heated to experimental temperatures, but very little void volume can be tolerated in the experiment. The welds between the headers and the calandria tubes and shell must be very precisely done. The welding techniques are still under development.

Type 304L stainless steel strip was received to begin shell, bulkhead, and header manufacture the first week in February. A shipment of 2004 ft of calandria tubes were received from Superior Tube Co. on February 25, 1969.

C. Component Development-- LMFBR

1. Reactor Mechanism and Instrumentation

a. Instrumentation Development (T. P. Mulcahey)

(i) Fission-Gas Pressure Transducer Evaluation and Development (J. R. Folkrod)

Last Reported: ANL-7513, p. 39 (Oct 1968).

(a) Null-balance System. A null-balance fission-gas pressure transducer identical to the unit tested last year for 8 months was installed in a fuel pin that was inserted into the CP-5 research reactor. The pressure reading was zero before reactor startup and rose to about 8 psig at reactor power. The pressure rose slowly to 15 psig after 2 weeks, then suddenly rose to 30 psig due to liberation of fission gases. The pressure continued to increase for 6 weeks until a maximum pressure of 130 psig was reached. Then, over a 2-day period the pressure began to drop to 120 psig. At that time, the reactor was shut down and the indicated fission-gas pressure went to 5 psig and never increased above that value for the duration of the transducer test. Every time the reactor was shut down, the fission-gas pressure would show a decrease in pressure due to the cooling effects of the gases. However, the sudden and sharp drop from 120 to 5 psig indicated only one thing: the pin failed and released fission gas to the second container, which had a large volume.

Postirradiation examination proved that to be the case. Thus the history of fuel-pin failure was recorded by its fission-gas pressure trace. The fission-gas pressure built up slowly at first, then suddenly increased, indicating that trapped fission gas suddenly was liberated from the metal fuel. Pressure increase was slow thereafter until a small leak appeared, which was indicated by the pressure transducer. Complete failure of the pin occurred at reactor shutdown, perhaps caused by thermal shock to the pin.

b. FFTF Instrumentation (R. A. Jaross)

(i) In-core Flowmeter Development (for FFTF) (R. A. Jaross)

Last Reported: ANL-7548, p. 30 (Jan 1969).

(a) Flow-sensor Feasibility Studies

Not previously reported.

Investigation of the feasibility of a probe-type permanent-magnet flow sensor for FFTF has been started. Two designs are being

considered, one with an O-shape cross section, the other with a C-shape cross section. Preliminary calculations and fabrication of parts for the former design (with an OD of 1.25 in.) are underway; Alnico-5 and -8 magnets have been purchased. Fabrication difficulties would delay development of the C-shaped design, so it will not be pursued at this time.

A small NaK loop (of 3/4-in. tubing) has been overhauled and modified for preliminary tests.

(b) Materials Procurement

Not previously reported.

Various sizes (AWG #34 to #19) of 1200°F ceramic-insulated nickel-coated silver magnet wire have been requisitioned for purchase to Technical Specification ANL-HTI-FFTF 503-4-G. The amount of wire to be ordered will permit fabricating coils for at least four eddy-current probe-type flow sensors and two eddy-current flowmeters.

Magnet wire suitable for coils required to operate in the FFTF, where the combined temperature effects of the liquid-metal coolant, gamma heating, and coil I^2R losses will exceed 1200°F, is also being sought.

(c) Magnet Irradiation Tests

Last Reported: ANL-7399, p. 44 (Nov 1967).

All preirradiation testing and stabilization of the Alnico-5, -6, and -8 magnet samples (96 total samples) prior to their irradiation in EBR-II have been completed. Irradiation capsules are being prepared; testing procedures and techniques to ensure high integrity in the EBR-II environment are being emphasized.

(ii) Signal Lead Connectors for Sodium Service (A. P. Grunwald)

Last Reported: ANL-7548, p. 31 (Jan 1969).

Tests of the FFTF prototype signal-lead connector involved several opening and closing cycles. The previously reported increase in release torque of the breech lock was found to be caused by in-seepage of ~20 cm³ of sodium past the main gasket. Apparently, the reduced mobility was not caused by sodium interfering directly, but by some corrosion and etching of stainless steel as well as gasket (Inconel) surfaces; such corrosion was present only where sodium was found. It is speculated that the reaction involved the Molycote (molybdenum disulfide) used as a lubricant in

the breech lock; although a thorough analysis of this reaction would be desirable, it will not be pursued. The appearance of the gasket suggests that the corrosion permitted the seepage of sodium in the first place.

The sealing surfaces have been reconditioned, and an attempt has been made to keep these surfaces free of MoS_2 when the unit was reassembled. No sodium was admitted in the subsequent two runs of the experiment into the test tank; the operation of the breech lock as well as the behavior of the gasket seem so far normal. Retesting with sodium will be undertaken before the experiment is terminated.

The pressure (leakage) tests of the gasket and of the nipples were extended to 20 and 200 psi, respectively. Results were as expected: leakrates varied approximately as the square of differential pressure, and no irregular releases or discontinuities of the leakrate as a function of pressure were observed until the pressure approached the "separation pressure" of a nipple, i.e., overcame the spring load that keeps the nipple seated. Separation on the 0.5-in.-dia nipple occurred at 170 psig. Reseating of the nipple after separation occurred when the pressure had dropped to ~130 psi, which is consistent with expectations. The smaller lines show a correspondingly higher capacity; in the present model these lines have also higher spring preloads because space for stronger springs was available. There is no point in testing for limits on these nipples as the regular and predictable behavior of the larger nipple allows extrapolation. Thus the designer can vary the bore dimension and spring-tension design for just about any pressure required (as long as the tubes used are strong enough to hold the pressure).

An observed tendency for the connector pins to buckle was found to be caused by imperfections in the connector supplied by Physical Science Co. The pin ends are typically rounded off to an approximately hemispheric shape, and the corresponding sockets have what appears to be a 45° camber. However, several pins and sockets show these relief operations (obviously made to facilitate entry of the pins into the sockets) to be incomplete. Magnified images of corresponding pins show partly flat "tops," noncoaxial "domes," and, in some places, edges instead of smooth transitions or continuous surfaces. All pins were straightened out laboriously, and the pin ends were filed to form a conical (pointed) end. So far, this has been successful in preventing buckling or misalignment of pins in the process of engagement through three cycles.

(iii) Failed-fuel Location Method Development (E. S. Sowa)

Last Reported: ANL-7548, pp. 31-32 (Jan 1969).

(a) Sodium Test Loop. Loop construction has been completed with wiring of heaters and thermocouples and installation of insulation, the second gas-detection loop, and the last protective-housing panel.

Operation of the instrumentation, heaters, sample-injection valve, and the nonfouling level detectors on the riser pipe was checked; small leaks at these detectors were corrected by welding their threaded fittings. Then sodium was loaded into the loop and operation was begun.

The activity-counting equipment has been ordered from the Hewlett-Packard Co.

2. Fuel Handling, Vessels, and Internals--Core Component Test Loop (CCTL) (R. A. Jaross)

Last Reported: ANL-7548, pp. 32-33 (Jan 1969).

The pressure differential across the FFTF prototype subassembly under flowtest has remained constant at 45.9 psig.

From January 23 through February 18, the CCTL has been in operation continuously for 647.5 hr; the pump was off for 0.5 hr on February 7 for an electrical change. The cumulative total operating time at any temperature is 3726.8 hr, of which 2346.9 hr were at 1060°F and 400 gpm.

a. Sodium-purity Measurements. The sodium-purity data in ANL-7548 were from the results of 24 runs of the plugging meter. The data were obtained with improved procedures for monitoring the purity of the sodium in CCTL. Additional measurements of flow and temperature conditions of the CCTL plugging meter and cold trap have led to further improvements; instead of cycling the plugging-meter valve, the valve is kept closed and at a low temperature. This change improves reliability by eliminating the need to cycle the valve; also, reliance on the on-line plugging meter for purity measurement (instead of obtaining sodium samples for laboratory analysis) eliminates the periodic need to shut down the pump and cut and reweld a bypass section from the CCTL.

In practice, the temperature of the plugging valve is maintained constant at about 250°F, and the sodium flow through the closed plugging valve is established at about 0.3 gpm by throttling the 2-in. control valve. The flows through both the cold trap and the plugging valve are constant within the statistical small variations of pressure head developed by the CCTL mechanical pump. The operators periodically monitor and record the flows through the cold trap and plugging valve; any increase in flow indicates an inadvertent change in the position of the 2-in. control-valve position or an inadvertent change of pump speed; but a decrease in these flows indicates either those inadvertent changes or a real increase in the sodium oxide concentration in the CCTL.

This mode of operating the plugging valve causes it, in effect, to serve as an on-line sodium-quality meter. Since the system began

operating in this mode on February 2 there has been no deviation in flow through the plugging valve. There also has been no change in the relative temperatures inside the cold trap.

b. Acoustic and Vibration Measurements

Not previously reported.

After being calibrated, two high-temperature accelerometers (Model-AQB4971, supplied by Gulton Industries, Inc.) were installed on the CCTL on February 7. One was installed on the high-temperature side of the test-vessel mounting pad at an elevation opposite the CCTL flow-inlet grid plate, which supports the FFTF subassembly. The second transducer was installed 33 in. downstream from the high-pressure outlet of the Byron-Jackson mechanical pump. Since installation, the sound intensities from the FFTF subassembly and the mechanical pump have not changed significantly.

Data analysis is being conducted in the program to develop an acoustic detector for boiling [see Sect. IV.C.1.a.(c)].

D. Systems and Plant--LMFBR

1. 1000-MWe Plant

a. 1000-MWe Contract Management, Technical Review, and Evaluation (L. W. Fromm)

Last Reported: ANL-7548, pp. 33-34 (Jan 1969).

The edited copy of the Westinghouse Task-I report is being published along with the other contractors' Task-I reports.

(i) Babcock & Wilcox Co. Subcontract. Volume 4, Trade-off Studies, and Volume 5, Parametric Studies, of the Task II and III report, BAW-1328, were received by ANL. Volume 1, containing the overall conceptual system design description (CSDD) and capital-cost estimate, and Volume 3, containing CSDDs, are expected within two weeks. Volume 2, which also contains CSDDs as well as the Task-IV report describing the requirements for research and development, is expected within a month.

(ii) Westinghouse Electric Corp. Subcontract. The architect-engineering portion of the cost optimization and parametric studies has been received by Westinghouse; it is being reviewed and incorporated into the Task-II and -III reports. Task-II system descriptions are being reviewed and revised. Research and development programs are being formulated in Task IV.

(iii) General Electric Co. Subcontract. Except for part of one of the fuel-design sections of the Task-III report, the Task-III and -V reports have been reviewed and approved by company management. That fuel-design section is being revised; the other sections are being prepared for publication. Material for the Task-IV report is being reviewed by management.

(iv) Combustion Engineering, Inc. Subcontract. Work on the follow-on study has been completed. The Task-IV report, which describes the required research and development, is expected within two weeks.

(v) Atomics International Subcontract. All technical activities of the follow-on study have been completed. Drafts of all task reports have been completed, reviewed, revised, and have been or are being edited. The Task-II report is being printed; all work is expected to be completed within a few weeks.

E. EBR-II

1. Research and Development

a. Reactor Experimental Support--Reactor Analysis and Testing (R. R. Smith)

Last Reported: ANL-7548, pp. 34-44 (Jan 1969).

(i) Nuclear Analysis and Safety

(a) Mark-IIA Static Calculations (J. R. Trinko)

Calculations have been made for two oxide cores containing 91 subassemblies; one contains the oxide-fuel composition originally agreed upon for Mark-IIA calculations, and the other contains the oxide-fuel composition proposed by G. H. Golden of ANL. The two fuels differ primarily in plutonium content. Originally ^{239}Pu was assumed to constitute 20 w/o of the fuel. Golden proposed 16 w/o ^{239}Pu and 4 w/o ^{240}Pu . Both cores were homogeneous and were surrounded by depleted-uranium blankets. A criticality enrichment search yielded 50.1 a/o ^{235}U for 16 w/o ^{239}Pu and 42.9 a/o ^{235}U for 20 w/o ^{239}Pu .

Six 127-subassembly cores (described in Table I.E.1) were also studied. Each core was assumed to be spherical and homogeneous. One-dimensional diffusion theory was used to calculate the number of structural subassemblies for criticality in cores 21, 22, and 23, for which the metal fuel was enriched to 52.5 a/o ^{235}U and the oxide fuel was 20 w/o ^{239}Pu , 30 w/o ^{235}U , and 50 w/o ^{239}U . The results of these calculations are shown in Table I.E.2.

TABLE I.E.1. Description of Hypothetical Mark-IIA Core Loadings Containing 127 Subassemblies

Core No.	Composition of Homogeneous Core Region (No. of Subassemblies)	Comments
21	57.0 Mark IIA 57.0 Oxide 13.0 Structural	Enrichment of 52.5 a/o ^{235}U ; critical on structural-subassembly search; depleted-U blanket
22	49.25 Mark IIA 49.25 Oxide 28.50 Structural	Enrichment of 52.5 a/o ^{235}U ; critical on structural-subassembly search; nickel inner reflector (Rows 8 and 9)
23	58.0 Mark IIA 58.0 Oxide 11.0 Structural	Enrichment of 52.5 a/o ^{235}U ; critical on structural-subassembly search; axial gap and reflector
24	45.5 Mark IIA 45.5 Oxide 36.0 Structural	Critical on Mark-IIA enrichment search; depleted-U blanket
25	45.5 Mark IIA 45.5 Oxide 36.0 Structural	Critical on Mark-IIA enrichment search; nickel inner reflector (Rows 8 and 9)
26	45.5 Mark IIA 45.5 Oxide 36.0 Structural	Critical on Mark-IIA enrichment search; axial gap and reflector

TABLE I.E.2. Calculated Parameters for 127-subassembly Cores Containing Structural Subassemblies and Equal Amounts of Metal and Oxide Fuel

Core No.	^{235}U Enrichment (a/o)	Number of Structural Subassemblies	Peak Flux ($\text{nv} \times 10^{-15}$)	Peak Power Density (MW/l)	Ratio of Peak to Average Power Density	β_{eff} ($\times 10^3$)	Average Flux Energy in Core (MeV)
21	52.5	13.5	3.18	0.649	1.50	6.356	0.715
22	52.5	28.5	3.46	0.627	1.31	6.375	0.683
23	52.5	11.0	3.37	0.705	1.41	6.224	0.723
24	79.2	36.0	3.74	0.725	1.62	6.355	0.649
25	60.5	36.0	3.96	0.678	1.40	6.306	0.611
26	83.8	36.0	3.93	0.763	1.51	6.27	0.652

Cores 24, 25, and 26 were assumed to contain 36 structural subassemblies and equal volume amounts of metal and oxide fuel. The enrichment of the metal fuel was varied to achieve criticality.

Peak neutron fluxes, peak power densities, ratios of peak to average power densities, β_{eff} , and core-averaged flux energies were also calculated and are presented in Table I.E.2.

Comparing the average flux energy of Core 21 with 24, that of 22 with 25, and that of 23 with 26, it is clear that the addition of structural subassemblies to the core softens the neutron-energy spectrum.

Furthermore, a nickel reflector produces a softer spectrum than either depleted uranium or the axial composition. The nickel reflector flattens the power distribution and adds reactivity, which permits the use of more structural subassemblies inside the core.

The replacement of a depleted-uranium inner blanket with a nickel reflector causes the peak flux to increase but the peak power density to decrease. This occurs because all cores have a very hard spectrum, and softening of the spectrum moves neutrons to energies where fission cross sections are lower.

(b) Analysis of Rod-drop Data for Run 29 (R. W. Hyndman)

The changeover from the stainless steel reflector to depleted uranium during Run 29 provided an excellent opportunity to evaluate the effects of the stainless steel reflector on the reactivity feedback function. Run 29 consisted of the following three segments: 29A, the reference loading with the stainless steel reflector in Rows 7 and 8; 29B, with the stainless steel in Row 7 replaced with depleted uranium; and 29C, with all stainless steel replaced by depleted uranium.

Rod-drop studies were conducted for both Runs 29A and 29C under conditions of 41.5-MWt power and 100% coolant flow, and 25-MWt power and 100% coolant flow. The time-dependent feedback functions resulting from the studies for Runs 29A and 29C at 41.5 MWt were then fitted to a six-term mathematical feedback model. The results of the model fitting are given in Figs. I.E.1 and I.E.2. In both cases an excellent fit was obtained.

The effects of replacing stainless steel with depleted uranium are illustrated in Figs. I.E.3 and I.E.4, which summarize the results of a simple linear scaling or extrapolation of the 41.5-MWt data to 25 MWt. For the case of Run 29C (depleted-uranium reflector), the linear scaling of the feedback resulted in an excellent fit. For Run 29A (stainless steel reflector), on the other hand, a marked difference may be noted.

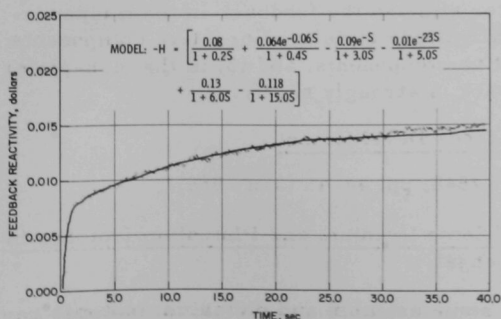


Fig. I.E.1

Comparison of Time-dependent Feedback Function from Run 29A Rod-drop Studies with Values Calculated with Mathematical Feedback Model (stainless steel reflector in Rows 7 and 8; 41.5 MWt; 100% coolant flow)

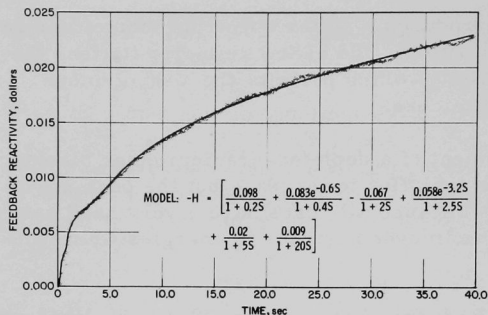


Fig. I.E.2

Comparison of Time-dependent Feedback Function from Run 29C Rod-drop Studies with Values Calculated with Mathematical Feedback Model (depleted-uranium reflector; 41.5 MWt; 100% coolant flow)

Fig. I.E.3

Results of Extrapolating Data in Fig. I.E.1 (Run 29A) to 25-MWt Power (model same as for Fig. I.E.1)

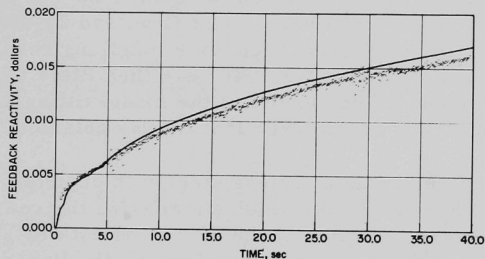
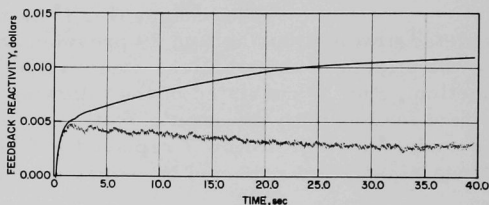


Fig. I.E.4

Results of Extrapolating Data in Fig. I.E.2 (Run 29C) to 25-MWt Power (model same as for Fig. I.E.2)

From these studies, the following conclusions may be made: (1) the prompt-feedback term was unaffected by the stainless steel reflector; (2) the installation of the stainless steel reflector affected the feedback in the midpower region either by decreasing the magnitude of delayed negative components or increasing the magnitude of positive components; and (3) in the high-power region (above 35 MWt), the feedback is strongly negative.

b. Nuclear Analysis Methods Development

Last Reported: ANL-7548, pp. 44-45 (Jan 1969).

(i) Fission Rates of Some Uranium and Plutonium Isotopes in EBR-II (B. R. Sehgal)

Fission rates of some uranium and plutonium isotopes have been calculated as a function of radial position in EBR-II. This information

will supplement the values of fission rates for ^{235}U , ^{238}U , and ^{239}Pu given in the guide for irradiation experiments.

Broad-group fission cross sections for the required isotopes were generated with the MC² code, using the ENDF/B data. The spatial dependence of the neutron spectrum for a recent configuration of EBR-II was used along with these cross sections to calculate fission reaction rates at various radial mesh points. The reaction ratios at the center of the core were calculated as: $1.184 \text{ }^{239}\text{Pu}/^{235}\text{U}$; $0.068 \text{ }^{238}\text{U}/^{235}\text{U}$; $6.341 \text{ }^{234}\text{U}/^{238}\text{U}$; $2.272 \text{ }^{236}\text{U}/^{238}\text{U}$; $0.406 \text{ }^{240}\text{Pu}/^{239}\text{Pu}$; $1.104 \text{ }^{241}\text{Pu}/^{239}\text{Pu}$; and $0.346 \text{ }^{242}\text{Pu}/^{239}\text{Pu}$.

(ii) Analysis of Some Critical Assemblies (B. R. Sehgal)

Ten fast critical assemblies have been analyzed with the ENDF/B cross-section data. The series includes ZPR-3 Assembly 6F, which has a composition and core volume very similar to those of EBR-II, and some assemblies which have a much harder spectrum (e.g., Jezebel) and a much softer spectrum (e.g., ZPR-3 Assembly 48). The details of the calculations and results have been reported in a paper submitted for presentation at the next American Nuclear Society meeting in June 1969. The trends shown by the results of the calculations lead to the following very preliminary observations:

(1) The ENDF/B ^{235}U σ_f above 2 MeV may be ~5% too high.

(2) Either the calculated spectrum is consistently softer than actually present in the assemblies or the ^{239}Pu σ_f and the ^{238}U σ_c are respectively ~5% too low and too high in the ENDF/B data set.

(iii) DSN Methods (L. B. Miller)

Implementation of the DSN numerical method as used with the IBM-360, Model 75 computer was continued with the adaption of the one-dimensional discrete-ordinates code ANISN. In addition to the obvious benefit provided by the speed and large, fast memory (256 K) of the Model 75 computer, implementation of the ANISN code provides the capability for performing one-dimensional neutron- and gamma-transport calculations with any order of anisotropic scattering.

Cross-section averaging and group collapsing can be done in regions or in a unit cell as a final edit option, using the space- and energy-dependent flux computed by the ANISN code. The averaged microscopic or macroscopic cross sections are punched in the format required for use in the ANISN and DOT codes.

The ANISN code on the IBM-360/75 computer also has a buckling-search option which was not available in the SNARG-1D code on the CDC-3600 computer. The code is written with variable dimensions so that the large, fast memory can be utilized to optimize the number of energy groups, the number of space points, and the degree of scattering anisotropy considered.

Like the DOT code, the ANISN code incorporates the step-function difference equations which always yield positive fluxes. These equations may be used exclusively or may be used in conjunction with the linear difference equations to recompute the flux whenever the linear difference equations produce a negative flux.

Six-group and 22-group cross sections averaged over EBR-II core, reflector, and blanket spectra have been prepared in the ANISN-DOT format.

(iv) Influence of Oxide-fueled Experimental Subassemblies on the Reactivity Coefficient of Axial Fuel Expansion
(J. T. Madell)

The influence of oxide-fueled experimental subassemblies on the reactivity coefficient of fuel expansion was studied in a realistic loading of EBR-II with Mark-IA fuel. The uranium enrichment of the mixed-oxide experimental subassemblies was set at 59.8 a/o to achieve criticality for this loading. Four calculations were performed to study the expansion coefficient--two in which the full core was expanded 0.2 and 0.4 in., and two in which all but the experimental subassemblies were expanded 0.2 and 0.4 in.

These calculations cover the range of situations in which the mixed-oxide fuel is assumed to expand as much as the metal fuel and in which the oxide fuel is assumed not to expand at all. The results of the calculations, presented in Table I.E.3, indicate a 17.7% reduction in the

TABLE I.E.3. Results of the Fuel-expansion Study
with Mixed-oxide Subassemblies

Rows Expanded	Approximate Weight of Fuel Expanded (kg)	Distance Expanded (in.)	$-\delta k \times 10^3$	$-\delta k / \delta L^a$ ($\times 10^2$)	$-\delta k / \delta L / \text{kg}^a$ ($\times 10^5$)
1 through 6	215	0.20	3.224	1.612	7.50
1 through 6	215	0.40	6.458	1.614	7.50
1, 3, 5, 6	180	0.20	2.646	1.326	7.37
1, 3, 5, 6	180	0.40	5.314	1.328	7.38

^aPer inch of fuel expansion.

magnitude of the expansion coefficient under the pessimistic situation in which the fuel of the experimental subassemblies does not expand. When the expansion coefficients are normalized per kilogram of ^{235}U (equivalent) being expanded, the differences in the results for the four cases becomes quite small ($\sim 2\%$). The reactivity coefficient of fuel expansion previously calculated for EBR-II Runs 24-27 is -1.59×10^{-2} ($\delta k/\delta L$ per inch of expansion).

A similar study was conducted of an EBR-II loading consisting of all Mark-IA subassemblies in which the influence of the expansion of metal fuel in the fourth row of the core was investigated. The loading of EBR-II for which the safety analysis was developed was similar to this loading. The results of this study (shown in Table I.E.4) are still being examined.

TABLE I.E.4. Results of the Fuel-expansion Study
with All-metal-fueled Core

Rows Expanded	Weight of Fuel Expanded (kg)	Distance Expanded (in.)	$-\delta k \times 10^3$	$-\delta k/\delta L^a$ ($\times 10^2$)	$-\delta k/\delta L/\text{kg}^a$ ($\times 10^4$)
1 through 5	158	0.40	7.81	1.95	1.24
1, 2, 3, 5	106	0.40	5.33	1.33	1.26

^aPer inch of fuel expansion.

The two core loadings are too different to permit a direct comparison of the calculated expansion coefficients. Investigation of the results so far reveals that the more negative values of $\delta k/\delta L$ and $\delta k/\delta L/\text{kg}$ for the metal-fueled core are due to the smaller and more compact loading. The loss of the fuel expansion in the fourth row has a greater effect on the core-expansion coefficient in the all-metal core because the fourth row represents a larger fraction of the total core loading. In both loadings, the expansion coefficient is linear with the amount of fuel expanded and the distance of the expansion.

(v) Nuclear Analysis for the Instrumented Subassembly
(J. T. Madell)

A possible, but highly unlikely, occurrence in the instrumented subassembly is the rupture of the two bellows in the pressure transducer and the passage of fission-product gas through the pressure tube to the reactor floor. As a part of evaluating the possible hazards involved in such an occurrence, the maximum activity of the fission-product gas in the fuel pin of the subassembly was calculated.

The equilibrium activity of the fission-product gases in Table I.E.5 will be present in the fuel pin of the subassembly operating at 8.8 kW (2.65×10^{14} fissions/sec) for 50 days. The calculation of the maximum activity yielded about 3000 Ci of gamma rays (≤ 1 MeV).

TABLE I.E.5. Description of Radioactive Fission-product Gases in Fuel Pin of Instrumented Subassembly after 50 days of Operation

Mass No. in Decay Chain	Fission Yield (%)	Isotope	Half-life	Decay Rate/sec ($\times 10^{-12}$)	Decay Energy (MeV)	
					β	γ
83	1.1	Br	2.4 hr	2.9	1.0	0.05
84	1.5	Br	31.8 min	4.0	3.0	1.5
85	2.0	Br	3 min	5.3	2.5	0.0
		Kr	4.4 hr	5.3	0.8	0.2
87	2.5	Kr	78 min	6.6	3.0	1.0
88	3.6	Kr	2.8 hr	9.5	0.5	1.5
131	4.1	I	8.05 days	10.9	0.6	-
132	5.0	I	2.3 hr	13.3	1.0	1.0
133	5.3	I	20.8 hr	14.0	1.4	0.5
		Xe	5.3 days	14.0	0.3	0.1
134	5.8	I	52.5 min	15.4	1.7	1.0
135	5.5	I	6.7 hr	14.6	1.0	1.0
		Xe	9.2 hr	14.6	0.9	0.5
138	5.2	Xe	17 min	13.8	2.7	1.5

(vi) Analysis of EBR-II Run 31F (J. T. Madell)

A large variety of neutron-sensitive foils were irradiated in three locations of EBR-II during Run 31F, with the objective of improving the definition of the flux magnitude and spectrum in the core. Because of its coarse group structure above 1 MeV, neutron cross-section set 238 is not well-suited to examine the data from the foil materials that are sensitive to high-energy neutrons. A new 22-group cross-section set (JM31F) was developed with 16 groups ($1/8$ lethargy units each) above 1.35 MeV. The broad group structure is sufficiently detailed to analyze threshold reactions such as (n,p) and (n, α). The MC² code generated the new set with weighting spectra characteristic of the core for Run 31F, depleted-uranium blanket regions, and the axial-reflector region, and the cross sections have been written in the formats required for diffusion- and transport-theory codes.

The new group structure also permits a direct comparison of the results obtained from Sets 238 and 23806 with the results to be obtained from Set JM31F. The energy limits of Groups 4, 5, and 6 in Set 238 are identical to those of Groups 17, 18, and 19, respectively, in Set JM31F; Groups 4 and 5 of Set 23806 have the same structure as Groups 20 and 21 of Set JM31F.

(vii) Effect of Xenon Tagging on Heat Transfer in Reactor Fuel Elements (R. K. Lo)

An analysis of the No. 3 element of the instrumented sub-assembly was made to predict the effect that adding a xenon tag would have on the thermal conductivity of the xenon-helium mixture in the element, the temperature drop across the gas gap between the fuel pin and the cladding, and the temperature of the center of the fuel. The analysis was based on a reactor power of 50 MWt, a location of the element at the midplane of the core, a plenum volume of 6.877 cm³, a maximum heat generation of 10.4 kW/ft, a coolant flowrate of 32 gpm, and a coolant temperature rise of 130°F. The analysis indicates that when the fuel element is charged with 1 cc xenon, the center temperature of the fuel would be about 3900°F, well below the melting point of the fuel (about 5000°F).

c. Fuel Performance Studies--Mark I Series (C. M. Walter)

(i) Driver Fuel Operation at High Temperatures and Burnups

Last Reported: ANL-7518, pp. 41-43 (Nov 1968).

(a) BEMOD Calculations for High-burnup Mark-IA Fuel Elements (V. Z. Jankus)

BEMOD* is a numerical program that calculates the stresses and strains of sodium-bonded metallic fuel elements under irradiation. In this program, the fuel, swollen under irradiation, is assumed to be compressible. The results of the calculations have been found to be quite sensitive to the assumed dependence of cladding creep on stress.

In BEMOD, the expansion of the fuel is a sum of thermal expansion, inexorable growth, and a compressible breakaway swelling:

$$(\Delta V/V) = (\Delta V/V)_{th} + (\Delta V/V)_{ing} + (\Delta V/V)_{bas}.$$

At sufficiently high burnups, the breakaway swelling is assumed to be

$$(\Delta V/V)_{bas} = G_2/[1 + (P/P_g)],$$

where P is the hydrostatic pressure, and G_2 and P_g are empirical parameters. This form has been found to fit the results obtained by K. F. Smith** on the swelling of EBR-II fuel in CP-5 under hydrostatic pressure. The

*Jankus, V. Z., BEMOD: A Code for the Lifetime of Metallic Fuel Elements, ANL topical report to be published.

**Smith, K. F., et al., The Effect of Hydrostatic Pressure on Irradiation Induced Swelling on EBR-II Fuel, ANL topical report to be published.

parameters G_2 and P_g , however, are subject to considerable uncertainty. For the present calculations, we have chosen G_2 equal to 0.7 and left P_g as an adjustable parameter.

Recent experiments by E. R. Gilbert* have demonstrated that at low temperature the creep of stainless steel in pile is much larger than the creep out of pile. Thus, in BEMOD we have assumed that cladding creep is a sum of temperature-dependent out-of-pile creep $\dot{\epsilon}_T$ and a flux-dependent creep $\dot{\epsilon}_\phi$, i.e.,

$$\dot{\epsilon} = \dot{\epsilon}_T + \dot{\epsilon}_\phi.$$

Also, we have assumed that at a given temperature flux-dependent creep is proportional to fast flux but is still of an undetermined dependence on stress:

$$\dot{\epsilon}_\phi = B(S_p/S_p^0)^n(\phi/\phi^0),$$

where B is the creeprate observed by Gilbert at stress S_p^0 and fast flux ϕ^0 , and where n is a still-undetermined constant.

Recent measurements of cladding strains of two Mark-IA fuel elements (BF05 and BF09) irradiated to 2.5 a/o maximum burnup (see Progress Report for November 1968, ANL-7518, pp. 41-43) provide a means of eliminating some uncertainties in the assumptions of fuel compressibility and cladding strain. In the present study, we have varied the cladding-creep parameter n and adjusted the fuel-compressibility constant P_g to obtain 0.6% creep at the fourth of six sections into which the fuel rod has been divided for purposes of identification in this analysis. (The sections are numbered from the bottom to the top of the fuel rod.) The initial length of the gas plenum in these calculations has been 2.128 in. (the nominal value for a Mark-IA fuel element), and BEMOD did not include cladding growth due to irradiation. (Growth of cladding due to accumulated fluence has been estimated as 0.2% by Harkness of ANL.)

For the chosen location and at 2.5 a/o maximum burnup, the values of the compressibility parameter P_g (in psi) to give 0.6% creep, and the corresponding calculated values for hoop stress S_p (in ksi), are given in the following table:

n	P_g (psi)	S_p^{**} (ksi)
7	406	23.5
5	341	19.7
3	222	12.8
1	15	1.2

*Gilbert, E. R., Battelle Northwest Laboratory, private communication, Oct 1968.

** S_p is the maximum hoop stress in the cladding at the point of maximum strain.

When we consider the relatively large uncertainty of the experimental strain values, the shapes of the axial strain profiles obtained with these calculations when $n = 7, 5$, and 3 are essentially the same, and agree fairly well with the shape of the profile made from BF05 and BF09 measurements. The shape of the profile when $n = 1$ is much flatter than the shape made from the measurements and is approximately the same as that of the profile of the fast flux. Also, the compressibility constant $P_g = 15$ is in distinct disagreement with Smith's measurements. At present, the choice $n = 3$ seems more attractive than the other choices shown in the table because of the theoretical considerations by Tesk at ANL and because the corresponding fuel-compressibility parameter P_g seems to agree somewhat better with Smith's data. However, the maximum stress of 12.8 ksi for $n = 3$ in the table is half to two-thirds the stress required for the same strain rate in out-of-pile tests at equivalent temperatures.

Greater difference in the values of strains calculated from the parameters in the table, with $n > 1$, may be expected when the length of the plenum chamber is changed. (Differences may also be expected when thinner cladding is used or when the element is operated at a higher temperature.) This might explain why BF09 experienced about 0.15% less average strain than BF05, even though both had been irradiated at essentially the same temperatures and flux distributions. The sizes of the plenum chamber of the two elements might have been slightly different. The normal volume of the plenum chamber in the Mark-IA element is barely sufficient to accommodate the bond sodium.

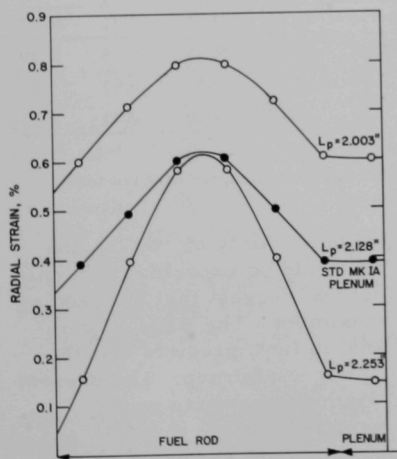


Fig. I.E.5. The Effect of Plenum Length (L_p) on the Radial Strain at 2.5 a/o Maximum Burnup for Mark-IA Encapsulated Fuel Element

To show the influence of plenum size (L_p), we have repeated the calculations using a somewhat smaller and a somewhat larger plenum size. In Fig. I.E.5, we have plotted the radial strains at 2.5 a/o maximum burnup, using $n = 3$ and $P_g = 222$. The calculated strain in the central sections (3 and 4) of the element remains the same when the standard plenum length is increased 1/8 in. This indicates that the strain there has been caused by direct contact between fuel and cladding. The shape of the axial-strain profile is much steeper than that obtained in the previous calculations. Further calculations performed with $n = 7$ and $n = 5$ produced no significant deviations from this shape.

The reduction of the plenum size by 1/8 in. increases the average strain considerably and makes the shape of the profile flatter, approaching the shape of the profile of fast flux. The average increase of the strain is more than the difference between the strains observed in BF09 and BF05. The strains calculated using $n = 7$ and $n = 5$ for the short plenum produced considerable deviations from the strains exhibited in Fig. I.E.5.

d. Mark II Driver Fuel Element Development (C. M. Walter)

(i) Element Irradiation Tests

(a) Irradiation of Encapsulated Mark-II Fuel Elements
(M. A. Pugacz)

Last Reported: ANL-7527, pp. 48-49 (Dec 1968).

Three encapsulated Mark-II fuel elements (201, 212, and 251) from Subassembly XO29, having maximum burnups from 1.9 to 2.3 a/o, have been diametrically profiled. The results are given in Table I.E.6.

TABLE I.E.6. Increase in Cladding Diameter of Mark-II Fuel Elements (%)

Capsule	Distance from Bottom End of Fuel, ^a in.									
	0.75	2.75	4.75	6.75	8.75	10.75	12.75	14.75	17.75	20.75
201	0.11	0.10	0.11	0.16	0.37	0.10	0.12	0.19	0.19	0.20
212 ^b	0.07	0.15	0.16	0.13	0.13	0.04	0.03	0.00	0.05	0.08
251	0.09	0.09	0.18	0.23	0.21	0.30	0.10	0.10	0.23	0.35

^aFuel pin initially 14.2 in. long.

^bPreirradiation diameter measurements not available; nominal diameter of 0.174 in. was used to calculate $\Delta D/D$.

Within the experimental uncertainty of $\sim \pm 0.1\%$, the values presented in this table are about what would be expected from only the irradiation swelling of the stainless steel and suggest that no cladding strain has occurred at burnups to 2.3 a/o maximum. The BEMOD computer code confirms these measurements and, in fact, predicts that the strain should be essentially zero up to about 6.5 a/o burnup. The present form of BEMOD shows that a Mark-II fuel element operating under 62.5 MWt conditions ($\phi = 2.9 \times 10^{15}$ n/cm²/sec, sodium $\Delta T = 300^\circ\text{F}$, and linear heat rating = 10.0 kW/ft) will go to a maximum burnup of about 11 a/o before 2% cladding strain occurs (see Fig. I.E.6). The cladding strain for a Mark-IA element operating at identical conditions is included in the figure for comparison.

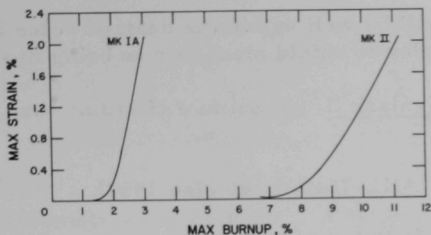


Fig. I.E.6

Calculated Maximum Strain vs
Maximum Burnup for Mark-II
and Mark-IA Fuel Elements

Because the calculations indicate that the Mark-II design should be capable of burnups considerably beyond 2.3 a/o, the subassembly has been returned to EBR-II for further exposure as Subassembly XO53 and will not be removed until the end of Run 34, at which time the elements will have accumulated about 4 a/o burnup.

The results of axial gamma scans of Elements 201, 212, and 251 are presented in Sect. I.E.2.b.(iii)(b).

e. Equipment--Fuel Related (E. Hutter)

(i) New Control Rod Subassemblies (O. S. Seim, T. Sullivan, and J. Pardini)

Last Reported: ANL-7548, pp. 45-46 (Jan 1969).

(a) Higher-worth Control Rod. Experimental design efforts were continued to achieve the desired 38.8-psi pressure drop with 61 gpm of flow through the higher-worth control-rod subassembly. Repetitive alterations of the subassembly have been made to reduce pressure drop. An orifice tube with orifice holes sized according to previous calculations was installed on the higher-worth control-rod prototype. Water-flow tests in the test loop with the equivalent of 61 gpm of sodium flow gave a total sodium pressure drop of 44 psi. This pressure drop is 3 psi higher than that obtained in the previous flowtest without the orifice tube and internal spring. The pressure drop was reduced to 41 psi by increasing the diameter of the orifice holes, but this was the maximum reduction which could be obtained by that method.

Modification of the lower shield piece has been decided on as the best way to reduce the pressure drop further. A study of the new design of the shield piece revealed a large increase followed by a large decrease in flow area where the transition between the annulus surrounding the 0.8-in.-ID rod and the 0.8-in.-ID hole occurred. Effort was directed toward redesign of the lower shield piece to eliminate variations in velocity when passing this point of flow restriction. Calculations indicate that the redesign will reduce the pressure drop approximately 3.5 psi. If subsequent flowtests substantiate the calculations, the overall pressure

drop through the subassembly will be well within the desired value of 38.8 psi at 61 gpm of flow. The lower shield piece is now being modified.

- (ii) Oscillator Rod--Mark II (O. Seim, J. Pardini, and T. Sullivan)

Last Reported: ANL-7548, p. 46 (Jan 1969).

The Mark-IIB oscillator rod has been flowtested in a water loop, and is being balanced and stress relieved. Detailed fabrication drawings of the modified drive shaft for the rod have been completed. The revised handling tool for the adapter sleeve has been fabricated and will be tested with the adapter sleeve after the sodium-test fixture has been assembled.

- (iii) Engineering Consultation (O. Seim, T. Sullivan, and J. Pardini)

- (a) Neutron-source Storage Thimble for Inner Blanket.

Engineering assistance is being provided to design a neutron-source storage thimble which will be located in Row 7 of the inner blanket of the reactor. This location is desirable for irradiation of an antimony-filled capsule in a region of high neutron flux for future use in neutron radiography. As much as possible of the design of the neutron-source storage thimble for the outer blanket was used in the design of the inner-blanket thimble, and a standard inner-blanket lower adapter was used.

Flow conditions associated with designing a storage thimble for reactor Row 7 were investigated, and the following values of heat generation for Row 7 were calculated as a basis to establish the design:

	Material	Total Weight (g)	Avg Heat Generation (W/g)	Total Heat Generation (W)
Core Section	Stainless steel	6,900	1.386	9,570
Core Section	Antimony oxide	425	1.500	637
Section above Core	Stainless steel	13,470	0.205	2,760
Section below Core	Stainless steel	12,220	0.231	2,820

These values lead to a ΔT of 36°F with a flow of 11.5 gpm through the assembly of the source and the thimble when an inner-blanket lower adapter

is used with the existing design of the storage thimble for the outer blanket. To prevent the discharge of relatively cool sodium from the assembly into the upper plenum, a ΔT of approximately 120°F is desired. To obtain this ΔT , the flow must be reduced from 11.5 to 3.5 gpm. An orifice assembly was designed for the lower hex of the thimble to reduce the flow to 3.5 gpm.

Detailed fabrication drawings of the new inner-blanket storage thimble were prepared. Flowtests will be conducted before inserting the assembly into the reactor.

f. New Subassemblies Design and Experimental Support
(E. Hutter)

(i) Irradiation Subassemblies (O. S. Seim and W. R. Ware)

Last Reported: ANL-7527, pp. 50-52 (Dec 1968).

(a) Reflector-material Test Subassembly. A subassembly was designed to evaluate the performance of bare and chrome-plated nickel as reflector materials in sodium-cooled fast reactors. Basically, the subassembly is a device that will support up to 30 samples of thin tubular material on a solid cylindrical spindle for irradiation in the blanket region of the EBR-II reactor.

Because the test subassembly will contain only reflector materials and no fuel, the cooling requirement is small. The predicted coolant velocity is 0.7 ft/sec at the innermost positions of the reactor (in Row 7). This velocity is duplicated in the subassembly. Since loss of metal by solution erosion increases with coolant velocity, the Row-7 location provides the most unfavorable condition in the reactor for the nickel and its plating.

The subassemblies for the EBR-II inner-blanket region require a pressure drop of 41 psig. This pressure drop was achieved by orificing in the design of the test subassembly. Three orifice plates, each containing two 0.086-in.-dia parallel holes, are positioned in series within the subassembly to provide a flowrate of 1.2 gpm. Hole sizes were determined by calculation and experimental flowtesting. Silicon carbide temperature sensors are mounted on the spindle at the top of the core and at the outlet for the subassembly coolant. These sensors are expected to confirm irradiation temperatures and may also be useful in checking heat generation.

Two reflector-material test subassemblies are being readied for insertion into the reactor.

(b) Mark-B61A Irradiation Subassembly. Detailed drawings of the Mark-B61A irradiation subassembly have been completed,

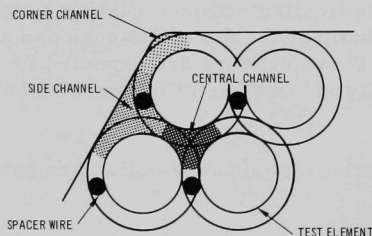
checked, and distributed. The final design will accommodate the expected 1.5% swelling of the walls of the stainless steel tubes in the core region. It will also allow disassembly and reassembly for interim inspections with a minimum of interference.

The internal distribution of flow through the subassembly before and after swelling has been calculated. The calculations were based on the flow areas and the equivalent dimensions for both conditions (before and after irradiation and swelling).

In the calculations for condition I (before swelling), the dimensions of the final design of the subassembly were used. The fuel elements are 0.230 in. in diameter and are wrapped with spacer wires having a diameter of 0.040 in. The elements were assumed to be clustered as tightly as theoretically possible in the center of their enclosing hexagonal tube, which measures 2.210 in. across its internal flats. Under these conditions, the clearance between the spacer wires around the elements in the outer row and the inner walls of the hexagonal tube would be 0.0147 in.

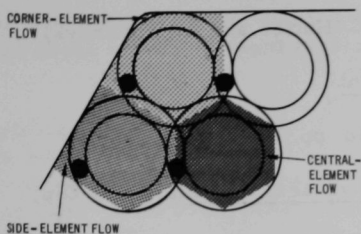
In the calculations for condition II, a 1% growth of the elements and spacer wires was assumed. It was also assumed that the fuel elements had been removed from their original hexagonal tube (for interim examination, for example) and had been inserted into a new tube having the same dimension across the flats as the original tube before irradiation. The elements were assumed to be clustered together as tightly as theoretically possible in the center of the tube. The diameter of the fuel elements would be 0.2323 in., and the diameter of the spacer wires would be 0.0404 in. The clearance between the spacer wires around the elements in the outer row and the inner walls of the hexagonal tube would be 0.0038 in. (A smaller clearance would make it difficult to insert the elements into the hexagonal tube.)

The calculated velocity distribution for both conditions are shown in Fig. I.E.7, and the calculated flow distributions are shown in Fig. I.E.8. In both figures, the values are reported as percentages of average velocity (or flow) through the subassembly.



Condition No.	Percent of Average Flow through Subassembly at Channel Location		
	Central	Side	Corner
I (before swelling)	94.1	110.3	96.4
II (after swelling)	96.9	106.8	87.3

Fig. I.E.7. Channel Velocities in Mark-B61A Subassembly



Condition No.	Percent of Average Flow through Subassembly at Element Location		
	Central	Side	Corner
I (before swelling)	72.2	137.5	159.3
II (after swelling)	78.3	130.2	142.8

Fig. I.E.8. Element Flows in Mark-B61A Subassembly

The flow distribution under condition I is somewhat less desirable than that under condition II. However, the difference between the flow in the central element under condition II is only 8% higher than that under condition I. This 8% difference is small in comparison to the 82% difference between the flows in the central and corner elements under condition II. The advantages of designing for an initial clearance that allows ample room for swelling appear to outweigh the disadvantages of an initial flow distribution that is slightly less desirable than that calculated for condition II.

Hydraulic pressure-drop tests will be made of a model of the subassembly in a water test loop.

(c) Mark-E61 Irradiation Subassembly. Design of the Mark-E61 subassembly is complete (see Fig. I.E.9). Flowtests of a mockup of the subassembly will be made in the water test loop after the design has been approved.

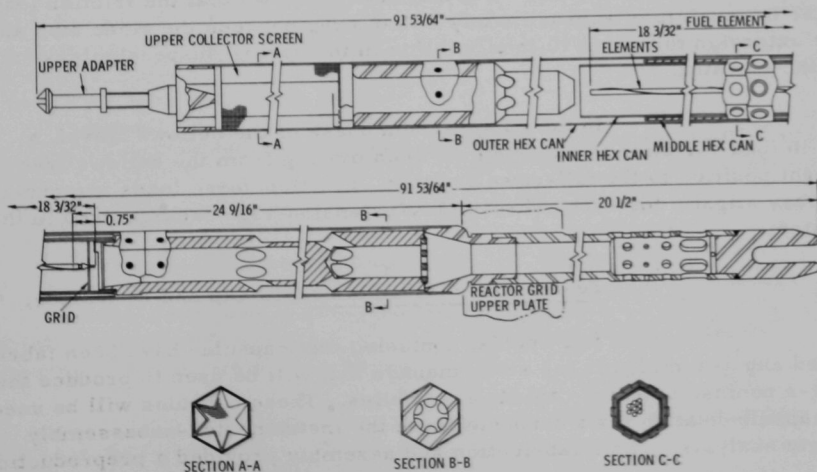


Fig. I.E.9. Mark-E61 Irradiation Subassembly

g. Instrumented Subassembly (E. Hutter and A. Smaardyk)

(i) Research and Development

Last Reported: ANL-7548, pp. 47-48 (Jan 1969).

(a) Drive System--Bellows-seal Assembly (R. Olp)

Operational tests were performed with the drive system of the instrumented subassembly to establish the amount of variable force loading contributed by the bellows-seal assembly as part of the operating load of the subassembly-extension tube (see Reactor Development Program Progress Report for October 1968, ANL-7513, p. 65). The amount of variation in the subassembly-extension-tube load experienced by the force transducer and other load-monitoring devices within the elevator support system is important when establishing the proper range of settings for the high- and low-limit switches of the drive system. The total operating load of the drive system, as measured by the load transducer in the system, varies from 279 lb at the full-down position to 348 lb at the full-up position ($94\frac{1}{2}$ in. of travel). This load variation is caused by the spring effect of the bellows assembly and by friction within the guide tube and support system.

The spring effect of the bellows when extended 72 in. above free height is 38 lb, which gives a bellows spring coefficient of 0.53 lb/in. for the bellows assembly in tension. Load-transducer readings from other assembly tests indicated a 55-lb total load variation at this elevation. A net friction load of 17 lb is indicated after accounting for the 38 lb of bellows spring load. Further testing shows that the friction load of 17 lb consists of approximately 7 lb of drag between the guide tube and the extension tube, and 10 lb of friction in the spring-suspension system of the elevator.

In the compression phase of the bellows travel, a 14-lb load variation is experienced when moving from the bellows free-height position to the full-down position. Friction-force loads are expected to vary slightly for each subassembly/extension-tube package used in the system.

(b) Test-capsule Assemblies (R. Olp and D. Walker)

Two special nonfueled test capsules have been fabricated and assembled in the same manner that will be used to produce the test-2 noninstrumented capsule assemblies. These capsules will be used in capsule-heating tests connected with the instrumented-subassembly safety analysis. Their fabrication and assembly provided a reproduction

check of the fabrication and assembly operations and equipment that will be used in the actual production of the fueled capsule assemblies for test-2.

The special capsules contain element tubes filled with depleted- UO_2 ceramic pellets of similar densities and dimensions; enriched- UO_2 fuel pellets will be used in the capsules for the actual test-2 subassembly. All other parts of the capsules and elements are identical to the test-2 capsules. Quality-assurance and quality-control programs have been developed for these capsules. These programs will be followed in the production of the capsule assemblies for test 2.

(c) Assembly of Test-1 Subassembly (C. Divona)

Assembly of the test-1 instrumented subassembly has progressed to the point at which the flexible leads are connected to the sheathed leads in the drywell area. The following operations have been successfully completed and tested:

- (1) assembly of the test-1 subassembly, including electrical testing and tensile testing to 2000 lb;
- (2) assembly of the bulkhead and the 27-ft drywell liner;
- (3) induction brazing of the 22 leads and tubes into the bulkhead as a single operation, in a hydrogen atmosphere; a leaktest with a helium mass spectrometer indicated leakrates no greater than 1×10^{-10} standard cc of helium per sec;
- (4) induction brazing of the four pressure-transducer junctions and one flux-monitor coupling in the drywell annulus. Because flux is thought to enhance corrosion, this operation was performed in a hydrogen atmosphere without the use of flux. Helium leaktests were used to verify the integrity of the joints.

h. Experimental Irradiation and Testing (H. Lawroski)

Last Reported: ANL-7548, p. 50 (Jan 1969).

(i) Experimental Irradiations (R. Neidner)

The exposure status of the experimental subassemblies in EBR-II remained the same as reported in the Progress Report for December 1968 (ANL-7527, pp. 59-60).

Listed below are new experimental subassemblies that have been approved for irradiation at the start of Run 33. These subassemblies have been assembled and pretested, and are available for loading.

Subassembly No.	Assigned Position	Capsule Content and Number of Capsules ()	Experimenter	Approved Subassembly Goal Exposure (fuels--a/o) (nonfuels--nvt x 10 ⁻²²)
X021B	2D1	FFTF Structural Materials (7)	PNL	3 (E > 0.1 MeV)
X043	4D2	UO ₂ -25 w/o PuO ₂ (37)	GE	3
X050*	4C2	UO ₂ -20 w/o PuO ₂ (4)	GE	3.3
		UO ₂ -28 w/o PuO ₂ (4)	GE	
		UO ₂ -20 w/o PuO ₂ (5)	ORNL	
		0.2 w/o Cr (U _{0.85} Pu _{0.2})C (2)	W	
		Structural Materials (5)	GE	
X055	6A4	(U _{0.85} Pu _{0.15})C (19)	UNC	4.4
X057	2B1	FFTF Structural Materials (7)	PNL	6 (E > 0.1 MeV)

(ii) Neutron-streaming Study. A study has been underway to compare neutron streaming from a Mark-A experimental subassembly with that from a standard EBR-II driver subassembly. The study compared the induced activity of webs from the castings of upper fixtures of driver and experimental subassemblies exposed in similar core locations. Subassemblies chosen for this study were C2166 and X039. Cobalt analyses were performed of each casting, and the activity from the ⁶⁰Co was measured.

Results of the study indicated that neutron streaming from both subassemblies was about the same. The Mark-A subassembly is a design in which neutron streaming was thought to have been a potential problem. However, for this typical case, there appeared to be no appreciable added neutron leakage to the upper plenum.

i. Feasibility Study of Fuel Failure Detection--Chemical and Mechanical Methods

(i) Trace Elements Analytical Techniques (C. E. Crouthamel)

Last Reported: ANL-7548, p. 53 (Jan 1969).

Before appropriate tags for identification of subassemblies containing failed fuel elements in EBR-II can be chosen, the identity and concentration of the impurities already present in the sodium coolant must be known. As a part of this evaluation, the trace elements in EBR-II primary-sodium samples were separated by precipitation on ferric hydroxide and subjected to neutron-activation analyses (see Progress Report for September 1968, ANL-7500, p. 71). The resulting gamma spectra were sufficiently complex to warrant computer analysis of the data. A Lawrence Radiation Laboratory computer program** was modified for the IBM-360 system, and the data library was expanded. Computer analysis of the neutron-activation spectra of the primary-coolant samples has been completed, and calculations of impurity levels in EBR-II primary sodium are

*Reconstituted partly from experimental Subassembly XG05.

**UCID-15140 (May 1967).

in progress. Upon completion of these calculations, further evaluations of the most promising tags will be made.

(ii) Sodium Loop--Tag Confirmation Study (N. R. Chellew and J. T. Holmes)

Last Reported: ANL-7548, p. 53 (Jan 1969).

Construction of a loop to be used in evaluating the stability of isotopic tags in circulating sodium is continuing. Wiring of instruments for control of the loop operation has been started. An ANL topical report is being prepared to document the construction, specifications, and capabilities of the loop.

j. Materials-Coolant Compatibility (D. W. Cissel)

Last Reported: ANL-7548, p. 54 (Jan 1969).

(i) Materials Evaluation

(a) Creep Rupture in Liquid Sodium. A modification of an existing sodium-test system is being used to evaluate the effects of mild carburization at 550°C on lifetime and elongation of stainless steel. Two creep-rupture tests in a 550°C clean-sodium environment have been completed as controls for the series to follow. Type 304 stainless steel wires, 0.010 in. in diameter, were loaded to a stress of 3.5×10^4 psi while in 550°C sodium containing ~3 ppm of oxygen. The data obtained from time to failure and percentage elongation are:

<u>Trial</u>	<u>Time to Failure (hr)</u>	<u>Elongation (%)</u>
1	124-140	Not available
2	151-166	6.7

(b) Compatibility of Sodium with Nitrided Stainless Steel.

Several sections of Type 304 stainless steel tubing whose surfaces had been inadvertently nitrided during annealing at 1050°C were exposed to 550°C sodium containing 3 ppm of oxygen for one week to determine the effect of sodium on the microstructure and on the chemistry involved. Samples of as-received tubing also were subjected to the same exposure. Metallographic inspection after annealing, but prior to sodium exposure, revealed grain-boundary precipitates having a platelet morphology. After exposure to sodium, the precipitates were unchanged but were slightly disguised because of the formation of carbides during sensitization. No preferential grain-boundary attack was observed in the as-polished condition. All samples lost a small amount of weight during the exposure to the sodium. The average weight losses were:

<u>Material</u>	<u>Initial Weight (g)</u>	<u>Final Weight (g)</u>	<u>Change in Weight (mg/cm²)</u>
As-received Tube	4.69359	4.69332	-0.011
Annealed Tube	5.73754	5.73701	-0.018

In this short-term exposure, sodium had no apparent significant effect on the nitrided stainless steel. Investigation is continuing.

(c) Nickel-reflector Experiment. A search of the literature about corrosion failed to answer satisfactorily the question of whether unclad nickel or chromium-plated nickel can be used safely as reflector elements in the EBR-II primary sodium. The basic difficulty is that mass-transport phenomena are poorly understood in a quantitative sense; no test has closely approximated the exposure conditions in the reactor.

An experimental subassembly has been prepared in which the hydraulic conditions are very close to those proposed for the actual reflector subassembly. Test specimens to be used in the subassembly are thin-walled nickel cylinders, some of which are chromium plated. They have been stacked on a solid nickel bar to provide the gamma heating equivalent to the actual reflector design. Weight losses for the individual rings will be determined after exposure to EBR-II primary sodium in the reactor. Metallography will be used as an additional check for the chromium plating. The subassembly will be ready for loading into EBR-II early in March 1969.

k. Study of Operation with Failed Fuel (R. R. Smith)

Last Reported: ANL-7518, pp. 57-59 (Nov 1968).

(i) Thermal Safety Analyses for a Mark-IA Irradiation-to-failure Experiment (J. F. Koenig)

The proposal has been made to irradiate a Mark-IA driver fuel pin to cladding failure in EBR-II. To accomplish this, a high-burnup fuel pin would be located in an assembly surrounded by virgin fuel. The assembly, assumed to be in a 4N2 position, would be irradiated to fuel failure or to 1.2% burnup of the virgin fuel if failure does not occur. The 1.2%-burnup fuel would be replaced with virgin fuel, and the process would be continued until failure of the high-burnup pin occurs.

Three possible modes of cladding failure have been considered: failure due to fuel swelling, to fission-gas pressure, and to bond-sodium pressure.

Fuel swelling can cause cladding strains sufficient to initiate failure. Previous experience indicates that maximum fuel swelling occurs in the upper half of the rod. If a crack in the cladding were to occur, the fuel exposed to the sodium coolant would be at the temperatures given in Table I.E.7. The fuel temperature would probably be between that for 17% expansion (initial contact with the cladding) and that for 30% expansion (initiation of gas release and reduction in swelling rate). Cladding failure is expected to occur before the strain reaches 4.3%, corresponding to 30% fuel expansion. Because the fuel would have displaced the bond sodium and would be in contact with the cladding, the radial-heat-transport mechanism would not be disrupted when failure occurs. The fuel temperatures, therefore, would be below the sodium saturation temperature and no boiling would occur.

TABLE I.E.7. Temperatures of Fuel in High-swelling Mark-IA Pin in Position 4N2

	Fuel Temperatures (°F)		
	Centerline	Average	Fuel
<u>At Axial Flux Peak</u>			
0% expansion (for reference)	1009	957	904
17% expansion	1059	974	888
30% expansion	1115	1000	884
<u>At Top of Fuel Pin</u>			
0% expansion (for reference)	1069	1033	997
17% expansion	1096	1041	986
30% expansion	1132	1058	983

Accumulation of fission gas in the plenum could cause cladding failure if the bursting pressure is reached. The plenum pressures with 100% release of fission gas and at various burnups are given in Table I.E.8.

TABLE I.E.8. Plenum Pressure in Mark-IA Element as a Function of Burnup^a

Burnup (%)	Pressure (psia)	Burnup (%)	Pressure (psia)
1	620	4	2360
2	1190	5	2940
3	1785		

^aAt 1000°F and with 100% release of fission gas.

Theory of the bursting of pressure vessels indicates that a minimum internal pressure of approximately 6500 psi would be required to cause failure of unirradiated cladding made of Type 304 stainless steel. Plenum pressure can build up when sodium is displaced from the fuel region to the gas plenum. Because the total volume of the sodium bond is greater than the volume of the plenum, the plenum pressure could possibly increase to the bursting pressure. A gas-type failure would probably occur near the top of the pin because of the lower tensile strength of the higher-temperature cladding. The gas leak could cause reduced flow on one side of the pin because of the increased pressure drop accompanying two-phase flow. Calculations indicate that at the top of the fuel pin, an arc encompassing 160° of the surface of a fuel pin containing 17%-expansion fuel could be insulated before the fuel adjacent to the cladding reaches 1340°F , the eutectic temperature. At 30% fuel expansion, the angle decreases to 130° . At the axial flux peak, 140° of the surface could be insulated for 17%-expansion fuel. At 30% fuel expansion, 110° of the surface could be insulated. Since these arcs are a large fraction of the total surface, it is not considered credible that a flow decrease on one side of a fuel pin could raise the fuel temperature to the eutectic point.

Cladding failure could occur from pressure buildup of trapped sodium in the lower half of the fuel pin. Fuel expansion in the upper half of the pin could form a seal between the fuel and cladding, thus preventing the sodium from expanding to the gas plenum. Further fuel expansion in the lower portion of the pin would build up a large hydrostatic pressure, resulting in cladding failure. This failure, which would occur in the lower half of the fuel pin, could result in loss of sodium bond between fuel and cladding above the rupture. Since the radial-heat-transfer mechanism would be lost, the fuel would melt, slump, and recast in contact with the cladding. The renewed heat transfer would limit the time above the eutectic temperature and the damage to the cladding. Should part of the molten fuel enter the coolant, the temperature of the molten fuel (1830°F) would be slightly higher than the saturation temperature of the sodium coolant (-50°F), and boiling may occur. The associated flow reduction on one side of the fuel pin would not result in heating of the fuel to the fuel-cladding eutectic temperature as shown previously.

Damage to adjacent pins could occur when the stored gas energy is released from the gas plenum. The gas volume, however, would be relatively small so that substantial velocities of high-pressure gas could not occur for any length of time. If the adjacent pin deflected 0.049 in. and contacted another pin, the maximum stress in the cladding would be less than the ultimate strength of the cladding; the cladding would not fail.

Failure of the fuel rod caused by the three mechanisms (or other mechanisms) could cause damage to adjacent pins due to

reduction of flow in coolant channels by release of gas or by ejection of molten fuel. Damage to adjacent fuel pins could occur from flow blockage due to accumulation of fuel in a coolant channel or on the surface of a fuel pin. Consequences of these events have been analyzed previously. The probability of damage to adjacent fuel pins is considered to be remote.

1. Driver Fuel Transient Performance Studies--TREAT Experiments (A. B. Rothman)

Last Reported: ANL-7548, p. 55 (Jan 1969).

(i) Mark IA Fuel TREAT Experiments. Leaks in both test capsules containing preirradiated, high-swelling Mark-IA driver-fuel elements were repaired at Test Area North (TAN) and shipped to the TREAT facility, where they passed instrumentation and leaktests on February 18. The first series of tests in TREAT will be performed on the pin with 1.2 a/o burnup. Presumably, the TREAT transients with both that pin and the pin with 2.5 a/o burnup will be completed by the first week in March.

The feasibility of making in-pile measurements of the motion of preirradiated fuel by the eddy-current method has been demonstrated by preliminary analysis of the motion of unirradiated fuel during TREAT tests. A summary of the results of this analysis has been prepared for the June 1969 meeting of the American Nuclear Society.

m. Systems Engineering (B. C. Cerutti)

Last Reported: ANL-7527, pp. 66-69 (Dec 1968).

All modification and maintenance work scheduled for the current shutdown of EBR-II was completed by February 15. The most important of this work is summarized below.

(i) Surveillance, Evaluation, and Studies of Systems

(a) Holddown Mechanisms for Reactor-vessel Cover
(H. W. Sine)

The motor operators for each of the three holddown mechanisms for the reactor-vessel cover were removed from their tie rods and disassembled to the point where all oil seals could be replaced. All components exposed by this disassembly were visually inspected and found to be in good condition, except the retaining bolt that holds the yoke nut in the spring support and bearing housing. In each mechanism this bolt was bent and had to be replaced. An investigation disclosed that this damage could not have occurred during normal operation of the mechanism, but only while removing and replacing the motor operator on its tie rod.

To prevent the recurrence of this damage, a special guide pin was made to align the thread of the yoke nut with the mating thread of the tie rod so that these parts could be engaged or disengaged easily. The applicable procedure has been revised to specify the use of this guide pin and to require that a dynamometer be used with a hand-operated chain fall to support the motor operator. This will ensure that excessive loads are not imposed on a tie rod while removing and replacing the motor operators.

(ii) Reactor and Primary System Improvements

(a) Revisions to Fuel Unloading Machine (FUM). The improved gripper-position indicator was installed. The modifications of the lower part of the FUM are complete and the port is ready for service.

(b) Reactor Systems Instrumentation. The auxiliary gripper plug was removed to allow installation of the new pressure-temperature sensor plug. (The radiation level at the lower end of the gripper plug was approximately 100 R/hr at 4 in.) The pressure-temperature sensor unit was then installed in the primary tank and will undergo an operational check during reactor run 33.

(iii) Secondary and Power System Improvements

(a) Removable Riser of Evaporator 702. Several years ago, a leak developed in evaporator 702. In searching for the source of the leak, the riser of the evaporator had to be cut loose and removed to gain access to the interior of the evaporator. The source of the leak--a defective weld joining a tube to the tubesheet--was quickly located. The weld was repaired immediately, the riser was welded back into place, and the plant was restored to service. Before the riser was replaced, however, the inside surfaces of the evaporator tubes were inspected.

Consideration was then given to the desirability of inspecting periodically at least this one evaporator to ascertain any change in internal conditions and to monitor the adequacy of feedwater treatment. It soon became apparent that complete removal of the riser was needed to meet the requirements of the inspection. A study was initiated to determine the best approach for periodic removal of the riser. Five approaches were considered:

(1) cutting the riser loose and rewelding it in place for every inspection;

(2) using a scale-free coupling--a device that provides for easier and faster removal and rewelding;

- (3) using conventional bolted flanges with a gasket;
- (4) using Conoseal couplings;
- (5) using Grayloc couplings.

Grayloc couplings were selected on the basis of reports of satisfactory and dependable experience by other users, reasonable first cost, and relative ease of disassembly and reassembly. During the January 1969 reactor shutdown, the riser from evaporator 702 was cut loose, and fitted for Grayloc couplings at the upper and lower ends. Coupling hubs were welded to the evaporator stub, the steam drum stub, and to both ends of the riser.

With the lower coupling securely in place, the cold-spring adjustment was checked at the upper joint; some correction was necessary to achieve satisfactory adjustment. The riser was then securely fastened, and the assembly was proved satisfactory by hydrostatic testing. In final steps to ready the evaporator for service, the pipe was insulated and changes were made in the pipe hangers to accommodate the added weight of the couplings.

Inspection of the header, walls, and tubesheets of the evaporator indicated that the conditions in the steam system were good. No significant corrosion was observed.

(b) Water-level Control for Steam Drum (K. J. Moriarty)

The existing servo-operated control system was replaced with a static system, and the installation was checked out.

(c) Drain Valves in Feedwater Line Downstream of Check Valve (M. B. Trillhaase)

Provision for draining the section of feedwater line downstream of the check valve was made by installing drain valves and a piping system to carry the drained feedwater outside the building.

(d) Venting and Draining of Superheater Steam-trap System (M. B. Trillhaase)

As originally built, the piping arrangement in the sodium boiler plant did not permit draining the steam-trap piping and lower ends of the superheaters for dry lay-up of the steam generator, a desirable practice to prevent corrosion. During the shutdown, a 3/4-in. drain manifold with 3/4-in. drain valve was installed for draining the

system, and a 1-in. check valve and 1-in. vent valve were installed in the condensate-collection piping.

(e) Steam Header Relief Valve. Installation of the Pressurmatic valve and its associated controls were satisfactorily completed.

(f) Relocation of the Pressure-controller Line for the No. 3 Feedwater Heater (M. B. Trillhaase)

The pressure connection for this line was relocated downstream of the check valve in the 200-psi makeup line to give a truer indication of actual plant conditions. Operation of the controller was not altered.

(g) Cooling Tower for EBR-II Plant Auxiliary System. This tower was completed and is ready for service.

(iv) Instrumentation Improvements (K. J. Moriarty)

(a) Console Changes. The changes scheduled for the control console were made and checked out.

(b) Constant-power Supply. The constant-power supply for the nuclear and process instrumentation was moved from the cable-routing room to the ground floor of the power plant. Because of this transfer, both the audible and electrical noise levels will be reduced in the cable-routing room.

(c) Circuit for Lowering Safety Rods. The circuit to permit lowering of the safety rods without causing unnecessary scrambling was installed.

(d) Temperature Compensation of Flowmeter for Reactor Outlet Flow. The reactor outlet flow (total flow of coolant from the reactor) includes the higher-temperature sodium from the core; therefore, the flowmeter measuring this total flow must be temperature compensated. Compensation will be programmed to the output signal of the flowmeter in steps of 0.8% flow for each 30°F of temperature difference. The installation and checkout have been completed for this change.

(e) Redundant Linear Channel. The installation work necessary for adding a second linear channel (channel 7A) to the operating instrumentation of the reactor was completed. This second channel will provide the redundancy necessary for continued reactor operation in the event of the loss of one linear channel.

n. Oxide Driver (G. E. Golden)

Last Reported: ANL-7548, pp. 57-58 (Jan 1969).

The following preliminary design parameters for the oxide core have been proposed:

Peak fuel temperature	$\leq 4800^{\circ}\text{F}$
Peak fuel linear power	$\leq 17 \text{ kW/ft}$
Peak sodium velocity	$\leq 30 \text{ ft/sec}$
Peak cladding temperature	$\leq 1200^{\circ}\text{F}$
Primary-loop ΔP	$\leq 60 \text{ psi}$
Primary-sodium flowrate	$\leq 9000 \text{ gpm}$
Hot-channel factor	1.20
Hot-spot factors	
convection	1.20
cladding	1.20
bond	1.20
fuel	1.20

Investigations are underway to refine these parameters. Closer estimates are required for the next phase of analysis of the oxide core, which is aimed at determining the relationship between peak fuel temperature and peak linear power. The core size is dependent on this relationship.

2. Operations

a. Reactor Plant (G. E. Deegan and J. R. Davis)

Last Reported: ANL-7548, pp. 58-62 (Jan 1969).

Maintenance and modifications progressed on schedule. After the modifications of the steam system had been completed, required hydrostatic tests were successfully carried out. All systems then were brought to 350°F , and the secondary system was filled with sodium. The plant has been heated to standby conditions, with the primary tank at 700°F . Pre-operational tests and calibrations are being made, and fuel handling for Run 33A has been started.

b. Fuel Cycle Facility (M. J. Feldman)

Last Reported: ANL-7548, pp. 62-77 (Jan 1969).

(i) Fuel Production

(a) Hot Line (N. R. Grant)

Table I.E.9 summarizes production activities for January 16 through February 15, 1969, and for the year to date.

TABLE I.E.9. Production Summary for FCF Hot Line
(Decanning and melt-refining steps have been discontinued)

	1/16/69 through 2/14/69	Total This Year
Subassemblies received		
Core, control, and safety	0	2
Other	2	2
Subassemblies dismantled for surveillance or examination	17	28
Subassemblies transferred		
To reactor	0	0
To L&O vault and interbuilding corridor for storage	0	0
Subassemblies transferred to ICPP for storage	1	1
Subassemblies returned from ICPP storage	2	2
Subassemblies fabricated	6	8
<u>Processing</u>		
Injection-casting runs	7	10
Elements processed		
Accepted	418	549
Rejected	116	164
Elements welded	495	535
Elements rewelded	0	0
Elements leaktested		
Accepted	499	499
Rejected	11	11
Elements bonded (including recycle)	658	841
Elements bondtested		
Accepted	712	841
Rejected	54	108
Elements to surveillance	227	774
Number from subassemblies	15	25
<u>Fuel-alloy and Waste Shipments</u>		
Cans to burial ground	2	6
Oxide and glass scrap to ICPP	0	2
Recoverable fuel alloy to ICPP		
Fuel elements	6 (104 kg of alloy)	6
Nonspecification material	3 (53 kg of alloy)	3

Phasing-out operations in the hot line are complete through the injection-casting step. The remainder of the fuel pins and elements in the argon cell are being processed for use in subassemblies.

(b) Cold-line Production and Assembly (D. L. Mitchell)

Table I.E.10 summarizes production activities for January 16 through February 15, 1969, and for the year.

TABLE I.E.10. Production Summary for FCF Cold Line

	1/16/69 through 2/14/69	Total This Year
Alloy-preparation runs		
New fuel	1	1
Remelts	1	1
Total	2	2
Injection-casting runs	3	8
Pins processed		
Accepted	269	758
Rejected	3	22
Elements welded	533	1042
Elements rewelded	0	0
Elements leaktested		
Accepted	840	840
Rejected	1	1
Elements bondtested		
Accepted	721	802
Rejected	103	118
Elements available for subassembly fabrication	548	1034
Subassemblies fabricated (cold-line fuel)	0	0
Elements received from vendor	4212	9763 ^a
Inspected and accepted	3795	8290 ^a
Inspected and rejected	63	760 ^a
Elements available for subassembly fabrication (vendor fuel)	2736 ^b	6791 ^c
Subassemblies fabricated (vendor fuel)	0	0

^aTotal to date.

^bMade available between 1/16/69 and 2/14/69.

^cTotal available as of 2/14/69.

One depleted-uranium-fissium casting batch of Mark-II fuel pins was made to verify the casting parameters. Ninety-eight pins of acceptable length were obtained from 102 castings made from the batch. These pins are being X rayed for internal voids or pipes to determine if any of them can be used as standards for the eddy-current inspection step of the pin-processing operation.

Processing equipment is being modified as required for converting from production of Mark-IA to Mark-II fuel pins and elements. Enough Mark-II elements for five subassemblies will be fabricated in the cold line.

(ii) Inspection of Vendor Fuel (D. L. Mitchell)

The acceptance rate for the ANL inspection of fuel produced by the vendor, Aerojet-General Corporation (AGC), has continued to be greater than 95%.

A test was made to compare the results of AGC and ANL inspections for bonds and sodium levels. Twenty fuel pins made by ANL were jacketed by AGC, and these pins plus twenty unbonded elements provided by ANL were centrifugally bonded by AGC. AGC inspected all of these 40 elements for bond and sodium level, and returned the elements and the eddy-current traces of the bond tests to ANL. ANL reinspected the elements with their eddy-current equipment. The results of this comparison are shown in Table I.E.11.

TABLE I.E.11. Comparison of Results of Inspection of the Same 40 Fuel Elements by AGC and ANL

Number of Elements	ANL Results	AGC Results
2	Accept	Reject--void and bubble
5	Accept	Reject--void
2	Accept	Borderline--void
4	Accept	Reject--bubble
2	Borderline	Reject--void and bubble
2	Reject--trap	Reject--void and bubble
2	Reject--trap	Reject--trap
1	Reject--bubble	Reject--void and bubble
20	Accept	Accept

These results indicate that AGC has established acceptance criteria that are at least as demanding as those used by ANL, with the possible exception of the interpretation of the criterion for trap defects.

These results do not reflect on the ability of AGC to bond elements properly; the purpose of the test was to compare evaluations of defects.

(iii) Surveillance (M. J. Feldman, J. P. Bacca, and
E. R. Ebersole)

(a) Chemical Analyses (E. R. Ebersole)

The number of fuel-product analyses of hot-line, cold-line, and vendor-fuel samples made during the reporting period, together with the average values and ranges, are tabulated in Table I.E.12.

TABLE I.E.12. Analyses of Fuel-product Samples

Analyzed for	Number of Analyses	Average Value	Range
Total U	14	94.45 w/o	94.13-95.10
²³⁵ U (% of total U)	14	52.13 w/o	52.02-52.26
Mo	14	2.50 w/o	2.39-2.60
Ru	14	1.88 w/o	1.78-2.06
Rh	14	0.277 w/o	0.242-0.307
Pd	14	0.192 w/o	0.163-0.212
Zr	30	0.069 w/o	0.029-0.110
Nb	14	0.011 w/o	0.007-0.013
Si	20	389 ppm	80-710
Al	14	95 ppm	59-162
Cr	15	56 ppm	30-145
Fe	19	280 ppm	73-666
Ni	14	151 ppm	70-193
C	11	246 ppm	98-434
Th	4	40 ppm	30-47
Total Analyses	225		

Analyses made for surveillance of irradiated pins from the reactor during the reporting period are tabulated below:

Analyzed for	Number of Analyses	Average Value	Range
Zr	20	0.113 w/o	0.074-0.177
Nb	20	0.010 w/o	0.007-0.014
Si	16	485 ppm	120-681
Al	2	192 ppm	157-227
Burnup	7	0.95 a/o	0.90-1.06
Total Analyses	65		

The Baird-Atomic densitometer reader for emission-spectrographic plates was delivered and checked out, and emulsion calibration was started.

(b) Postirradiation Analysis of EBR-II Fuel (J. P. Bacca)

(1) Surveillance of Mark-IB Fuel. Postirradiation examinations of the fuel elements from Mark-IB surveillance Subassembly C2136 were conducted. This subassembly, the fifth of the Mark-IB program, attained a calculated maximum burnup of 1.18 a/o during Run 32. The data for composition and irradiation swelling of the elements from the subassembly are summarized in Table I.E.13. These data show the beneficial effects of silicon in concentrations greater than 200 ppm in the fuel on reducing irradiation-induced swelling of the fuel.

TABLE I.E.13. Fabrication and Irradiation-performance Data for Mark-IB Surveillance Driver-fuel Subassembly C2136

Injection-casting Batch No.	Silicon Content of Fuel (ppm)	Number of Elements	Element Burnup Range ^a (a/o)	Total Volume Swelling of Fuel ($\Delta V/V$, %)	
				Average	Range
4243	320	10	1.09-1.16	5.8	4.9-8.7
4245	150	11	1.09-1.17	14.2	10.8-15.5
4246	290	9	1.10-1.17	5.5	4.2-9.5
4247	224	5	1.11-1.18	7.4	6.0-8.7
4248	340	13	1.09-1.12	4.9	4.3-5.3
4250	230	14	1.10-1.18	5.0	4.1-5.4
0456	396	8	1.11-1.17	6.2	5.4-6.8
0457	230	21	1.09-1.18	7.4	6.0-8.9

^aMax burnup, 1.18 a/o; avg burnup, 1.02 a/o.

The data obtained from all of the Mark-IB fuel indicate that these elements show a slightly larger volume increase than the average for all Mark-IA elements at comparable burnups and silicon concentrations. Figure I.E.10 shows swelling-versus-burnup curves obtained by averaging the surveillance results for more than 6000-Mark IA driver-fuel elements produced in the hot line.

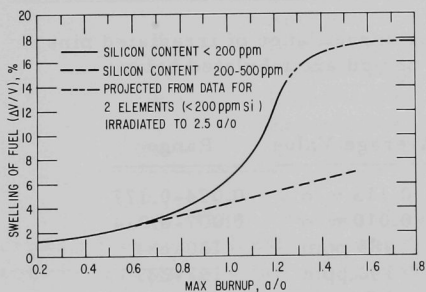


Fig. I.E.10. Effect of Silicon Content in Mark-IA Fuel Alloy on Fuel Swelling at Various Burnups (derived from analysis of hot-line fuel)

1.25 a/o during Run 32. The data for fuel composition and irradiation swelling of the elements of C2120 are presented in Table I.E.14. The obvious effectiveness of trace-element silicon in the U-5 w/o Fs alloy in the

(2) Surveillance of Cold-line Fuel. Postirradiation examinations were completed of elements from Mark-IA cold-line Subassembly C2120. This subassembly, the fifth and final subassembly of the first phase of this surveillance program, attained a calculated maximum burnup of

enhancement of irradiation-swelling resistance can be noted. These data points exhibit excellent fits on the curves of Fig. I.E.10.

TABLE I.E.14. Fabrication and Irradiation-performance Data for Mark-IA Cold-line Surveillance Driver-fuel Subassembly C2120

Injection-casting Batch No.	Silicon Content of Fuel (ppm)	Number of Elements	Element Burnup Range ^a (a/o)	Total Volume Swelling of Fuel ($\Delta V/V$, %)	
				Average	Range
003-I	320	53	1.16-1.25	5.1	4.3-5.9
005-IH	145	38	1.17-1.24	13.3	10.5-14.9

^aMax burnup, 1.25 a/o; avg burnup, 1.08 a/o.

(3) Encapsulated Mark-II Driver-fuel Experiment.

Gross axial gamma scans (⁹⁵Zr-⁹⁵Nb) were made for Mark-II Elements 201, 212, and 251, which had been irradiated to approximately 2 a/o burnup in

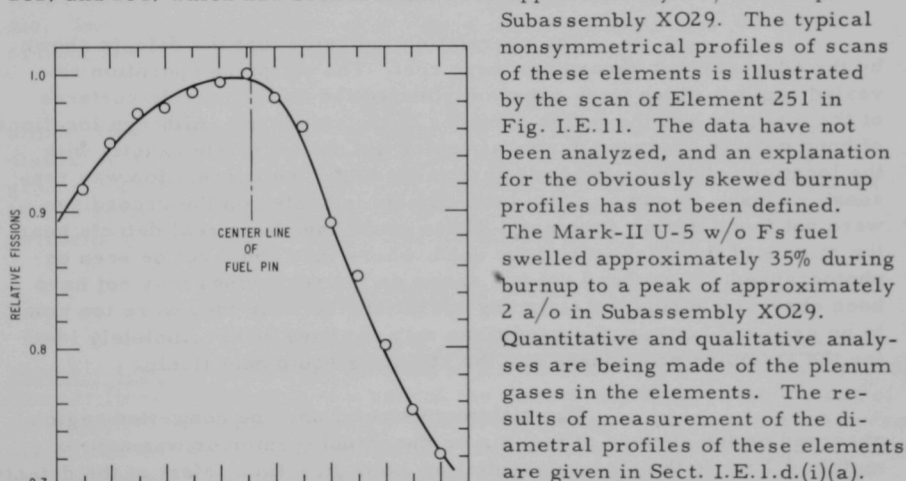


Fig. I.E.11. Results at Axial Gamma Scan (⁹⁵Zr-⁹⁵Nb) of Element 251 from Subassembly XO29

Subassembly XO29. The typical nonsymmetrical profiles of scans of these elements is illustrated by the scan of Element 251 in Fig. I.E.11. The data have not been analyzed, and an explanation for the obviously skewed burnup profiles has not been defined. The Mark-II U-5 w/o Fs fuel swelled approximately 35% during burnup to a peak of approximately 2 a/o in Subassembly XO29. Quantitative and qualitative analyses are being made of the plenum gases in the elements. The results of measurement of the diametral profiles of these elements are given in Sect. I.E.1.d.(i)(a).

(4) Sodium-bond Defects Observed in Irradiated EBR-II Driver-fuel Elements. Following irradiation in EBR-II, Mark-I

and Mark-IA driver-fuel elements nearly always show indications of defects in the sodium bond when subjected to pulsed eddy-current bond testing in the Fuel Cycle Facility. These indications of defects are observed when the irradiated elements are tested at the nominal in-cell temperature of approximately 35°C. They are still observed, however, when the elements are bond tested at approximately 135°C, a temperature at which the bond

sodium in the element is molten. Even irradiated elements that have been subjected to a postirradiation impact-bonding operation (500 impacts delivered to the element at 450°C) show these persistent bond-defect indications during eddy-current bond testing at both of the test temperatures.

An effort has been started to determine whether defect indications are showing real defects or are the result of other phenomena which cause regions of high electrical resistance to the flow of eddy currents during inspection of the element bonds.

Irradiated Mark-IA driver elements were transferred from Idaho to Illinois, where special equipment and procedures had been set up to strip the Type 304L stainless steel jackets from the U-5 w/o Fs fuel pins. The sodium bonds of the elements had previously been tested by eddy current in the FCF. The bonds of the elements were examined visually and photographically as the jackets were stripped from the pins. These observations were correlated with the recordings of the eddy-current bond tests made previously.

The correlation indicated that the defects shown by the eddy-current recordings were real. The stripping operation revealed regions which were apparently nonwetted on the outside surfaces of the fuel pins and the inside surfaces of the claddings. Although locations of bond defects observed during stripping did not correlate exactly with the locations shown on the bond-test recordings, the correlation was reasonably close. In some cases, bond defects indicated on the recordings were not found during stripping. These could have been real defects near the middle of the thickness of the bond, where they could not be seen or photographed. Some bond defects shown on the recordings may not have been observed during the stripping operations because they were too small to be seen and because the conditions may not have been completely ideal for the stripping procedures and the stripping equipment itself.

The maximum size of any one nonwetted region observed on the surface of fuel pin or the cladding interior was approximately 0.1 in. in the circumferential or axial direction. Most of the defects observed were much smaller than this. Clusters of very small voids were frequently observed; these appeared to be located most prevalently at the inside surfaces of the cladding. These clusters apparently were not indicated well on the bond-test recordings. Nonwetted regions on the surfaces of the fuel pins were observed to be black, typical of the cast U-5 w/o Fs pin surface. On the other hand, nonwetted regions on the cladding surfaces were bright and lustrous. No correlation of bond defects with the degree of fuel burnup was readily apparent from this investigation.

The following hypotheses are offered to explain the cause of the development of bond defects during irradiation:

(1) Sodium bonding is complete in the element as manufactured, but nonwetted regions develop as a result of irradiation or other parameters of reactor service, or both.

(2) Sodium bonding of small areas is not complete in the element as manufactured, but the bond-testing eddy-current system is not able to resolve nonwetted regions on the surfaces of the fuel pin or jacket because the bond annulus is completely filled with sodium. As a result of irradiation, various reactions (e.g., fission-gas release) at these nonwetted regions may occur, thereby increasing the physical size of the defects to the extent that they become resolved in the postirradiation bond test.

(3) Sodium bonding is complete in the element as manufactured, and wetting at the surface of the fuel pin is a sodium-uranium oxide interaction. Spalling of finite thicknesses of this oxide during irradiation--resulting from thermal shock and other causes--leads to the formation of isolated nonwetted regions on the surface of the fuel pin. These defects are then indicated in postirradiation bond tests and are not rewetted during the postirradiation rebonding treatment.

The eddy-current recordings of all of the almost 10,000 driver elements whose bonds were tested following irradiation as a part of the FCF fuel surveillance and product-analysis programs indicated bond defects similar to those shown by the elements used in this stripping investigation. In every case, these 10,000 elements performed satisfactorily in the EBR-II without known incidents.

(c) Failure Analysis (J. P. Bacca and R. V. Strain)

Examination of Suspect Element E57 from Subassembly L462. Further examination of Element E57 from Subassembly L462 has verified the presence of a hole in the element cladding at the top end of the spacer wire, approximately 0.9 in. from the top of the element. A hydrostatic flowtest was made to determine the flowrate of water through the hole, and additional macrophotographs of the hole were taken (one is shown as Fig. I.E.12).

The section of the element cladding containing the hole was flowtested with a constant head of water at 80°F. Listed in Table I.E.15 are data from the test and the values for hole size that were calculated using the formula for a standard thin-plate orifice: $Q = 0.65 A \sqrt{2gh}$, where Q is flowrate, A is the area of the hole, g is gravitational acceleration, and h is the height of the head. These calculated values for the area of the hole are in fair agreement with the approximations of the area that was calculated from measurements made from the macrophoto of the hole shown in Fig. I.E.12. The approximate size of the hole is shown in Fig. I.E.13. The irregular shape of the hole probably accounts for the

discrepancy between the areas calculated from the flowtest data and the area calculated from the measurements of the hole.

Metallographic examination of the area near the hole is in progress.

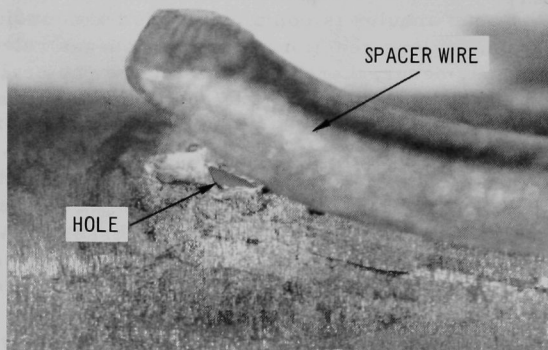


Fig. I.E.12. Macrophoto of the Hole in the Cladding of Element E57 from Subassembly L462 (16,55X)

TABLE I.E.15. Flowtest Data and Calculated Areas of Hole in Cladding of Element E57

Flowtest Data				Equivalent Dimensions of Hole with Area A		
Head h (in.)	Time (sec)	Volume (ml)	Flowrate Q (ml/sec)	Calculated Area A (in.)	If Circle, Dia (in.)	If Square, Side (in.)
35.38	47	11	0.234	0.000133	0.0130	0.0115
30.25 ^a	300	56	0.187	0.000115	0.0121	0.0107

^aA duplicate run gave results identical to those tabulated.

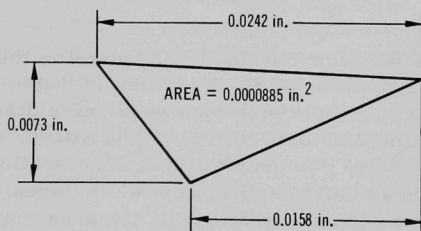


Fig. I.E.13

Geometrical Approximation of the Dimensions of the Hole in the Cladding of Element E57 from Subassembly L462

- (d) Materials Surveillance and Compatibility Studies
(J. P. Bacca, R. V. Strain, C. L. Meyers, and
S. T. Zegler)

(1) Postirradiation Examination of Safety-rod Thimble 3D1. Separate, full-length gamma scans were completed of each of the six flats cut from the safety-rod thimble that was removed from core position 3D1 in November 1968. In each scan, a rather broad activity peak was located between 31 and 35 in. from the top of the thimble. The six activity-peak maxima around the thimble sides differed by only 5 to 7%. This is to be expected because the neutron flux in this region of the core was reported to be nearly level.

The six individual flats were mechanically separated, and all except one that is assigned to ORNL were shipped to the laboratories that will participate in more-detailed examination of the thimble. Two flats will be examined by ANL, and one each by ORNL, PNL, and GE-NSP. The sixth flat will be reserved for additional tests or as a historical sample.

Chemical analysis of a sample of the thimble has confirmed that the thimble was fabricated from a Type 304L stainless steel which originated from vendor heat No. 890810. The following room-temperature mechanical properties were listed on the receiving-inspection report: ultimate test strength, 92,000 psi; yield strength (0.2%--offset), 37,500 psi; total elongation, 60%. Since this heat is the same as that from which the control-rod thimble examined last year was fabricated, a much more extensive evaluation of its mechanical and physical properties has already been made and reported by ANL.

Analyses of fluence by radiochemistry techniques is being performed at ANL on specimens from two flats, one from the ORNL flat, and one from the ANL reserve flat. Samples for fluence analyses from the other four flats will be made available soon by the other investigators, after they have taken their test specimens from the flats they have.

(2) Postirradiation Microstructures of 70%-enriched Driver Fuel (Simulation of EBR-II Higher-power Operation). Optical metallographic studies have been made of 70%-enriched and 52%-enriched fuel pins that were irradiated together in Subassemblies C2138, C2166, and C2165 to approximately 0.3, 0.5, and 0.8 a/o burnup, respectively. The microstructures of the two materials differ mainly with respect to the particle size of microconstituents. With 70% enrichment, particle size is generally larger, a factor related to the generally higher (approximately 100°F) temperatures of irradiation. No microstructural evidence of melting,

diffusion of the alloying elements of the Type 304 stainless steel jacket into the fuel, or of formation of fission-gas bubbles was apparent in any of the examined fuel pins and jackets. Irradiation-induced hardening is apparent in both materials, particularly in the 70%-enriched material at a burnup of 0.3 a/o. The hardness of both materials decreases as temperature and length of irradiation increase.

Optical metallographic studies are now in progress on a similar pair of 70%- and 52%-enriched pins that were irradiated in Subassembly C2174 to approximately 1.0 a/o burnup.

(3) Compatibility of U-5 w/o Fs Alloy with Types 304 and 316 Stainless Steels. Diffusion-couple compatibility tests were completed for a U-5 w/o Fs alloy (batch R-409) containing 75 ppm silicon and 196 ppm aluminum coupled with Types 304 and 316 stainless steel. The tests using Type 304 stainless steel were made at temperatures of 550, 600, and 650°C and for times of up to 10,000 hr. The tests using Type 316 stainless steel were made at the same temperatures and for times of up to 10,000 hr.

Similar tests were made for a modified U-5 w/o Fs alloy (batch R-410) containing 734 ppm silicon and 1406 ppm aluminum coupled with Type 316 stainless steel only. These tests were made at 650°C and for times of up to 10,000 hr.

Presented in Table I.E.16 are the penetration coefficients K which were determined for the several combinations. In all cases the diffusion obeys the rate law $P^2 = Kt$, where P is the penetration in cm, K is the penetration coefficient, and t is the annealing time in seconds.

TABLE I.E.16. Penetration Coefficients for Combinations of U-5 w/o Fs Alloy and Stainless Steel Alloys

Fuel Alloy	Jacket Alloy	Annealing Temp (°C)	Penetration Coefficient K (cm ² /sec) ^a	
			For Total Band Width	For Steel Penetration
U-5 w/o Fs Batch R-409 ^b	304 SS	550	4.55×10^{-12}	1.3×10^{-14}
		600	2.23×10^{-11}	7.8×10^{-14}
		650	2.87×10^{-10}	3.1×10^{-13}
U-5 w/o Fs Batch R-409 ^b	316 SS	550	3.85×10^{-12}	1.0×10^{-14}
		600	2.71×10^{-11}	7.5×10^{-14}
		650	3.45×10^{-10}	4.3×10^{-13}
U-5 w/o Fs Batch R-410 ^c	304 SS	650	4.0×10^{-10}	3.3×10^{-13}

^a $K = P^2/t$, where P is the penetration in cm, K is the penetration coefficient, and t is the annealing time in sec.

^bBatch R-409 contains 75 ppm silicon and 196 ppm aluminum.

^cBatch R-410 contains 734 ppm silicon and 1406 ppm aluminum.

(4) Compatibility of Fuel-element Jackets with Flowing Sodium. Metallographic examination of 10 sections of the jackets of Elements 26 and 10 from Subassembly C2165 (0.8 a/o burnup) revealed no cracks in the stainless steel after the samples had been ground to remove cracks produced by the tubing cutter used in taking the samples.

No effects of the primary sodium or the sodium-removal wash were found. The samples exhibited degrees of sensitization that varied according to their position along the length of the element. No sensitization was found at the lower end of the elements; sensitization increased to a maximum at the top of the fuel pin. The degree of sensitization at the inner and outer surfaces of the tubing was greater than that for the bulk of the tubing material. Previous examinations have shown this to be caused by high carbon concentrations in the surfaces of the as-received tubing rather than by carburization of the cladding by the primary sodium. The differences in the degree of sensitization from sample to sample are caused by the variation in temperature along the length of the element while it is in the reactor.

Tests were made to determine why the tubing cutter caused cracks in the tubing during sampling. The tubing cutter did not cause cracking when used to sample empty tubing. When the same tubing contained fuel or fuel and bonding sodium, however, the surface of the jacket adjacent to the cut contained small cracks. Apparently, the presence of the backing material changed the characteristics of the cutting action of the tubing cutter.

(iv) Experiment Handling and Interim Examination
(V. G. Eschen and N. R. Grant)

No irradiated experimental subassemblies were transferred to the FCF during this reporting period. Six irradiated capsules that had been removed from Subassembly XO21A were used together with one new capsule to fabricate Subassembly XO21B. This subassembly will receive additional irradiation in EBR-II.

PUBLICATIONS

Digital Data Recording Using High-Speed Framing Cameras

A. DeVolpi

High-Speed Photography, Proc. 8th Intern. Congr., Stockholm,
June 23-29, 1968. John Wiley and Sons, New York, 1968,
pp. 485-487

The Recording of Transient Nuclear Data at 10^9 Counts/Second

A. DeVolpi

Proc. Intern. Symp. on Nuclear Electronics, Versailles, France,
September 10-13, 1968, French Soc. for Electronics and
Radioelectronics and Intern. Union of Pure and Appl. Phys.,
pp. 112-1--112-11

An On-Line Method of Transfer Function Analysis in EBR-II

R. W. Hyndman and M. R. Tuck

Nucl. Appl. 6, 137-141 (February 1969)

Analysis of the Static Power Coefficient of EBR-II with Reduced Coolant Flow

J. K. Long

Nucl. Appl. 6, 116-125 (February 1969)

Separation Technique for Nonconducting Solids in Liquid Sodium

P. Vilinskas and R. J. Schiltz

Nucl. Appl. 6, 176-177 (February 1969)

Performance Tests on an Eddy-Current Flowmeter

D. E. Wiegand and C. W. Michels

IEEE Trans. NS-16(1), 192-195 (February 1969)

II. OTHER FAST REACTORS--CIVILIAN--OTHER FAST BREEDER REACTORS

A. Fuel Development

1. Corrosion of Fuel Jacket Alloys

- a. Sodium Corrosion of Austenitic Stainless Steels (J. Y. N. Wang and K. Figlik)

Last Reported: ANL-7527, p. 79 (Dec 1968).

(i) Corrosion Tests. The corrosion of stainless steels in sodium is being investigated to identify and to study the metallurgical and environmental parameters that may influence the failure of Types 304 and 316 stainless steels because of penetration by sodium at reactor operating temperatures. The effect of carbon content on the corrosion behavior is of major interest because of the close relationship observed between carburization and intergranular penetration of these materials.

A long-term corrosion evaluation is being conducted with specimens of Types 304, 304L, 316, and 316L stainless steels. Material analyses are given in Table II.A.1. Prior to sodium exposure, coupon specimens (2.54 cm long by 0.64 cm wide) of either 5- or 10-mil thickness were solution-heat-treated for 2 hr under vacuum (3×10^{-5} Torr) at 1050°C and then oil-quenched at 0°C. The corrosion test is being performed in an autoclave, in which the maximum flowrate of sodium is about 70 cc/min, the temperature of the sample section is 650°C, and the cold trap is held near 100°C to obtain an initial oxygen level of 3 ppm in sodium (determined by vacuum distillation). Thirty-two samples were originally exposed, and all were withdrawn every 90 days and cleaned. Two specimens of each type were retained for examination, and the remainder were re-exposed. A total test time of 360 days is planned.

TABLE II.A.1. Composition of the Tested Stainless Steels

Type of Stainless Steel	Composition (w/o)									
	C	Ni	Cr	Mo	Mn	Cu	Co	Si	P	S
304	0.07	8.71	18.59	-	1.50	-	-	0.59	0.026	0.005
304L	0.03	10.96	18.74	0.48	1.66	0.25	-	0.75	0.021	0.015
316	0.06	12.86	17.66	2.82	1.77	0.14	0.15	0.65	0.016	0.012
316L	0.03	12.74	17.45	2.10	1.60	0.13	0.18	0.74	0.022	0.014

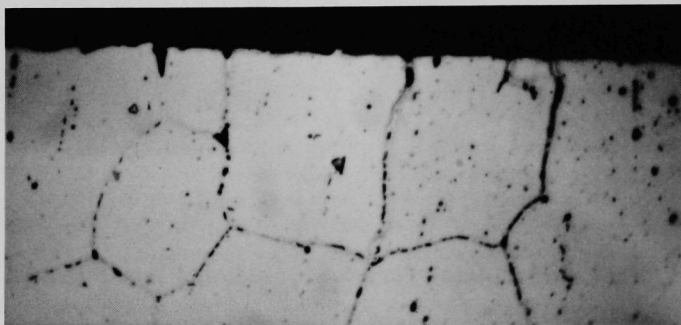
Evaluation methods include a determination of weight change as well as metallographic inspection. Each group of specimens was cleaned in ethanol, followed by ultrasonic cleaning in distilled water. Microscopic examination followed an electrolytic etch in 5% oxalic acid.

Weight changes for the first two 90-day periods are shown in Table II.A.2. A trend toward increased weight loss with time of exposure is evident, as are the greater weight losses of the low-carbon alloys (304L and 316L specimens). Examples of intergranular penetration of these samples are shown in Fig. II.A.1. After two 90-day test periods the 316L specimen showed intergranular attack to a maximum penetration of 14 μ . Such

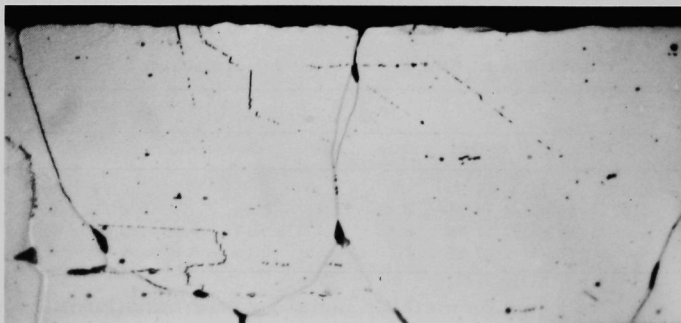
TABLE II.A.2. Weight Losses of Stainless Steels Exposed to Sodium at 650°C^a

Type of Stainless Steel	Weight Loss of 5-mil Specimens ($\mu\text{g}/\text{cm}^2$)		Weight Loss of 10-mil Specimens ($\mu\text{g}/\text{cm}^2$)	
	90-day Exposure	180-day Exposure	90-day Exposure	180-day Exposure
304	4	36	5	23
304L	17	65	10	64
316	10	50	12	47
316L	18	75	11	60

^aSodium is cold-trapped at $\sim 100^\circ\text{C}$.



Type 304L Stainless Steel



Type 316L Stainless Steel

Fig. II.A.1. Intergranular Penetration of Stainless Steels after Exposure to Sodium at 650°C for Six Months (750X)

intergranular attack was absent in specimens examined after the first 90 days. The intergranular attack of the 304L specimen was less severe; penetration occurred to a maximum depth of $7\ \mu$. The intergranular attack at the surface of standard 304 and 316 specimens is just detectable.

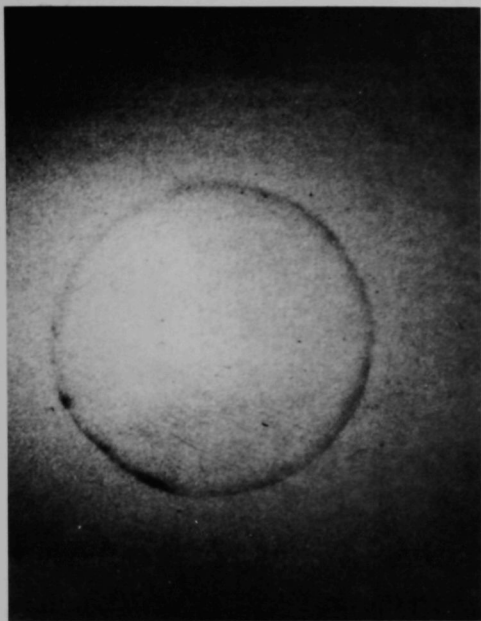


Fig. II.A.2. Autoradiograph Showing Sodium Retention on Steel ($\sim 3X$)

Electron-microscope and microprobe analyses are planned, and the oxygen content of the sodium will again be analyzed. Until all the data are examined and analyzed, no speculation as to the cause of this phenomenon will be expressed.

(ii) Development of Tracer Techniques. A radioactive-tracer technique is being developed to study the preferential diffusion of sodium into grain boundaries or through the matrix of stainless steel. Active sodium was prepared by ion exchange of liquid sodium with active $^{22}\text{NaCl}$. One capsule of Type 304L stainless steel has been prepared and tested with a mixture of ^{22}Na - ^{23}Na for 250 hr at 650°C . An autoradiograph of a transverse section of the capsule after removal of the sodium, shown in Fig. II.A.2, revealed that the activity of ^{22}Na

in the residual sodium caused a photographic image on the film. If, after removal of surface sodium, an image can still be produced, then sodium penetration of the stainless steel is implied. Further work is in progress to improve this technique.

2. Other Fuel Jacket Alloy Studies

a. Mechanical Properties of Fuel-jacket Alloys (F. L. Yaggee)

Last Reported: ANL-7548, p. 78 (Jan 1969).

(i) Effect of Flowing Sodium on the Creep of Vanadium Alloys.

The sodium loop designed for creep measurements has successfully completed 500 hr of continuous operation at 650°C and a sodium flowrate of 7 gal/min. Two creep tests have been initiated with 0.020-in.-thick sheet specimens of V-15 w/o Cr-5 w/o Ti alloy under a uniaxial stress of

42,600 psi. After 250 and 350 hr of testing, the steady-state creep rates for these specimens were of the order of 3.0 and 2.5×10^{-5} /hr, respectively. The corresponding total strains were about 0.5 and 0.3%. The specimen with the slightly faster creep rate and higher total strain had been exposed to flowing sodium at 650°C in the unstressed state for approximately 100 hr before the creep test was started.

Apparent temperature fluctuations have occurred in the flowing sodium passing through the creep testing ports. These fluctuations are reflected as displacement oscillations on the recorded creep curve. An effort is being made to determine the source and nature of this problem.

III. GENERAL RESEARCH AND DEVELOPMENT--CIVILIAN-- STUDIES AND EVALUATIONS

A. Evaluation of Fast Reactor Analysis Methods and Data (K. A. Hub and T. Wolsko)

Not previously reported

1. Thermal-Hydraulic Analysis

A computer program has been formulated to analyze the thermal-hydraulic characteristics of fast reactors. This program, SAM-1, evolved from a previous thermal-hydraulics code called EVALUATE.* Unlike its parent program, which is applicable to only sodium-cooled reactors, SAM-1 calculates thermal-hydraulic characteristics of fast reactors designed to be cooled by sodium, helium, carbon dioxide, or steam.

A quasi-one-dimensional program, it analyzes the temperature and flow characteristics of individual subassemblies or rows of subassemblies. Both hexagonal- and square-subassembly geometries can be treated. Three different coolant-orificing conditions are possible: (1) coolant orificed for a constant outlet temperature at nominal midcycle conditions, (2) coolant orificed to a maximum clad temperature at peak conditions, and (3) coolant flow unorificed.

Temperature and coolant velocities are calculated for several reactor conditions (nominal, peak, and peak-hotspot). In addition to the peaking conditions, a time variation is available to account for power-density changes during the burnup cycle. Both carbide and oxide fuels can be used with this program. Due to the central voiding of mixed uranium-plutonium dioxide, a routine is incorporated to make fuel-conductivity corrections.

In the particular case of gas-cooled designs (helium, carbon dioxide, and steam), partially or fully roughened fuel-pin designs can be analyzed. For partially roughened fuel pins, the temperature of the fuel and cladding is calculated both at the point of maximum temperature and at the transition point between the roughened and unroughened surfaces. It is assumed that the convective heat-transfer coefficient experiences a step change at the point of transition between roughened and unroughened surfaces.

In addition to the temperatures and velocities, peak pressure drop, maximum bending and tensile stresses, and maximum subassembly deflection are calculated.

*Thompson, D. H., EVALUATE, A Thermal-Hydraulics Computer Program for Sodium-cooled Fast Reactors, Argonne National Laboratory, to be published.

IV. GENERAL REACTOR TECHNOLOGY

A. Applied and Reactor Physics Development

1. Theoretical Reactor Physics--Research and Development

a. Cross Section Data Evaluation (D. A. Meneley)

Last Reported: ANL-7518, p. 81 (Nov 1968).

Calculations of perturbation cross sections for the materials present in ZEBRA 6A and ZPR-3 Assemblies 50 and 52 have been performed. A FORTRAN program was written for the purpose to use the cross sections and fluxes from the corresponding MC² problems. The results will be compared with those from the GAFGAR, ETØX, and ENDRUN codes.

Most of the ENDF/B materials from the revised category-1 data tapes have been processed through the system 360 versions of DAMMET, ETØE, and MERMC2 to form a library for the 360 version of MC². Some preliminary data were included for materials for which revised category-1 data are not yet available. A total of 66 materials is present in the library.

Improvements have been made in program MAGIC, which plots data from the MC² library tape on the CDC-3600. The work is complete except for the addition of routines to plot unresolved resonance cross sections.

b. Reactor Computations and Code Development (B. J. Toppel)

Last Reported: ANL-7548, pp. 82-83 (Jan 1969).

(i) Variational Synthesis Code. A variational synthesis code has been developed (see Progress Report for January 1968, ANL-7419, pp. 91-95). At present the code produces two-dimensional fluxes in r,z or x,y geometry with a maximum of 30 energy groups and 30 synthesis regions. There is no explicit limitation on the number of mesh points or in the number of trial functions per synthesis region handled.

The generation of a variety of one-dimensional trial functions is being implemented within the ARC system.

Test runs made using trial functions which are actual one-dimensional profiles of simple two-dimensional flux shapes in one, two, and six energy groups have produced synthesis results in excellent agreement with the exact two-dimensional fluxes. Use of the same type of exact trial

functions in a more complex situation has produced qualitatively good results, but it is believed that the synthesis results should be much closer to the two-dimensional results than they are at present. A series of test cases of increasing complexity will be used to investigate these discrepancies in a systematic manner.

As the number of trial functions per region increases, difficulties probably connected with the quasi-linear dependence of the trial functions begin to show up. These are slow or no convergence of the fluxes and the appearance of some values of flux clearly in error. Criteria to diagnose and eliminate this difficulty are being worked out.

Future steps to be taken are: continue debugging of the code in its present two-dimensional version until satisfactory agreement is obtained when using exact trial functions; experiment with sets of non-exact realistic trial functions in order to learn which is a good choice of trial functions in a variety of physical situations; calculate adjoint fluxes; extend the capability of the code to three dimensions.

(ii) Argonne Reactor Computation System. A series of problems are being run to test the one-dimensional perturbation-theory module and its associated standard path, PERT1D. These problems are designed to uncover potential programming and systems errors and to test the accuracy of the module by comparison with k calculations made with the one-dimensional diffusion-theory module and its associated standard path, PATH1D.

The description of the critical, reference configuration is given in Tables IV.A.1 and IV.A.2. The reactor is a finite cylinder of 36.3-cm half-height and with an extrapolation distance of 16.254 cm. There are 22 groups of neutrons.

TABLE IV.A.1. Description of the Critical,
Reference Configuration

Region	Outer Radius (cm)	Mesh Points	Material ^a
1	56.8325	40	M1 M6
2	137.6299	30	M2 M7
3	181.8767	40	M5 M8
4	227.5967	20	M9

^aSee Table IV.A.2.

TABLE IV.A.2. Isotopic Concentrations in the Materials

Material	Isotope Number	Isotope Name	Concentration (10^{24} atoms/cm ³)
M1	53	U-235	0.00003156
	68	U-238	0.01035688
M2	8	Pu-241	0.00007676
	53	U-235	0.00002201
	55	Pu-239	0.0010974
	64	Pu-240	0.00039041
	68	U-238	0.00722140
M5	53	U-235	0.00003892
	68	U-238	0.01277050
M6	34	Na	0.007696
	35	O	0.0207769
	37	Fe	0.0101123
	38	Ni	0.0010399
	39	Cr	0.0026407
M7	34	Na	0.0078528
	35	O	0.0176160
	37	Fe	0.012836
	38	Ni	0.00132
	39	Cr	0.003352
M8	34	Na	0.0045745
	35	O	0.0256184
	37	Fe	0.0124689
	38	Ni	0.0012822
	39	Cr	0.00325613
M9	34	Na	0.010689
	37	Fe	0.030564
	38	Ni	0.003143
	39	Cr	0.007983

Three problems were run to test the module with respect to changes in buckling. In one problem, the height of the reactor was changed; in the second problem, the extrapolation distance was changed; in the third problem both the height and the extrapolation distances were changed such as to result in no net perturbation. The results of these calculations are given in Table IV.A.3, from which it is seen that there is excellent agreement between the perturbation and the diffusion theory calculations.

TABLE IV.A.3. Results of Buckling Perturbations

Problem	Perturbed		$\Delta k/k^2$	
	Half-height (cm)	Extrapolation Distance (cm)	PERT1D	PATH1D
1	39.3	-	0.016228	0.016456
2	-	19.254	0.016228	0.016456
3	39.3	13.254	0.0	0.0

Five problems are being run to test the module with respect to changes in the isotopic composition of materials. In four problems, the composition of one region is perturbed; in the fifth problem the compositions of all regions are perturbed simultaneously. In the third region (material M8) isotopes are removed; in the fourth region (material M9) a fissile isotope is added. These calculations are summarized in Table IV.A.4. For the problems that have been run there is excellent agreement between the perturbation and diffusion theory calculations.

TABLE IV.A.4. Results of Isotope Perturbations

Problem	Perturbed			$\Delta k/k^2$	
	Material ^a	Isotope ^a	Concentration (10^{24} atoms/cm ³)	PERTID	PATHID
4	M1	53	0.00015	0.0023298	0.0023962
5	M2	55	0.0010426	-0.0234203	-0.0234902
6	M8	37	0.0	-0.0047456	
		38	0.0		
		39	0.0		
7	M9	53	0.05		
8	M1	53	0.0015		
	M2	55	0.0010426		
	M8	37	0.0		
		38	0.0		
		39	0.0		
	M9	53	0.05		

^aSee Table IV.A.2.

Five problems are being run to test the module with respect to changes in the volume fractions of materials in compositions. In four problems, the composition of one region is perturbed; in the fifth problem, the compositions of all regions are perturbed simultaneously. These problems are described in Table IV.A.5.

TABLE IV.A.5. Results of Composition Perturbations

Problem	Perturbed			$\Delta k/k^2$	
	Composition ^a	Material ^a	Volume Fraction	PERTID	PATHID
9	C1	M1	0.5	-0.00027826	
10	C2	M2	1.05	0.0249018	
11	C3	M8	0.5	-0.0017729	
12	C4	M2	1.0		
		M9	1.25		
13	C1	M1	0.5		
	C2	M2	1.05		
	C3	M8	0.5		
	C4	M2	1.0		
		M9	1.25		

^aSee Table IV.A.2.

Further problems will be run to test the module with respect to composition-region assignments and with respect to the imposition of internal boundary conditions.

2. Nuclear Data--Research and Development

a. Reactor Code Center (M. Butler)

Last Reported: ANL-7527, p. 98 (Dec 1968).

During the last quarter of 1968, 214 programs were distributed by the Code Center; of these 53 were in answer to requests from universities.

This month Supplement 1 to ANL-7411, Compilation of Program Abstracts, was distributed. This supplement contains the abstracts of 57 additional programs (ACC Nos. 280 through 336), and a number of revisions and modifications to the original document. ANL-7497, the Director of Cooperating Installations, was also issued this month. Supplements to this directory will be published periodically.

Additions to the library since the first of the year include: 349, TOODEE, a two-dimensional time-dependent heat-conduction program written for the IBM 7040 by Phillips Petroleum Company; 355, MC², the Argonne CDC-3600 multigroup cross-section-calculation program using ENDF data; 356, ZPR GAF/GAR DATA, the UNIVAC 1108 GAF/GAR data tapes prepared by Gulf General Atomic for ZPR-3 Assembly 48 ENDF/B benchmark testing; 357, SUPORAN, the core-support-structure stress-analysis program written at Argonne for the CDC-3600; and the ENEA Computer Programme Library program E084, OLDERIC, a CDC-3600 two-dimensional few-group diffusion program.

A revised version of the CDC-6600 TWIGL program received from Bettis has replaced an earlier version; GE625 versions of the FOG (No. 28), EXTERMINATOR 2 (No. 156) and GAMTEC2 (No. 185) programs distributed by Bechtel Corp. have been added to the Center's library.

A CDC-3600 version of the ENEA E066 LOUISE-3 program for three-dimensional diffusion-theory studies and an IBM-360 version of E135, HECTIC2, a heat-transfer analysis program, have been received from Ispra.

B. Reactor Fuels and Materials Development

1. Fuels and Cladding

a. Research and Development

(i) Chemistry of Irradiated Materials (C. E. Crouthamel)

(a) Development of Analytical Facilities, Microstructure Sampling Techniques and Analytical Procedures for Analysis of Irradiated Fuels

Last Reported: ANL-7518, p. 90 (Nov 1968).

The Shielded Fuel Evaluation Facility (SFEF) is nearly ready for shakedown tests. Relocation of the metallograph within its shielding completed the major installation work. The in-cell metallographic equipment for cutting, polishing, vacuum coating, and cathodic etching is being set up and checked prior to filling the cell with helium.

The pneumatic sample-transfer tube that connects the SFEF and the analytical facility has been installed and leaktested. The control system and auxiliary piping are in place. The pneumatic switching devices for the sending and receiving stations are being fabricated. Upon completion of this work, the entire transfer system will be tested.

(b) Postirradiation Studies for Reactor Fuel

Last Reported: ANL-7513, p. 103 (Oct 1968).

Work is underway to examine specimens of five UO_2 -20 wt % PuO_2 fuel pins clad with stainless steel, which were irradiated in EBR-II to burnups ranging from 4 to 7 at. %. Specimens are being ground and polished in the metallographic facilities of the General Electric Company, Pleasanton, California. Eight transverse and four longitudinal sections representative of the five fuel pins are being ground to thicknesses of 1 to 3 mils so that each section will have a gamma-activity level ≤ 1 R/hr at 1 ft. One longitudinal and two transverse sections have been delivered. Succeeding sections will be delivered in groups of three at three-week intervals.

Optical examinations of the sections are being carried out in the Shielded Fuel Evaluation Facility. One specimen, a transverse section of a pin of 5.6 at. % burnup, is now being analyzed with an unshielded electron-probe microanalyzer. Preliminary results have been obtained for the distributions of uranium, plutonium, and fission products, and the degree

of interaction of cesium with the stainless steel cladding. The data obtained to date are similar to those previously reported for SOV-6, a UO_2 -20 wt % PuO_2 pin irradiated in EBR-II to 2.7 at. % burnup (see Progress Reports for November 1967, ANL-7399, p. 121; February 1968, ANL-7427, p. 102; and July 1968, ANL-7478, p. 100).

In other work, laser-beam vaporization has been used to sample selected areas of a cross section of SOV-6. Gamma-spectrometric analysis of the laser samples showed ^{125}Sb to be concentrated in the region of the fuel-cladding interface; however, none was detected in the equiaxial and columnar grain regions. Antimony-125 was also found previously in laser-beam samples taken from the fuel-cladding interface of a 13% enriched, stainless steel-clad UO_2 pin irradiated in MTR to 6.8 at. % burnup (see Progress Report for December 1967, ANL-7403, pp. 109-110).

2. Coolants, Moderators, and Control Materials--Fundamentals of Corrosion in Liquid Metals

a. Corrosion Mechanisms (D. L. Smith)

Last Reported: ANL-7527, pp. 101-104 (Dec 1968).

The equilibrium distribution of nonmetallic impurities between liquid sodium and the Group V refractory metals is being determined. Although oxygen is of primary importance, nitrogen, carbon, and hydrogen are also being considered. The distribution coefficients are determined by exposing refractory-metal wires to sodium for periods sufficient to equilibrate the impurity of interest. Both hot-trapped and cold-trapped sodium are being investigated over the temperature range from 500 to 800°C.

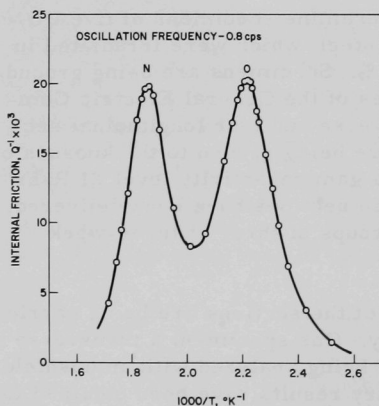


Fig. IV.B.1. Typical Internal-friction Curve for Vanadium after Exposure to Low-oxygen Sodium

The internal-friction technique is being used to measure the nonmetallic interstitial concentrations in the Group VB metals. This method has proved to be sensitive for low concentrations in the small wire samples. An automated internal-friction apparatus that uses a solar cell to measure oscillation amplitude has been constructed and is now in operation. The amplitude, cycle number, and sample temperature are printed on a teletype. Figure IV.B.1 is a typical plot of the internal friction as a function of temperature for a vanadium wire exposed to sodium. The relationship between the peak height Q of internal friction and the oxygen concentration based on vacuum-fusion data at relatively high concentrations is given by

$$C_O \text{ (ppm)} = 55,000Q^{-1}.$$

This linear relation is valid up to 3000 ppm oxygen in vanadium.

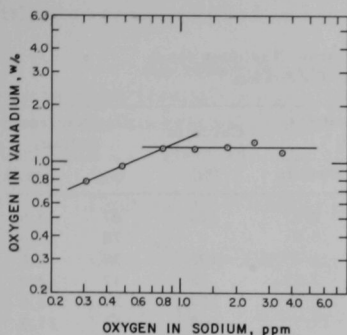


Fig. IV.B.2. Oxygen in Vanadium Wires Exposed at 600°C to Cold-trapped Sodium

removal of the sodium. The oxygen solubility in vanadium at 600°C obtained in this experiment is 1.2 w/o. Although the temperature dependence of the solubility of oxygen in vanadium is not well-known, this value compares favorably with other reported values.

A few more tests will be run at 600 and 700°C with different oxygen concentrations in sodium. Also, wires will be exposed at 50° temperature intervals from 500 to 750°C, with oxygen concentration in sodium held constant.

- b. Corrosion Inhibition by Dissolved Getters in Liquid-sodium Environment (K. Natesan, C. A. Youngdahl, and W. McFall)

Last Reported: ANL-7527, p. 104 (Dec 1968).

Additions of alkaline-earth elements to liquid sodium are being considered as a means of lowering the activity coefficient of nonmetallic impurities such as oxygen and nitrogen. Preliminary investigations of the Na-O-Ca system are in progress, with emphasis on calcium recovery and the analysis for total oxygen in the ternary system.

The experiment consisted of equilibrating under vacuum (10^{-5} Torr) varying amounts of metallic calcium and about 10 g of sodium at 400°C for about 1 hr in a sealed molybdenum crucible. The crucible was cooled to 300°C, then opened, and the distillation of the sodium started. The maximum distillation temperature reached about 500°C in 50° increments.

After distillation, the residue was hydrolyzed and acidified with hydrochloric acid, and the solution was analyzed for sodium and calcium by flame photometry. The calculations of oxygen content in sodium were made by assuming that all the sodium was present as sodium oxide. The results are listed in Table IV.B.1.

TABLE IV.B.1. Analyses of Vacuum-distillation Residues from the Equilibrium Studies of the Na-O-Ca System^a

Run	Sodium (g)	Calcium			Flame Analysis ($\mu\text{g}/\text{ml}$)		Calcium Recovery (%)	Oxygen from Sodium	
		(g)	(ppm)	($\mu\text{g}/\text{ml}$)	Calcium	Sodium		(μg)	(ppm)
R4	6.44	0.0150	2340	150	153	2.5	102	87	13.5
R5	7.56	-	-	-	-	5.0	-	178	23.6
R6	12.16	0.0010	82.5	10	10.5	1.7	105	59	4.8
R7	11.80	0.0051	432	51	50	1.35	98	47	4.0
R8	9.44	0.0020	212	20	21.5	0.7	108	24.4	2.6
R9 ^b	12.83	0.0003	23.4	12	13.0	17.5	108	153	11.9
R12	10.78	-	-	-	-	6.6	-	229	21.3
R13	15.04	-	-	-	-	10.1	-	351	23.3
R15 ^c	11.74	0.0021	179	21	16.7	0.10	80	4	0.34
R16 ^c	10.10	0.0009	89	9	9.7	0.50	107	17.4	1.7

^aAll residues were diluted to 100-ml solutions unless otherwise specified.

^bCalcium addition as Na-Ca master alloy with Ca \approx 1.8 w/o; the residue was diluted to a 25-ml solution.

^cDouble distillation: 500°C for sodium and 820°C for calcium.

In several experiments a double distillation was attempted; following the distillation of sodium at 500°C, the distillation of calcium was attempted at 800 to 820°C in vacuum (2×10^{-6} Torr) for 1/2 to 1 hr. After this second distillation, the residue was again hydrolyzed and acidified with hydrochloric acid, and the solution was analyzed for sodium and calcium by flame photometry. The results are also given in Table IV.B.1.

In the absence of any calcium, the oxygen content in sodium was about 21-23 ppm. The addition of calcium to sodium lowers the oxygen concentration associated with sodium in the residue. However, there is not sufficient oxygen in the original sodium to convert all the calcium to calcium oxide. Thus, sodium oxide, calcium oxide, and calcium may be present in the distillation residue. Thermodynamically this does not seem feasible since the reaction



is expected at all temperatures. The sodium resulting from this reaction will be distilled off, leaving behind calcium oxide and excess calcium. But if sodium oxide and excess calcium are physically separated in the crucible after distillation, then the above reaction will not occur.

In Experiment R15, some of the free calcium appears to have distilled off, whereas in R16 no distillation of free calcium is noted (both runs were double distillations). This may be due to an insufficient temperature or length of time for distillation. Experiments with higher distillation temperatures and longer distillation times will be attempted.

An alternative approach for total-oxygen analysis is to distill the sodium (containing calcium and oxygen) at 500°C and hydrolyze the residue under controlled conditions. During hydrolysis the following reactions proceed:



The hydrogen released will be collected and analyzed by gas chromatography. From the amount of hydrogen liberated, the free calcium in the residue can be calculated. From the free calcium values and the flame analysis of total calcium and sodium, the total oxygen in the ternary system can be calculated. A gas-chromatography unit is being set up for this purpose.

An apparatus is also being constructed for measurements of the solubilities of alkaline-earth metal oxides (e.g., CaO and MgO) in liquid sodium. The experiment will consist of equilibrating solid CaO in liquid sodium at different temperatures. Samples of sodium, which have passed through a 5- μ stainless steel filter, will be taken by a dip-sampling technique. The sodium samples will be distilled, and the residue will be analyzed for sodium and calcium.

3. Radiation Damage on Structural Materials--Research and Development--In-Reactor Creep Studies

a. In-pile Creep (J. A. Tesk and W. F. Burke)

Last Reported: ANL-7548, pp. 92-93 (Jan 1969).

The creep rate of a 0.020-in.-dia specimen of V-15 w/o Cr-5 w/o Ti alloy was measured in a neutron flux of 3×10^{13} n/cm²-sec ($E > 0.1$ MeV) at ~650°C while under a uniaxial stress of 55,000 psi. The specimen was annealed for 1 hr at 1250°C prior to the test. After a brief incubation period of 10 hr, the creep rate continually increased until fracture occurred at 63.5 hr. The deformation rate just before fracture was 2.35×10^{-4} /hr at 657°C. The strain just before fracture was 0.87%, about 20% (or 0.15% strain) of which occurred during a rise in stress because of electronic

failure in the stress-control system. Strain was uniform during the test, and total strain at fracture was 2.5%. The specimen was extremely brittle after the test and fractured again during postirradiation handling.

During the experiment, the test temperature was changed from $645.2 \pm 0.5^\circ\text{C}$ to $661.2 \pm 0.5^\circ\text{C}$ at constant stress, and the resultant change in creep rate from $1.75 \times 10^{-4}/\text{hr}$ to $2.96 \times 10^{-4}/\text{hr}$ yielded an activation energy of $93,000 \pm 7500$ kcal/mole. This value is close to the 89,000 cal/mole found by Yaggee* in out-of-reactor tests with other vanadium-base alloys.

b. Void Formation and Growth (S. D. Harkness)

Last Reported: ANL-7548, p. 93 (Jan 1969).

(i) Small-angle Scattering Studies of Void Formation. Comparisons between void-size distributions measured by X-ray small-angle scattering (SAS) and transmission electron microscopy (TEM) are now complete for three samples of Type 304 stainless steel. The form of the size-distribution curve was generated from the results of the SAS measurements by means of a method discussed elsewhere.** The results of the present comparison, listed in Table IV.B.2, indicate that SAS can be used with some confidence in measuring void-size distributions.

TABLE IV.B.2. Comparison of SAS and TEM Measurements of Void Size

Irradiation Temperature ($^\circ\text{C}$)	Estimated Fluence ($\text{n}/\text{cm}^2 \times 10^{22}$)	R_G (\AA)	R^* (\AA)	R (X ray) (\AA)	$\langle R^3 \rangle^{1/3}$ (X ray) (\AA)	$\langle R \rangle$ (TEM) (\AA)
460	1.4	126	74	56	64	58
450	4.1	74	69	68	69	59
463	3.1	148	83	61	72	82

The SAS size parameters used in this analysis are defined as follows:

$$R_G = \left[\frac{5 \ln I(s)}{4\pi^2 s^2} \right]^{1/2} \quad (1)$$

and

$$R^* = \frac{3}{8(1-f)} \frac{\int_0^\infty s I(s) ds}{s_0^3 I(s_0)}, \quad (2)$$

*Yaggee, F. L., Gilbert, E. R., and Brown, A. R., Metallurgy Division Annual Report, ANL-7299 (1966) p. 80.
 **Harkness, S. D., Gould, R. W., and Hren, J. J., Phil. Mag. 19, 115 (1969).

where

$$s = 2\theta/\lambda;$$

2θ = angular position above main beam;

λ = X-ray wavelength;

$I(s)$ = scattered intensity at s ;

f = volume fraction of scattering phase;

s_0 = value of s at which the product $I(s_0)s_0^3$ becomes constant.

These measured parameters are then used to generate a size distribution from which actual size moments may be derived. The measured X-ray size parameters should not be directly related to the actual moments of the size distribution.

(ii) Swelling in Irradiated Type 304 Stainless Steel. Immersion densities from a flat of the hexagonal can of Subassembly XG05 appear to confirm the results obtained with the recently analyzed control-rod thimble. These results are presented in Table IV.B.3.

TABLE IV.B.3. Immersion-density Results for Subassembly XG05

Axial Distance from Top of Flat (in.)	Estimated Fluence, $E > 0.1$ MeV ($n/cm^2 \times 10^{22}$)	Irradiation Temperature (°C)	Density (g/cm^3)	Swelling (%)
2	0.12	470	7.906	-
9.6	0.31	470	7.896	0.12
18	1.2	470	7.898	0.101
26	3.8	460	7.818	1.11
31.6	5.0	430	7.831	0.95
37	4.2	380	7.871	0.44
40	2.9	371	7.869	0.47

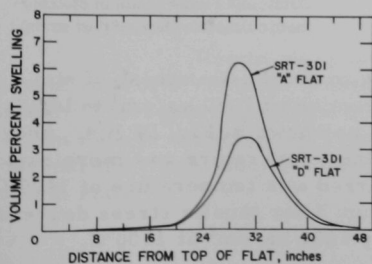


Fig. IV.B.3. Predicted Density Profiles of Two Flats of a Safety Thimble

Studies are in progress with a safety guide thimble (removed from position 3D-1 of EBR-II) that reached an estimated peak fluence of $10^{23} n/cm^2$. Predicted density profiles of two of the flats of the hexagonal-shaped thimble are presented in Fig. IV.B.3. The expected difference between the two flats is due to the difference in irradiation temperature. Flat A was positioned next to a driver fuel subassembly during most of its exposure, whereas flat D was usually adjacent

to a structural subassembly. The outlet temperature calculated for flat A is 474°C, whereas for flat D the calculated value is 440°C.

4. Engineering Properties of Reactor Materials--Research and Development--High Temperature Mechanical Properties of Ceramic Fuels

a. High Temperature Mechanical Properties of Fuel Oxides (R. J. Beals)

Last Reported: ANL-7527, pp. 110-114 (Dec 1968).

(i) Stress Dependence on Strain Rate and Temperature. The effects of temperature and strain rate upon the mechanical properties of stoichiometric uranium dioxide are being investigated. The mechanical properties under study include the maximum fiber tensile stress (sometimes termed ultimate tensile strength), the flow stress (yield stress), and the plastic strain. Specimens were sintered to 97% of theoretical density with an average grain size of $5\ \mu$. Data were obtained with bars of square cross section by the four-point bending technique. The values presented in Figs. IV.B.4 and IV.B.5 represent an average of at least five determinations at each test condition.

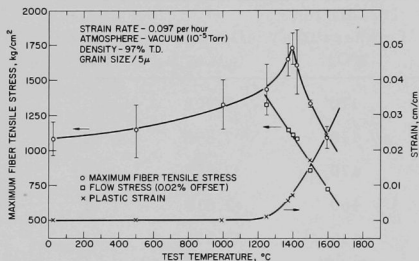


Fig. IV.B.4. The Effect of Temperature on the Maximum Fiber Tensile Stress, Flow Stress, and Plastic Strain of Stoichiometric Uranium Dioxide (slow strain)

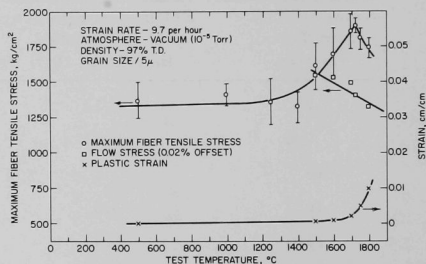


Fig. IV.B.5. The Effect of Temperature on the Maximum Fiber Tensile Stress, Flow Stress, and Plastic Strain of Stoichiometric Uranium Dioxide (fast strain)

There was a small increase in the tensile stress of stoichiometric UO_2 from the room-temperature value of 1080 kg/cm² to 1440 kg/cm² at 1250°C for a strain rate of 0.097/hr, as shown in Fig. IV.B.4. Above 1250°C, the increase in stress with increasing temperature was more rapid, and a maximum stress of 1720 kg/cm² occurred at a temperature of 1400°C. Above this critical temperature, the maximum fiber tensile stress decreased considerably, with an average stress of only 1090 kg/cm² at 1600°C.

The UO_2 deformed in a brittle fashion with essentially no plastic strain until the test temperature was increased to 1250°C . At this temperature the strain was 0.009 cm/cm . Above 1250°C , the brittle-to-ductile transition, there was a marked increase in strain to 0.024 cm/cm at 1600°C .

The flow stress of the uranium dioxide was measured at 0.02% strain, and the first deviation of the stress-strain curve from a linear relationship occurred at 1250°C . Figure IV.B.4 shows that the extended stress curve intersects the curve of ultimate tensile strength at 1250°C and then decreases linearly with increasing temperature. This would appear to be a further indication of the transition at 1250°C . By a linear least-square regression interpretation, the relationship between flow stress and temperature at a strain of 0.097 is

$$\sigma_f = 3620 - 1.812t, \quad (1)$$

where σ_f is the flow stress in kg/cm^2 , and t is the test temperature in $^\circ\text{C}$.

The effect of a strain rate of $9.7/\text{hr}$ on the mechanical properties of stoichiometric UO_2 is shown in Fig. IV.B.5. Although the curve of maximum fiber tensile stress is similar in appearance to that for the slower strain rate, the brittle-to-ductile transition region now appears to be around 1500°C , and the critical temperature at 1725°C . The ultimate tensile strength at the critical temperature was 1800 kg/cm^2 . There was considerably less deformation, or plastic strain, in the rapidly strained specimens; at 1600°C the plastic strain was 0.0004 cm/cm , whereas at 1800°C , it was 0.0076 cm/cm .

The flow stress was considerably higher for UO_2 strained at the rapid rate ($9.7/\text{hr}$). The extended flow-stress curve intersects the curve of ultimate tensile strength at 1525°C , and then decreases linearly with increasing temperature (Fig. IV.B.5). The relationship between flow stress and temperature at a strain rate of $9.7/\text{hr}$ is given by

$$\sigma_f = 2580 - 0.675t. \quad (2)$$

Preliminary data have been obtained for the effect of a strain rate of $0.97/\text{hr}$ on the maximum fiber tensile stress of uranium dioxide. The relative position of the critical temperature at this intermediate strain rate is compared in Fig. IV.B.6 with the strain rates previously discussed; the figure shows that the critical temperature increases with the strain rate.

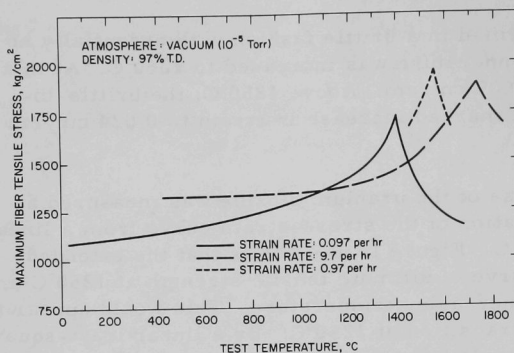


Fig. IV.B.6

The Effect of Temperature and Strain Rate on the Maximum Fiber Tensile Stress of Stoichiometric Uranium Dioxide

(ii) Fracture Mechanisms in UO_2 (R. F. Canon and R. J. Beals)

Not previously reported.

A study is in progress to provide a semiquantitative explanation of the experimental observations resulting from the measurements of the high-temperature mechanical properties of UO_2 . In particular, possible fracture mechanisms are proposed to explain the dependence of the maximum strength on temperature and strain rate.

The "peaking" behavior of UO_2 at high temperatures has been qualitatively observed,* but not discussed. In fact, the large experimental uncertainties associated with previous data have prevented a true assessment of thermal effects. Figures IV.B.4, IV.B.5, and IV.B.6 illustrate the behavior of the ultimate tensile strength (UTS), the yield stress, and the plastic deformation at different strain rates as a function of temperature. The UTS has a well-defined peak at a specific temperature, T_C (hereafter referred to as the critical temperature). The critical temperature increases with increasing strain rate.

Typical stress-strain curves for various temperature regions of interest are presented in Fig. IV.B.7. At the lowest temperatures ($T \ll T_C$), the UTS is relatively independent of temperature, and specimen failure is completely brittle. At intermediate temperatures ($T < T_C$), the onset of plastic deformation occurs with a subsequent increase in the fracture

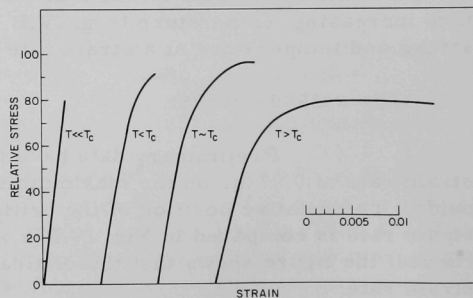


Fig. IV.B.7. Typical Stress-Strain Curves for Stoichiometric Uranium Dioxide

*Tottle, C. R., ANL-7070 (1965); Beals, R. J., and Handwerk, J. H., Materials Technology - An Interamerican Approach, Proc. Conf. on Materials Technology, pp. 136-143 (1968).

stress, but the fracture mode seems to remain relatively brittle in nature. For temperatures very close to T_C , significant plastic deformation begins, and the stress-strain curve flattens out. As the test temperature is increased, the plastic strain increases rapidly with an accompanying sharp decrease in the UTS.

The critical temperature is probably associated with a brittle-to-ductile fracture transition. For temperatures less than T_C , the ultimate strength can be characterized by the Griffith crack criterion.* At temperatures greater than T_C , the behavior of the UTS is similar to the stress-strain-rate behavior, which is observed in high-temperature creep experiments with uranium dioxide. Therefore, the region around T_C should be accompanied by a transition from a transgranular to an intergranular fracture mechanism. (Fractographic studies will be performed to check this hypothesis.)

An important aspect of the mechanical behavior at temperatures $< T_C$ is the strengthening that is noted in the region of brittle fracture. The UTS is relatively constant up to the onset of plastic deformation. After the commencement of plastic deformation, there is a marked increase in the fracture strength. This strengthening behavior can be qualitatively explained by the effect of plastic deformation on the mechanism of brittle fracture associated with the Griffith theory. Specifically, plastic strain would have a "blunting" or rounding effect on the crack fronts, which would reduce the stress-concentration factor. Therefore, a higher stress would be required for crack propagation. Work is presently underway in an effort to describe this behavior quantitatively.

The critical temperature is associated with the onset of significant plastic strain, and, at temperatures greater than T_C , the UTS is associated with an almost perfectly plastic deformation behavior (see Fig. IV.B.7). This maximum strength behavior can be thought of as a "forced creep" effect (i.e., for any imposed strain rate, the material deforms under a maximum load-bearing stress, the UTS). The temperature dependence of the UTS in this region is characterized by a rate-limiting diffusion mechanism for deformation and fracture. This observation is supported by the increase in the critical temperature with increasing strain rate.

If one assumes that the critical temperature is associated with the onset of significant plastic strain resulting from a diffusion-controlled mechanism that limits the maximum fracture stress, then the peak shift can be described by an activation energy. If one assumes a constant stress, the strain-rate dependence on temperature can be expressed as

*Griffith, A. A., Phil. Trans. Roy. Soc., London, A221, 163 (1920).

$$\epsilon \propto \exp(-Q/RT), \quad (1)$$

where ϵ is the strain rate, Q is the activation energy, and T is the absolute temperature. By using Eq. (1), the peak shift observed in Fig. IV.B.6 was found to correspond to an activation energy of ~ 94 kcal/mole. This value is in excellent agreement with values associated with creep in stoichiometric UO_2 .[†] For an intermediate strain rate, the relative position of T_c for the preliminary strength data can also be described by an activation energy of about 94 kcal/mole. Also, for the slowest strain rate, the dependence of stress on temperature is within experimental error of this value of the activation energy, assuming a stress exponent, n , of 4.5 to 5. Future work will extend the UTS measurements to temperatures $>1800^\circ\text{C}$ in an effort to provide a more precise determination of the activation energy.

Plastic deformation at temperatures $>T_c$ probably occurs by means of grain-boundary sliding.^{††} The proposed model for this behavior is a dislocation climb and glide process along the grain boundaries, such as that proposed by Ishida and Henderson-Brown[‡] and supported by Horton and Beevers.^{‡‡} The rate-limiting process for the deformation is probably dislocation climb within the boundary. The activation energy would then correspond to the value for grain-boundary diffusion. This climb-glide mechanism would explain the good agreement in the activation energies for the present deformation behavior, creep, and grain-boundary self-diffusion in UO_2 .[§] The climb and glide of dislocations along the boundaries would lead to fracture by the growth of cavities (or pores), as envisaged by Ishida and McLean.^{§§}

(iii) High-temperature Stress Relaxation of UO_2 (J. T. A. Roberts)

Last Reported: ANL-7527, pp. 111-114 (Dec 1968).

(a) Stress Relaxation. Measurements of stress relaxation were made with stoichiometric UO_2 (95% of the theoretical density, grain size of $\sim 4 \mu$) at a strain rate of 0.097/hr (\equiv a crosshead speed of 0.005 cm/min), in the temperature range from 1300 to 1800°C . At least two specimens were tested at each temperature. As reported in ANL-7527, the relaxation of stress with time could be described in all cases by the equation

$$\sigma_0 - \sigma = s \log_{10} (1 + t/t^*). \quad (1)$$

[†] Scott, R., Hall, A. R., and Williams, J., *J. Nucl. Mater.* **1**, 39-48 (1959); Armstrong, W. M., and Irvine, W. R., *J. Nucl. Mater.* **12**, 261-264 (1964); Wolfe, R. A., and Kaufman, S. F., WAPD-TM-587 (Oct 1967); Bohaboy, P. E., and Asamoto, R. R., paper presented at Fall Mtg., Nuclear Division, Am. Ceram. Soc., Pittsburgh, Pennsylvania, October 6-8, 1968.

^{††} Poteat, L. E., and Yust, C. S., Ceramic Microstructures, Their Analysis, Significance and Production, R. M. Fulrath and J. A. Pask, eds., J. Wiley and Sons, Inc., New York (1968), pp. 646-655.

[‡] Ishida, Y., and Henderson-Brown, M., *Acta Met.* **15**, 857 (1967).

^{‡‡} Horton, C. A. P., and Beevers, C. J., *Acta Met.* **16**, 733 (1968).

[§] Reiman, D. K., and Lundy, T. S., unpublished data.

^{§§} Ishida, Y., and McLean, D., *J. Met. Sci.* **1**, 171 (1967).

The strain-rate sensitivity s [defined as $(\partial\sigma/\partial \log \dot{\epsilon})_T$] increased linearly with increasing applied stress σ_0 , and generally the slope increased with increasing temperature (see Fig. IV.B.8). The relaxation time t^* was assumed independent of σ_0 , since no clear trend existed. As shown in Fig. IV.B.9, computed standard deviations varied from 10 to 20% of the mean values.

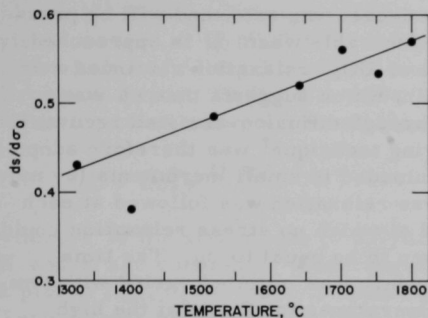


Fig. IV.B.8. Plot of $ds/d\sigma_0$ vs Temperature (strain rate of 0.097/hr)

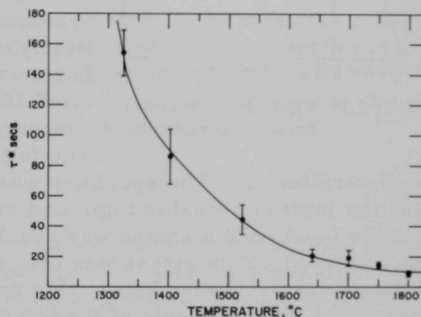


Fig. IV.B.9. Plot of t^*_{av} vs Temperature (strain rate of 0.097/hr)

The strain-rate sensitivity is directly related to the activation volume V for the deformation process. From the work of Feltham[†]

$$V' = 2.3RT/s, \quad (2)$$

and a factor of 3 was used to convert V' into the normally quoted activation volume V for shear; thus, $V = 6.9RT/s$. The corresponding activation energy U can be given by

$$U = U_0 - V'\sigma^* (= U_0 - VT^*), \quad (3)$$

where U_0 is the energy barrier associated with the deformation process and σ^* is the effective stress. In turn, the relation

$$\sigma^* = \sigma_0 - \sigma\mu \quad (4)$$

gives the effective stress, where σ_0 is the applied stress, and $\sigma\mu$ is the internal (or athermal) stress component.^{††}

[†]Feltham, P., Phys. Stat. Sol. 3, 1340 (1963).

^{††}Hull, D., Introduction to Dislocations, Pergamon Press (1968), p. 246.

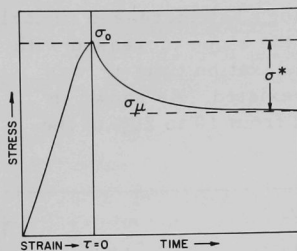


Fig. IV.B.10. Typical Stress-Strain and Stress-Relaxation Curves

The stress-relaxation technique was used in an attempt to measure $\sigma\mu$, which would then allow the calculation of the product $V'\sigma^*$ in Eq. (3). An ideal stress-relaxation curve is shown in Fig. IV.B.10. Since the plastic-strain rate is governed by the thermal component of stress, σ^* , stress relaxation occurs at a progressively decreasing rate, and will be practically unobservable when $\sigma\mu$ is approached. In the case of UO_2 , relaxation continued even after 30 min, which suggests that $\sigma\mu$ was changing through diffusion-assisted recovery. The following technique[†] was therefore adopted to determine $\sigma\mu$. The specimen in small increments (by moving the Instron crosshead up), and stress relaxation was followed at each stress level until a stress was reached at which no stress relaxation could be observed. This stress was then taken to be equal to $\sigma\mu$. The time allowed for relaxation before this procedure was initiated varied with temperature: from ~20 min at the low temperatures to ~5 min at the high temperatures.

The plot of V' versus σ^* in Fig. IV.B.11 shows that a universal curve fits values obtained at all temperatures. The trend is identical to that observed in metals at low temperatures;^{††} $V \simeq 80b^3$ at $\tau^* = 200 \text{ kg/cm}^2$ (i.e., $\sigma^* = 600 \text{ kg/cm}^2$), increasing rapidly to values in excess of $300b^3$ at low stresses, and decreasing to $\sim 40b^3$ at high stresses. The corresponding values for bcc metals reported by Conrad and Hayes are $50b^3$, $>100b^3$, and 2 to $5b^3$, respectively.

In the region $\sigma^* \geq 200 \text{ kg/cm}^2$, the product $V'\sigma^*$ ($= V\tau^*$) was independent of both σ^* and temperature, and gave a mean value of $14.75 \pm 1 \text{ kcal/mole}$.

In calculating an activation energy U , the assumption was made that the so-called relaxation time

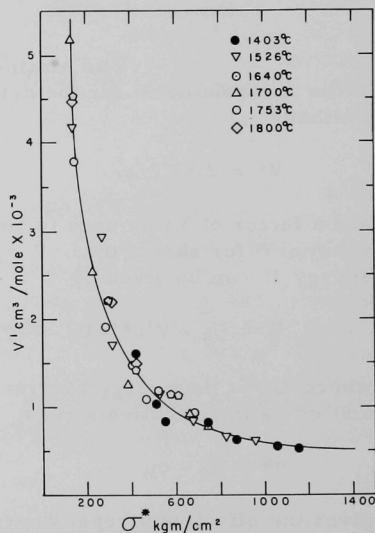


Fig. IV.B.11. Plot of V' vs σ^* (strain rate of 0.097/hr)

[†]Rodriguez, P., J. Mater. Sci. 3, 98 (1968).

^{††}Conrad, H., and Hayes, W., Trans. ASM 56, 249 (1963).

t^* was a true relaxation time as measured, for example, in anelastic stress relaxation. The rate of relaxation is then given by an Arrhenius-type relation

$$t^{*-1} = t_0^{-1} e^{-U/RT}, \quad (5)$$

where t_0^{-1} is a pre-exponential constant. A plot of $-\log_{10} t^*$ versus $1000/T$ yields a value of U of 37.5 ± 2 kcal/mole. This value can be compared with a value of 32 ± 4.5 kcal/mole calculated from the data of Beals (see Progress Report for October 1968, ANL-7513, pp. 110-111) by using the following relationship for thermally activated deformation:

$$\dot{\epsilon} = K \sigma_f^n e^{-U/RT}, \quad (6)$$

where $\dot{\epsilon}$ is the strain rate (0.097/hr), σ_f is the yield or flow stress, and K and n are constants. Rearranging the equation for a constant strain rate, a plot of $\log_{10} \sigma_f$ versus $1/T$ should give a straight line of slope $U/2.3nR$. Term n was obtained from the slope of a plot of \log true stress versus \log true strain in the strain-hardening region of the stress-strain curve (i.e., $\dot{\epsilon} = \text{a constant} \times \sigma^n$). A mean value of 3.23 ± 0.45 was obtained from eight results computed at 1375, 1425, 1500, and 1600°C. Term σ_f was taken to be the proportional limit at 0.02% offset. These values might suffer a certain amount of inaccuracy due to strain hardening.

The good agreement between activation energies for yielding or flow and stress relaxation leads to the conclusion that the same mechanism is operative. This means that "unlocking" and movement of unpinned dislocations are controlled by the same thermally activated process.

A value of U_0 can now be obtained from Eq. (3), i.e., $U_0 = U + V'\sigma^*$, giving $U_0 = 50 \pm 5$ kcal/mole. Such a low value precludes the possibility of the rate-controlling process being cation diffusion (as suggested for creep, for example), since reported values are about twice as high. There are several dislocation mechanisms for yield and flow that would result in a low activation energy, e.g., interaction with forest dislocations, nonconservative motion of jogs in screw dislocations, cross slip of screw dislocations, and overcoming Peierls-Nabarro forces. At the present time there are insufficient data for any one mechanism to be preferred.

Although there appears to be a discrepancy between the activation energies associated with initial plastic flow and fracture, two different processes are being considered. Initial dislocation motion results in yielding, but a different rate-controlling process is characteristic of the plastic deformation associated with the ultimate tensile strength and ultimate specimen fracture.

C. Engineering Development

1. Research and Development

a. Instrumentation and Control

- (i) Boiling Detector (T. T. Anderson, B. B. Spillane, and R. H. Selner)

Last Reported: ANL-7548, pp. 98-100 (Jan 1969).

(a) Acoustic Method

(1) High-temperature Detector Development. Fabrication of the high-temperature detector reported previously has been completed by welding the transducer container and assembling a 2-ft-long electrical lead that is insulated with alumina. Equipment is being assembled for determining the sensor response to sonic and ultrasonic signals.

An alternative bonding method, involving silver-brazing of rf-sputtered electrodes, is being evaluated. Materials Research Corp. demonstrated rf sputtering performed on samples of lithium niobate and annealed stainless steel diaphragms. The process included sputter-cleaning of electrodes and successive deposition of a nickel film over a chromium film without intermediate exposure to the atmosphere. The coated samples are being tested.

(2) Irradiation Tests of Piezoelectric Materials. The uses and benefits of an immittance-measuring instrument for determining the dynamic properties of piezoelectric materials during irradiation has been discussed with personnel at a U.S. Navy underwater sound laboratory.

(3) Sound Measurements in EBR-II. Acoustic tests are being performed on the Core Components Test Loop (CCTL) to corroborate the results obtained from tests on the EBR-II reactor. High-temperature accelerometers (650°C max) are attached to the outside of sodium-filled components, on the pump-discharge line, and at the test-vessel base. Results indicate that background noise at the base of the test-vessel base is related to flow in a similar fashion to background noise from the four locations on the EBR-II primary system (see Fig. IV.C.1). The EBR-II and CCTL measurements are comparable in respect to system size, pump style, pump manufacturer, argon gas over the free sodium surface, and type of measurement device.

(4) Heater Tests for Sodium-boiling Detection. Fabrication of the dummy subassembly, which is 90% complete, is awaiting delivery of the power lead for the high-temperature heater. Preparations are being made to detect the boiling acoustically.

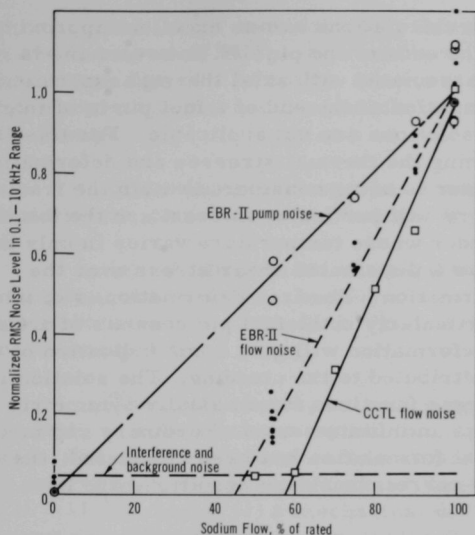


Fig. IV.C.1
Flow-related Acoustic Noise in EBR-II
Primary System and in the Core Com-
ponent Test Loop

b. Heat Transfer and Fluid Flow

(i) Electron Bombardment Heater Test Facility (R. D. Carlson and R. E. Holtz)

Last Reported: ANL-7548, p. 101 (Jan 1969).

Because of binding problems in the high-vacuum environment, modifications are being made to the spring support structure of the 7-pin cluster that is of 3/8-in. diameter and 24 in. long; the other 7-pin cluster of 5/16-in. diameter and also 24 in. long, is also being modified.

A single pin, 1/4 in. in diameter and 24 in. long, has been fabricated. The design of the 7-pin cluster of 1/4-in.-dia pins and a 36-in. heated length is continuing.

c. Engineering Mechanics

(i) Anisotropic Thermoelasticity Studies (R. A. Valentin)

Last Reported: ANL-7518, pp. 99-101 (Nov 1968).

(a) Isotropic Solutions for Comparison

Not previously reported.

It is common practice in computing steady-state thermal stresses in fuel pins to employ plane-strain solutions because it

is known that the results of such calculations are an excellent approximation in all regions except near the ends of the pin. If, however, one is investigating reactivity effects associated with axial thermal expansion, a detailed description of the deformation of the end of a fuel pin is of interest and, by definition, plane-strain solutions are not applicable. For this reason, the problem of determining the thermal stresses and deformations of a finite heat-generating cylinder is being considered within the framework of classical elasticity theory. Of particular interest are the exact shape of the end of a short cylinder whose temperature varies in only the radial direction and, further, how a distributed shear stress over the lateral surface affects this deformation. The free deformation is of interest in reactivity calculation, particularly if the fuel pin consists of a stack of pellets; the shear effect on deformation will give some indication of the degree of axial restraint to be attributed to the cladding. The solution is being formulated in terms of stress functions for an axially symmetric cylinder and will be expressed as an infinite series of ordinary and modified Bessel functions. The initial formulation has been completed; the algebraic details of applying the correct boundary conditions are in progress.

D. Chemistry and Chemical Separations

1. Aqueous and Volatility Processes--Research and Development--Fluoride Volatility Process

a. Engineering Design, Analysis, and Evaluation (N. M. Levitz)

Last Reported: ANL-7548, p. 107 (Jan 1969).

The applicability of fluoride volatility processes to the reprocessing of LMFBR fuels is being assessed in conceptual plant-design studies. The aims of this effort are to assess process feasibility, define areas requiring development or confirmation, and estimate the magnitude of the development task.

The application of fluoride volatility processing to LMFBR fuels is supported by a substantial body of basic and technological information that has been generated over the past 15 years in reprocessing work on other nuclear fuel materials and in related processes. The most important and pertinent areas of earlier work utilizing fluoride volatility and fluid-bed techniques by ANL and other organizations include the following:

(a) commercial refining of uranium in the Allied Chemical Corp. plant at Metropolis, Illinois;

(b) extensive development work on fluoride volatility processing of fully enriched uranium fuels, exemplified by the startup of a hot pilot-scale facility in France;

(c) basic and pilot-plant (kilogram-scale) work on the preparation and transport of PuF_6 ; the results of this work are now finding application in the design of a prototype facility for recovering plutonium scrap and recycle material, planned for installation in 1969 at the AEC-owned Rocky Flats Plant;

(d) plant-scale experience with the fluid-bed calcination of radioactive waste solutions at the Idaho Nuclear Corp. plant;

(e) the first planned commercial application of volatility processing to irradiated fuels, namely, fluoride volatility processing of the uranium stream of the Aquafluor Process in the General Electric Midwest Fuel Recovery Plant.

The draft of a report on a large conceptual fluoride volatility plant (with a capacity of one metric ton of actinides per day) has been completed. The report presents reference process and engineering flowsheets. The reference process (see Progress Report for November 1968, ANL-7518, pp. 107-110) includes (1) a mechanical decladding step, (2) fluorination of uranium and plutonium in two in-series fluid-bed reactors, (3) separation and purification of plutonium in a thermal decomposer, (4) purification of uranium by cold trapping, selective sorption, and distillation, and (5) conversion of the combined uranium and plutonium streams to the oxide. The conclusions that were reached in the conceptual plant design study are summarized below.

The techniques and operations adopted for use in the conceptual fluoride volatility plant--such as continuous fluid-bed fluorination, solids handling, cold trapping of hexafluorides, fractional distillation, and sorption of impurities on solids--represent well-developed existing technology in the nuclear chemical industry. Extension of these techniques to highly radioactive systems, however, requires further development.

Of the areas requiring work defined by the conceptual plant-design study, some involve the investigation and confirmation of concepts that are already partially developed but not fully proven. For example, confirmation is needed that plutonium losses and plutonium decontamination will meet all of the requirements. Other areas involve engineering development of techniques and equipment. Thus, development of the head-end step for separation of fuel from cladding and development of reliable equipment for continuous fluorination in remotely operated facilities are needed. Work on these problems would represent the first stage of a development program on the fluoride volatility process.

The conceptual plant design includes promising solutions to a number of problems raised by the application of volatility processing to a

LMFBR fuels. The process equipment is designed to handle the large heat load from radioactive decay of fission products. Criticality control is provided by safe-by-shape geometry (slab-shaped vessels), and by avoiding neutron moderation and reflection. Provision is made for sampling the fuel input for fissionable-material accountability and burnup analyses. Waste control is handled by complete containment of effluent gases and storage of solid wastes in cylindrical vessels in a storage pool. Waste volumes are moderate. A preliminary analysis of plant safety was made.

The scope of the study did not include detailed layout of equipment and process piping to establish the size of the radiochemical-processing cells and the entire plant. However, a preliminary layout of plant equipment was made, and from this, the processing cells and the building appear to be comparable in size to other reprocessing plants of similar capacity.

The study indicates that the volatility process shows excellent potential for handling highly radioactive, short-cooled LMFBR fuels with virtually no emission of radioactivity to the environment. The process appears capable of handling high concentrations of fissile material in the feed, implying a potential for high throughput. With optimization, a substantially improved process could be expected.

2. Closed Cycle Processes--Research and Development--Compact Pyrochemical Processes

a. Supporting Chemical Studies (I. Johnson)

Last Reported: ANL-7518, p. 111 (Nov 1968).

The solubility of zirconium in liquid Mg-Cu-Ca alloys that are in equilibrium with a solid phase containing zirconium is being investigated to obtain data for use in quantitative predictions of the behavior of fission product zirconium in the reduction step of the salt-transport process.

An experiment was performed in which the solubility of zirconium was determined in Mg-Cu alloys, containing from zero to 35.2 at. % calcium over a temperature range from 550 to 850°C. The experiment was conducted in tantalum apparatus in a helium-atmosphere glovebox. The original charge to the experiment contained copper, magnesium, and zirconium. Calcium was added to the melt in increments to give the desired alloy compositions. Each alloy was stirred at 500 rpm for 2 hr at each temperature and allowed to settle for 20 min before sampling. Samples were taken in tantalum sample tubes through tantalum filters (medium-porosity tantalum frits with a density of 8.3 g/cc). Results of analyses performed on samples taken at 850°C show that the solubility of zirconium

varied from 2.9 at. % in the Mg-42.4 at. % Cu alloy to 0.024 at. % in the Mg-26.6 at. % Cu-35.2 at. % Ca alloy. These results indicate that the presence of calcium in the Mg-Cu reduction alloy suppresses the solubility of zirconium in the alloy. The samples taken at other temperatures are now being analyzed to provide additional data.

b. Process Engineering Studies (R. D. Pierce)

Last Reported: ANL-7548, p. 108 (Jan 1969).

Various structural materials are being tested to evaluate their suitability for use in pyrochemical-processing equipment. A tantalum-base alloy designated T-111 (Ta-8.5% W-2% Hf) was exposed to a system of molten Mg-44 at. % Cu/MgCl₂-30 mol % NaCl-20 mol % KCl for 98 hr at 750°C. The tantalum alloy was exposed to the system in the form of agitator blades mounted on a shaft, turning at ~200 rpm. The blades were positioned in the metal phase, metal-salt interface, salt phase, and vapor phase. Visual examination of the test specimens after the experiment indicated very good corrosion resistance to the molten metal alloy-salt system. The hardness of the specimens increased only ~1.5%, and the weight changed less than 0.03%.

A Nb-1% Zr alloy was also tested as a candidate material for pyrochemical-process equipment. This alloy was tested because it is somewhat stronger than pure niobium, which has shown promise for these applications (see Progress Report for September 1967, ANL-7382, p. 121). In a previous experiment (see Progress Report for December 1968, ANL-7527, p. 121), the Nb-1% Zr alloy appeared to be attacked by the salt phase in a Mg-Cu-U/MgCl₂-NaCl-KCl system. In the latest experiment, four coupons of the alloy were attached to an agitator shaft that was rotated at ~25 rpm in a MgCl₂-30 mol % NaCl-20 mol % KCl salt mixture for 194 hr at 650°C. Examination of the coupons after the experiment revealed that one coupon had cracked and that all of the coupons were severely corroded. The weight of the coupons decreased ~10%, and the hardness increased ~36%. Because of these results, Nb-1% Zr is no longer considered a candidate material, and no further tests with it will be performed.

Two separate corrosion experiments were performed to relate the corrosion resistance of pure niobium and pure tantalum to the results obtained with Nb-1% Zr above. The conditions in these two experiments were the same as those for the Nb-1% Zr experiment (MgCl₂-30 mol % NaCl-20 mol % KCl at 650°C and ~25 rpm). Visual examination of the coupons from these two experiments indicated that both materials fared much better than the Nb-1% Zr. None of the coupons decreased in weight. However, the niobium increased in hardness ~20%, and the tantalum hardness increased ~34%. These coupons will be bend-tested and then examined metallographically.

c. Experimental Flowsheet Investigations (R. D. Pierce)

Last Reported: ANL-7548, pp. 108-109 (Jan 1969).

Work is continuing on the construction of the Plutonium Salt Transport Facility (see Progress Report for September 1968, ANL-7500, p. 115). The installation of piping between vacuum pumps in the auxiliary equipment enclosure and glovebox equipment was completed except for connections at the glovebox-equipment end. Helium-supply piping and glovebox-pressure-control piping for glovebox 3 were installed except for lines that will supply helium to the process-furnace piping system. Fabrication of the top flanges for the three main processing vessels in box 3 was completed, and fabrication of the top flanges for the four receiver vessels in the same box has been completed except for welding.

Parts for the agitator drives for the processing vessels in box 3 have been received, and the agitator motor mounts are being fabricated. Sliding trays have been installed in pass-through 6 and locks 7 and 8. These trays move horizontally on ball-bearing slides, and can extend from the locks or pass-through into the gloveboxes to allow heavy objects to be introduced into or transferred between gloveboxes. The trays have been tested with 300-lb loads, which are similar to those expected when the facility is operational, and performed satisfactorily.

Windows and gloves have been installed in glovebox 4 to permit leak testing.

d. Liquid Metal-Molten Salt Contactors (R. D. Pierce)

Last Reported: ANL-7548, pp. 109-110 (Jan 1969).

A multistage mixer-settler is being developed for use with liquid metal-molten salt systems in the Plutonium Salt Transport Facility. A high-temperature single stage extractor for determining extraction performance has been designed, and fabrication of the unit has begun.

Tests with a plastic model of a single mixer-settler stage were continued to provide design information for high-temperature mixer-settlers. An inverted cup to confine the discharge of the mixer-pump was tested with the plastic model. In a high-temperature mixer-settler, the outer edges of the cup would be submersed in the molten salt phase, thereby preventing exposure and vaporization of the liquid metal from the pump outlet to the furnace atmosphere.

A stainless steel mixer-pump (see Progress Report for November 1968, ANL-7518, pp. 112-113) that will be used in the high-temperature single-stage tests has been used with an aqueous-organic

system in the plastic model to determine pumping capacity. Earlier tests demonstrated that the volumetric pumping rate is essentially independent of the density of the liquids being pumped (see Progress Report for December 1968, ANL-7527, p. 122). Therefore, calibrations made with water will be applicable to the liquid metals and molten salts that will be used in later experiments. Pumping rates were measured at pump speeds from 550 to 710 rpm, pump inlet openings from $5/32$ to $1\frac{7}{8}$ in. in diameter, and pumping lifts from $6\frac{1}{4}$ to 8 in. The results of these tests show that the pumping rate increases as the size of the inlet opening is increased, but the pumping rate also becomes more sensitive to pump speed. Reducing the size of the inlet opening reduces the pumping rate significantly, but the pumping rate also becomes more independent of pump speed.

Measurements of mixing efficiency are currently being made with a plastic mixing chamber and the stainless steel mixer-pump mounted on a dynamometer test stand. Various mixer-blade and baffle configurations are being tested to achieve a high intensity of mixing. Preliminary measurements indicate that the proposed high-temperature extractor will operate satisfactorily at ratios of mixing power to solvent-flowrate that are more than ten times higher than those normally required to achieve complete extraction in mixer-settlers.

3. General Chemistry and Chemical Engineering--Research and Development

a. Determination of the Solubility of Helium in Sodium (F. A. Cafasso)

Last Reported: ANL-7548, p. 112 (Jan 1969).

The solubility of helium in liquid sodium is being measured by a procedure that employs helium-3 as a tracer (see ANL-7548). Two preliminary experiments have been completed at 500°C. The results yield a solubility of about 25 parts per billion per atmosphere of helium pressure. (Expressed in terms of the Ostwald coefficient, this corresponds to 3.3×10^{-4} volume of helium dissolved per unit volume of sodium.) This value is higher than our previously determined solubility values for argon (17 ppb/atm), krypton (5.0 ppb/atm), and nitrogen (0.017 ppb/atm) at 500°C. Further experimentation to define the temperature dependence (300-600°C) and pressure dependence (3-10 atm) of the helium solubility is in progress.

b. Total Vapor Pressure and Oxygen Potentials in the Ternary U-Pu-O System (P. E. Blackburn)

Last Reported: ANL-7518, pp. 115-116 (Nov 1968).

Transpiration equipment for the study of the Pu-O system is nearing completion. The gas-handling system has been assembled and is

being leaktested. The cooling system, including the necessary safety devices for glovebox operation with plutonium, has been completed.

Testing and calibration of various flowmeters, measurement of prism and window adsorption, and the optical pyrometer calibrations are in progress to prepare for initial tests of the system. Experiments with U_4O_9 - U_3O_8 will start shortly. These studies, which will serve to test the equipment, will be followed by measurements of oxygen activities and total pressures over PuO_{2-x} .

- c. Total Effusion of Pu-O and U-Pu-O (P. E. Blackburn and R. K. Edwards)

Last Reported: ANL-7518, p. 116 (Nov 1968).

The effusion apparatus, previously used to determine the congruently vaporizing composition of urania as a function of temperature, is being installed in a glovebox so that effusion studies of plutonium-bearing materials may be carried out. The apparatus has been modified so as to incorporate a quadrupole mass spectrometer into the system. Incorporation of the spectrometer as a part of the effusion apparatus and the coupling to the glovebox are presently under way. Construction of internal components of the effusion apparatus (Knudsen cell, mounting device, etc.) has been completed; the components are currently being assembled for testing. This equipment will also be used to measure the relative ionization cross sections for U-O and Pu-O molecules essential for the partial vapor pressure studies of U-Pu-O (see Progress Report for October 1968, ANL-7513, p. 127).

PUBLICATIONS

Acoustic Boiling Detection in Reactor Vessels

T. T. Anderson and T. A. Grate

IEEE Trans. NS-16(1), 260-265 (February 1969)

Final Surveillance of EBWR Pressure Vessel Following the Plutonium Recycle Program

N. Balai, C. R. Sutton, and M. R. Sims

ANL-7117 (Supplement) (September 1968)

Argonne Code Center: Compilation of Program Abstracts

M. K. Butler, Marianne Legan, and L. Ranzini

ANL-7411 Supplement 1 (October 1968)

Constitution of Plutonium Alloys

F. H. Ellinger,* W. N. Miner,* D. R. O'Boyle, and F. W. Schonfeld*

LA-3870 (December 1968)

Development of Brazing Techniques and Procedures for Fabricating Fuel Subassemblies for the Argonne Advanced Research Reactor (AARR)

V. M. Kolba, C. V. Pearson, and W. C. Kramer

ANL-7458 (August 1968)

Production of Plutonium Hexafluoride by Fluorination in a Fluidized Bed

N. M. Levitz, G. J. Vogel, E. L. Carls, D. E. Grosvenor, B. Kullen,
D. Raue, and W. MurphyNucl. Appl. 6(2), 147 (1969)

The Interaction of Two-dimensional, Stratified, Turbulent Air-Water and Steam-Water Flows

John H. Linehan

ANL-7444 (May 1968)

Activation Gamma Rays

A. E. McCarthy and Marshall Grotenhuis

Engineering Compendium on Radiation Shielding, Ed. R. G. Jaeger
et al. Springer-Verlag, Berlin, 1968, Vol. I, pp. 91-100

Coolant-structure Coupling during a Rapid Insertion of Energy

K. Y. Narasimhan, G. S. Rosenberg, and M. W. Wambsganss, Jr.

ANL-7502 (October 1968)

ENDF/B Neutron Cross-section Data for Natural Helium (ENDF-125)

E. M. Pennington

ANL-7462 (October 1968)

*Los Alamos Scientific Laboratory.

V. NUCLEAR SAFETY

A. Reactor Kinetics--Other Reactor Kinetics1. Core Structural Safety (C. K. Youngdahl)

Last Reported: ANL-7548, pp. 119-122 (Jan 1969).

a. Dynamic Plasticity Analysis of Circular Shells. A computer program AXRECT has been written to evaluate the closed-form solution for the plastic deformation of a circular shell loaded by a pulse whose axial and time distributions are each rectangular, i.e., the internal pressure is given by

$$\begin{aligned}
 P(z,t) &= \frac{\sigma_0 h}{R} \phi(\xi) \psi(\tau); \\
 \phi(\xi) &= \frac{1}{a}, \quad |\xi| \leq a, \\
 &= 0, \quad |\xi| > a; \\
 \psi(t) &= \psi_M, \quad 0 \leq \tau \leq \tau_0, \\
 &= 0, \quad \tau > \tau_0,
 \end{aligned} \tag{1}$$

where σ_0 , R , and h are the yield stress, radius, and thickness of the shell, respectively and ξ , τ , and a are the dimensionless axial coordinate, time, and half-length of the loaded region, respectively. The results calculated by AXRECT will be compared with those from the computer program being prepared to calculate loads that are arbitrary functions of axial position and time.

For the rectangular axial distribution, the static yield load of the shell is given by

$$\psi_S = \frac{1}{2} (a + \sqrt{a^2 + 4}). \tag{2}$$

The deformation is entirely of the Phase-1 type if ψ_M and a are such that

$$\psi_M^3 a + (2a^2 - 3) \psi_M - 3(a^2 + 2) a \psi_M - 3a^2 \leq 0. \tag{3}$$

Otherwise the motion begins in Phase 3 with a hinge band in the vicinity of $\xi = 0$. The initial type of deformation is indicated in Fig. V.A.1, which shows for a given load length a the intervals of ψ_M that produce Phase 1, Phase 3, or no deformation at all. From Fig. V.A.1 it is apparent that for

$a = 0$, which corresponds to the concentrated ring load previously treated, the deformation must begin in Phase 1; for loads that are more spread out axially, only a narrow band of values of ψ_M will produce initial Phase-1 deformation.

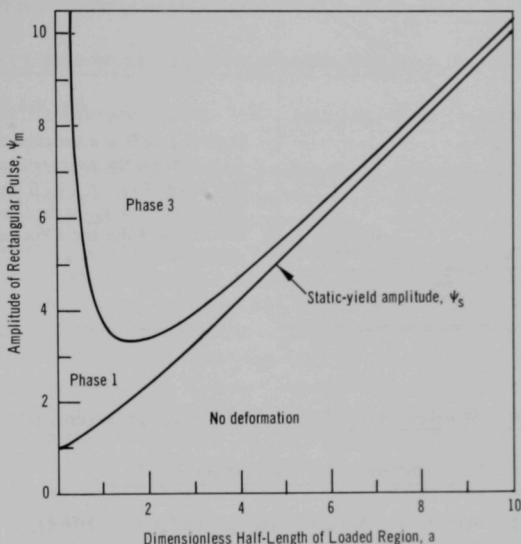


Fig. V.A.1. Initial Deformation Phase for Rectangular Load Distribution over the Length $2a$

As shown in Fig. V.A.2, a tentative conclusion that can be drawn from the rectangular-load results is that

$$\frac{I}{\tau_f - \tau_y} \approx \psi_s, \quad (4)$$

where τ_y and τ_f are the times at which plastic flow begins and ends and I , the impulse of the load over this time interval, is

$$I = \int_{\tau_y}^{\tau_f} \int_{-a}^a \phi(\xi) \psi(\tau) d\xi d\tau. \quad (5)$$

This conclusion seems to be supported by the preliminary results for Phase-1 deformation with other load shapes. Equation (3) implies that the average load over the time interval of deformation is approximately the load for static yield. For a given shell material and geometry and a given

axial load distribution, the static-yield load can be determined either analytically or experimentally. For any time distribution of the pulse, Eq. (3) estimates the duration of the deformation.

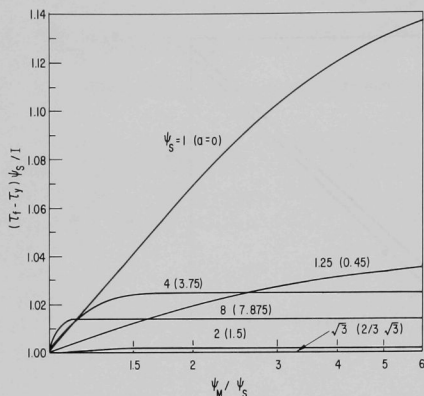


Fig. V.A.2

$(\tau_f - \tau_y) \psi_S / I$ as a Function of ψ_M / ψ_S , where $I / (\tau_f - \tau_y)$ Is the Average Load over the Deformation Interval $\tau_f - \tau_y$, ψ_S Is the Static-yield Amplitude, and ψ_M Is the Load Amplitude for a Rectangular Pulse and a Rectangular Axial-load Distribution

2. Fuel Meltdown Studies with TREAT (C. E. Dickerman)

a. Meltdown Studies with Ceramic Fuels

Last Reported: ANL-7518, p. 121 (Nov 1968).

(i) Prototype Fast-reactor Mixed-oxide Pins. Mixed-oxide "Prototype Fast Reactor" fuel pins have been supplied by the UKAEA for a joint program of experimental safety studies in the TREAT reactor. These pins are clad with 0.015-in.-thick 316L type stainless steel jackets of 0.230-in. outer diameter. The smeared oxide density is approximately 81%. Sixty-six unirradiated pins and seven pins irradiated in the Dounreay Fast Reactor to a maximum burnup of 5 a/o have been received, although their use has been delayed by slippage in the schedule of experimental facilities and apparatus being developed for fuel-safety experiments with mixed oxide. These pins provide a well-defined fuel design, backed by extensive irradiation experience on a subassembly scale, with design features similar to fuel being developed domestically. Their study is thus an integral part of the LMFBR fast-reactor safety programs.

Inspection of the two groups of pins is being scheduled, with the aim of characterizing them as completely as feasible prior to TREAT experiments. Measurements scheduled for the unirradiated pins include profilometry, radiography, weight, and volume.

Examinations planned for the seven irradiated pins include profilometer, radiography, weight, volume, axial balance point, and

axial gamma-ray scans, including spectrum checks. After the nondestructive examinations, one pin is to be given a detailed destructive examination, including fission-gas release (quantity and analysis), metallographic examinations of cladding penetrations and voids, fuel and fission-product distributions, and ceramographic examinations of fuel.

b. Development of Experimental Methods

Last Reported: ANL-7548, pp. 122-127 (Jan 1969).

(i) Proof test of Prototype Mark-II Integral Sodium TREAT Loop. A Mark-II integral sodium loop is being developed for TREAT safety experiments with fast-reactor oxide-fuel pins. The loop is designed to have higher operating temperature, pressure containment rating, and more complete instrumentation than the original, Mark-I integral sodium TREAT loops which have been used extensively for TREAT experiments with metallic fuel pins. After completion of the preliminary testing of the prototype Mark-II (see ANL-7548), the loop was given a high-pressure proof test. The steady-state temperature of the loop sodium during the test was 427°C. Sodium was circulated through the loop during the test at 3-4 m/sec through the test section. Current through the annular linear induction pump of the loop was 15 A, and the total time at temperature was 6 hr. Target pressure for the test was 378 atm (5550 psig). Total time at pressures above 204 atm (3000 psig) was approximately one hour. The maximum pressure of the test was 422 atm (6200 psig), which was reached from 204 atm in steps of approximately 40 atm.

Difficulties were encountered in operating the gas-pressure-intensifier unit, and after the loop was at temperature the air-driven hydraulic pressure source of the unit failed to function. An alternative, electrically driven, hydraulic pressure source was hurriedly obtained and connected directly to the accumulator of the intensifier unit. Test pressure of this hybrid system was read directly on the 0-10,000 psig pressure gauge of the substitute pressure source. This gauge was calibrated after completion of the loop pressure test, and the pressure results quoted above are the actual pressure values using the gauge calibration results.

Our experiences with the gas-pressure-intensifier unit were reported to the manufacturers' representative. He supplied a new set of spring-loaded check valves which, upon inspection, proved to be of a design different from the ones originally supplied in the unit. After replacement of the check valves and springs, the unit has been found to operate satisfactorily.

(ii) Checkout of Full-scale TREAT Fast-neutron Hodoscope. A fast-neutron hodoscope is under development for use in TREAT experiments to detect fuel locations and motions inside opaque apparatus, e.g.,

sodium loops. Preliminary, small-scale versions of the device have been used for loop experiments since TREAT transient 1007 during May 1966. During the last report period, tests were conducted at TREAT with a full-scale version of the hodoscope, incorporating the new semiautomated data-handling system (see Progress Report for October 1968, ANL-7513, pp. 138-140). On the basis of these tests, the fast-neutron hodoscope for TREAT may now be considered operational in its full-scale form. After installation and preliminary testing, the static features of the system appeared to be satisfactory. The dynamic characteristics remain to be demonstrated, with two unevaluated tests having been made. Even so, the hodoscope should be used for every possible transient in which there is a clear slot through the reactor with the dual purpose of providing supplementary data from the transient and of obtaining operating experience with the hodoscope.

Various precautions were successful in reducing noise interplay between channels. Also, the amount of external noise picked up from operating relays and machinery was tolerable. In view of the large number of channels, these two problems could have been major stumbling blocks for the full-scale system. Although some external pickup remains, it appears that during transients this should not interfere with proper operation of the hodoscope.

Future effort will be directed primarily towards "fine tuning" of the hodoscope. In particular, attention can now be focussed on sodium loops and on questions of count-rate limitations. Although previous efforts established that a small sample of channels could meet the count-rate requirements of transients, only a series of high-power transients can proof-test the full system of 334 channels.

(a) Calibration Procedure. Calibration of all detectors is based on a single plutonium-beryllium reference source. A positioning mechanism allows the source to be located in front of any channel with relatively high precision.

Use of a neutron source is necessary in order to account for as many factors influencing efficiency as possible: intrinsic Hornyak button detector, coupling with photomultiplier tube, phototube gain, voltage divider, signal cable, and to a lesser extent, the X206 processing board containing integrator, amplifier, and discriminator.

The initial calibration (excluding failures) requires about 2 min per channel. Once the defective channels have been weeded out, it should be possible to conduct a review of all channels at the rate of about one minute per channel, assuming that minor readjustments are not required.

(b) Integral Bias Curves. In order to derive some measure of gamma-ray rejection, as well as to correlate present data with past tests, two sets of integral bias curves were obtained.

The first set was based on the plutonium-beryllium reference source. There is at least an order-of-magnitude difference in amplitude between the gamma-ray background and the neutron level. Thus, considerable pileup would be required before gamma-ray pulses would begin to be counted at the neutron-discriminator level. Unfortunately there is not only gamma-ray (and noise) pileup at high count rates, but there are certain instrumental effects which may tend to augment these spurious pulses: for example, the decay components from ZnS(Ag) stretch out long enough to produce a pedestal effect for smaller pulses.

With the TREAT reactor operated at 50 kW, bias curves were obtained for the same four channels. It is important to note that there is no apparent shift in gamma-ray sensitivity when using the reactor as a source. This confirms that the plutonium-beryllium source adequately represents the reactor radiation spectrum seen by the hodoscope.

(c) Stationary Scan Analysis. Prior to the transient a stationary scan was conducted; an initial scan revealed that the hodoscope was focussed too far to the right of the pin; readjustment slightly over-corrected. The pin appeared initially to be tilted about 0.15 in. along its length. The neutron data suggested a length of fuel of about 14.3 ± 0.4 in. and a diameter of 0.15 ± 0.3 in. The actual fuel length is ≈ 14.2 in. and diameter is 0.144 in.; the cladding length is about $17\frac{1}{2}$ in.

The transient power level was chosen to remain below failure threshold. It was apparent from post-transient visual observation of the transparent capsule that the pin was not destroyed, although it ended up in a state of high distortion.

The post-transient stationary scan with the hodoscope is shown in Fig. V.A.3 and is consistent with this picture. The pin appears intact but severely bent in the focal plane of the hodoscope. The final limits of movement represent a distance of up to 0.65 in. at the extreme or about 0.50 ± 0.05 in. measured from the pin axis.

From the color photographs taken with the Fastax camera, it should be possible to compare the hodoscope against high-speed optical-camera data.

At this point one may conclude that the static characteristics of the hodoscope, as originally designed, are satisfactory.

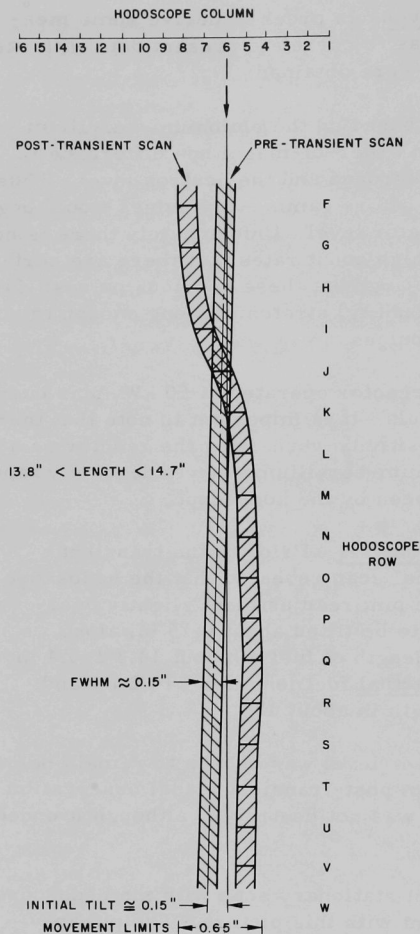


Fig. V.A.3. Stationary Scan Analysis with
Fast-neutron Hodoscope

been development of the semiautomated system for taking data from the high-speed film record from the fast-neutron hodoscope and reducing it to a form suitable for analysis. The CHLOE scanning system and computer code-data reduction have been checked out on simulated full-scale hodoscope film output. Film for the checkout tests (see Sect. b above) is being fed through the data-readout and -reduction systems as a test. If successful, analytical development work can then be concentrated on ways of displaying the hodoscope "pictures" and analyzing them.

(d) Transients. Two transients were conducted to test dynamic aspects of the system. The first was a mock transient in which no neutrons were produced by the reactor, but all other noise-producing features of a transient were simulated.

Power and duration for (the second) transient 1255 were chosen to be below the threshold of destruction for the single EBR-II 6% pin (sodium bonded) enclosed in a transparent capsule. The Fastax camera viewed the pin through the window. Intended peak power was about 50 MW. The hodoscope camera was loaded with 500 ft of film run at 1000 pictures/sec, giving 6-msec time resolution. All indications of operation were satisfactory. The pin was visually observed to have ended up in a highly contorted shape (see Fig. V.A.3).

A series logic string with lamp indicators, establishing the proper functioning of many of the hodoscope elements, worked properly.

c. Analytical Support
(C. E. Dickerman)

Last Reported: ANL-7513,
pp. 138-140 (Oct 1968).

The principal activity under analytical development has

3. Materials Behavior and Energy Transfer (R. O. Ivins)

Last Reported: ANL-7518, pp. 123-125 (Nov 1968).

a. Pressure Generation due to Violent Melt-down

To measure the pressures generated and the momentum transfer during a nuclear transient of energy sufficient to rupture stainless steel cladding tubes containing UO_2 fuel specimens, a third meltdown experiment (Run CEN-S3) has been performed in the sodium-filled piston autoclave in the TREAT reactor. The run involved two transients, with reactor periods of 82 and 53 msec, during which fission-energy releases were 344 and 669 MW-sec, or 236 and 460 cal/g UO_2 , respectively.

For the experiment, the autoclave was loaded with about 200 g of sodium (which was heated to 175°C before the transient) and an array of five fueled rods and four dummy rods. The stainless steel tubing for each of the nine rods was 0.29 in. in OD, 12 in. long, had 15-mil walls, and end caps that sealed in helium at 15 psi. Each fuel rod consisted of two sections: an upper or "blanket" section that was designed to collapse under external pressures of approximately 6000 psi, and a $5\frac{5}{8}$ -in.-long lower fuel section consisting of ten sintered pellets (of 0.250-in. dia and 0.50 in. long) of 10%-enriched UO_2 . A 3/32-in. axial gap was provided above the pellets. A stainless steel dowel (~0.5 in. long) joined the two sections. Each of the five fuel pins contained about 41 g UO_2 .

The 460-cal/g transient caused the rupture and destruction of all five fuel rods. The pressure-response trace (see Fig. V.A.4) showed five separate pressure pulses, which perhaps were caused by the separate failures of the five fuel rods. The first two pressure pulses (I_1 and I_2) occurred almost simultaneously near the end of the transient (at 645 MW-sec and 444 cal/g UO_2); the first pressure spike also coincided with a rapid acceleration of the piston from a velocity of 6 to 302 cm/sec. The third pressure pulse (I_3), the largest, had an amplitude of 540 psi and a band width of 2.7 msec, and caused piston velocity to increase from 302 to 472 cm/sec. The final two pressure pulses (I_4 and I_5) occurred after the piston was locked in its final position; Pulse I_5 , which occurred considerably later than the previous pulses, was essentially identical to Pulse I_4 . The maximum piston velocity (472 cm/sec) was higher than that observed in Run CEN-S2 (270 cm/sec), which was reported erroneously as 27 cm/sec in Table IV.A.1, p. 124, ANL-7518.

The pressure-response data could be correlated with the change in momentum of the piston. The values of impulses $I_{1,2}$ and I_3 obtained from the pressure-response data (88.6 and 70.5 g-sec, respectively) agree reasonably with the change in momentum of the piston calculated from the output of the linear-motion transducer. The work required to

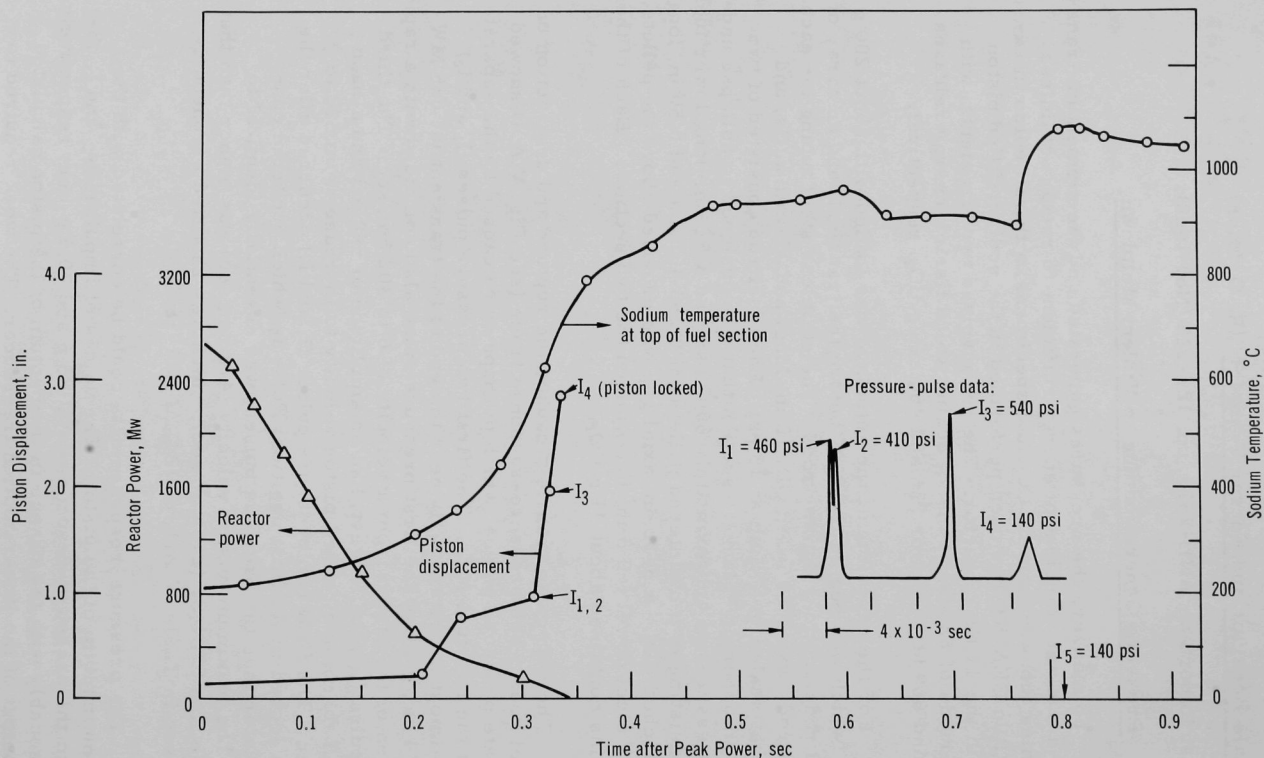


Fig. V.A.4. Linear Motion, Pressure Response, and Sodium Temperature for Sodium Autoclave Test CEN-S3

accelerate the 260-g piston during $I_{1,2}$ and I_3 (12×10^6 and 16×10^6 ergs, respectively) can be explained readily in terms of the release of high-pressure gas from the fuel rods. The work available from the isentropic expansion of 0.8 cm^3 (STP) of helium at 1000 psi and 3000°K to 100 psi is 11×10^6 ergs and to 25 psi is 15×10^6 ergs.

A peak sodium temperature of 1100°C was recorded by a thermocouple located at the upper part of the fueled section of the fuel rod 0.8 sec after peak power. All other thermocouples recorded temperatures below 500°C.

Preliminary calculations indicate that acceleration forces of 400-500 g occurred during the first three pressure pulses. About $5 \times 10^{-3}\%$ of the nuclear energy was converted to mechanical energy.

The residue from test CEN-S3, as shown in Fig. V.A.5, indicated that the five fuel rods were completely destroyed during the transient. Only small (~0.5 in. long) cylindrical sections of fused UO_2 remained; these sections were hollow (of 3/16-in. ID) and had an outside diameter of 0.265 in. This behavior might be explained in the following manner: because the resulting UO_2 diameter is greater than that of the original pellet

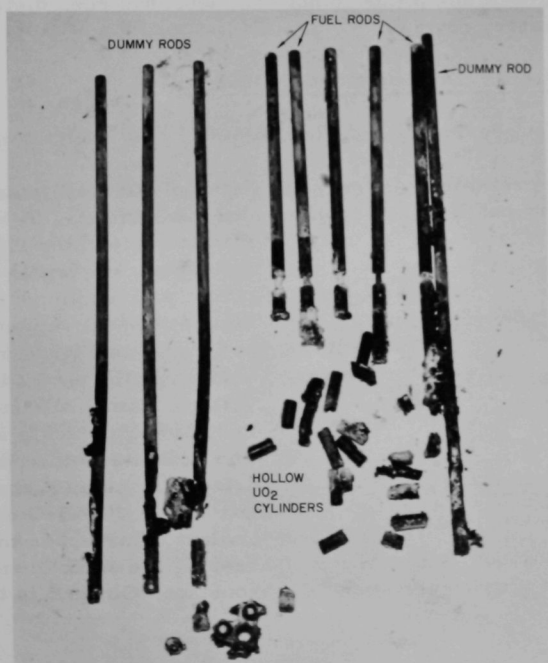


Fig. V.A.5. Residue of 9-rod Cluster from Sodium Autoclave Test CEN-S3

(0.250 in.), the UO_2 pellets apparently expanded by virtue of partial melting and thus contacted the cladding (cladding ID was 0.260 in.), whereupon the cladding melted, and perhaps vaporized, and the outer portion of the UO_2 solidified. The hollow core was the result of molten oxide flowing from the solid oxide annulus.

All dummy rods suffered cladding failure in the form of melted sections at the lower portions of the rods. Except for slight bowing, the rods were otherwise undamaged; a section of one fuel rod was welded to a dummy rod. Most likely, the mechanism of failure of the dummy rods involved the rods being contacted by molten UO_2 expelled from the fuel rods, especially since the first indication of failure occurred at 444 cal/g UO_2 , nearly 100 cal/g above the melting point of UO_2 .

4. Fast Reactor Safety Test Facility Study (C. N. Kelber)

a. Program Justification and Definition

Last Reported: ANL-7548, p. 130 (Jan 1969).

The preliminary (Phase 1) draft of the report on program definition and justification, although not complete, has been distributed for internal laboratory review.

b. Facility Definition and Utilization

Not previously reported.

A preliminary survey has begun of the facility capabilities needed to carry out various recommended experiments. A survey has been made to determine the power in a fast-spectrum driver necessary to induce a given steady-state power load in the test region. The results are shown in Fig. V.A.6. The abscissa is the power in the test region, varying from 1 MW (about 19 pins) to 15 MW (full-scale subassembly). The ordinate is the power in the driver, based on a simple representation of a UO_2 -BeO core with sodium coolant. Curve 1 is the result of keeping the enrichment in the driver constant. Curve 3 is the ratio of

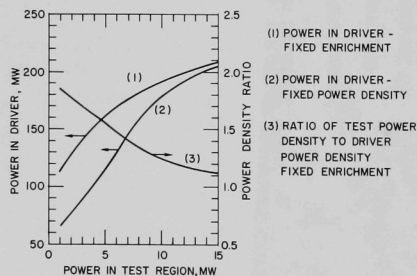


Fig. V.A.6. Power in a Fast-spectrum Driver to Induce a Steady-state Power Load

average power density in the test region to that in the driver. Desirable values for this ratio depend on the particular experiment, but for purposes of illustration a value of 1.125 was taken as optimum. Curve 2 is the estimate of power in the driver when the ratio of average power densities is fixed at 1.125.

What is most significant is the variation of this curve. This variation is almost linear from 1 to 10 MW, but then tends to saturate quickly. In computing trade-offs it must be recalled that Curve 2 represents a limit probably unobtainable in practice because of design compromises. The best available curve probably lies between Curves 1 and 2, and hence saturates somewhat more quickly than Curve 2.

5. 1000-MWe Safety Studies (L. W. Fromm)

Last Reported: ANL-7500, p. 130 (Sept 1968).

a. Contract Management, Review and Evaluation

(i) Westinghouse Electric Corp. Subcontract. The topical report on the Task-V safety studies has been completed. A report of the calculations of the reference core design using the MC² computer code and the ENDF/B data file has been drafted.

B. TREAT Operations

1. Reactor Operations (J. F. Boland)

Last Reported: ANL-7548, pp. 130-131 (Jan 1969).

Installation of the electronics for the 340-channel fast-neutron hodoscope (see Progress Report for June 1968, ANL-7460, p. 126) was completed and the system was tested under steady-state and transient conditions with an EBR-II fuel element as a target (see Sect. V.A.3). Results of the steady-state tests were satisfactory, but results of the transient test will not be available until the photographic film is processed and analyzed.

An EBR-II fuel element previously irradiated to a burnup of 1.2% in EBR-II was subjected to two transient tests. This element is instrumented with eddy-current-type motion detectors to measure the expansion of the fuel inside the cladding. Testing of this element will continue until the cladding fails. Results of similar tests using unirradiated elements were reported in Progress Report for August 1968, ANL-7487, p. 65.

C. Chemical Reaction--Research and Development--Chemical and Associated Energy Problems (Thermal)

1. Analysis of Excursion Accidents (J. J. Barghusen)

Last Reported: ANL-7518, pp. 126-130 (Nov 1968).

a. TREAT Experiments with Zircaloy-2-clad UO_2 Fuel. In the continuing in-pile study of the characteristics of fuel failure, a series of three photographic experiments are being planned with Zircaloy-clad, vibrationally compacted UO_2 powder fuel specimens. The additional data on cladding temperature will help explain why the extent of metal-water reaction for powder fuels is consistently less than for pellet fuels at identical fission energy levels.

2. Pressure Generation due to Particle-Water Energy Transfer (R. O. Ivins)

Last Reported: ANL-7527, pp. 135-138 (Dec 1968).

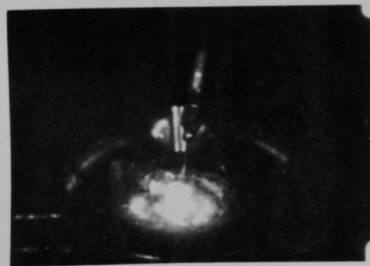
a. Steam-explosion Experiments

Not reported previously.

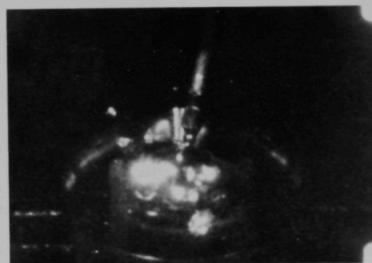
Experimental work has been initiated to study explosive interactions between molten materials and water, i.e., "steam explosions." The objective is to establish whether destructive pressures can be generated when molten reactor fuel materials intimately contact water in accident situations.

The preliminary tests were performed in a laboratory hood shielded with 1/4-in.-thick aluminum plates, one of which had a 1/2-in.-thick Plexiglas window for observation. After a 100-g sample of molten tin or potassium iodide material was heated to about 600°C in a 1.25-in.-ID graphite crucible, about 1 ml of water (at room temperature) was injected into the molten mass through a stainless steel hypodermic tubing and a "Hycam" high-speed motion-picture camera photographed the reactions. When the water was injected, explosions were observed; molten material was dispersed widely inside the hood. The explosion with tin was sufficiently violent to shatter the upper half of the graphite crucible. Figure V.C.1 shows five selected frames from the pictures taken in the experiment with molten tin at 600°C. A similar sequence of events was observed for the case of molten potassium iodide at 800°C.

The water-injection experiments are continuing with other molten materials, such as aluminum, silver, and sodium chloride. A technique is being developed to measure the thrust resulting from the explosions; it employs a 1.5-in.-ID stainless steel crucible whose top is open



195.9 msec



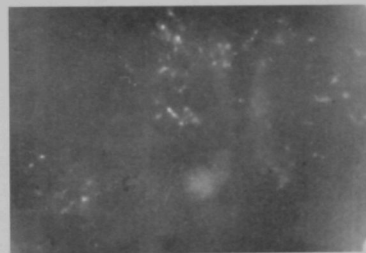
233.6 msec



303.7 msec



304.2 msec



337.5 msec

Fig. V.C.1. Events after 1 ml of Room-temperature Water Was Injected Just under Surface of 600°C Molten Tin at Various Times from Start of Injection. Immediately after injection (195.9 msec), tin surface bulged, probably because of sudden generation of steam; surface continued to bulge (233.6 msec) until certain size was reached, whereupon (303.7 msec) sudden explosion occurred (304.2 msec, which is only 0.5 msec later); at 337.5 msec can be seen pieces of shattered crucible flying in a cloud of mixed steam and tin particles.

to the atmosphere; the bottom of the crucible is connected to a force transducer by a 0.5-in.-dia stainless steel rod, 8 in. long. The transducer measures both compressive and tensile forces transmitted through the rod. The thrust (compressive force) measured equals the rate of momentum outflow from the crucible into the atmosphere that occurs during an explosion.

D. Engineered Safety Features

1. Safety Features Technology--Containment

a. Hydrodynamic Response to High-energy Excursion (Y. W. Chang and G. Cinelli, Jr.)

Last Reported: ANL-7527, pp. 139-140 (Dec 1968).

(i) Programming and Checking Axisymmetric Computer Code.

The preliminary version of the two-dimensional computer code for the numerical calculation of hydrodynamic response of primary containment to a high-energy excursion has been completed. Outstanding features of the code are that it (a) contains equations of state of reactor materials (the present version of the code contains the equations of state of core, breeding blankets, plenum, sodium, steel, and argon), (b) gives the energy partition at all times, (c) gives the motion of the medium at all times, (d) determines whether or not and when the reactor vessel breaks, (e) gives the pressure loading on the plug and determines when the plug jumps, and (f) provides input to the plug-jump problem.

The code output is on printed sheets that give the displacements, velocities, pressures, internal energies, densities, and strains at every time step for all spatial points. The output of displacements and pressures can also be given pictorially, showing the movements and deformations or magnitudes of pressure of all spatial points at any instant of time. It is believed that this code will give the reactor designer information with which to adjust the geometry of the layout and the strength of structural components to achieve a balanced design or a design that will dissipate the excursion energy with least hazard to the primary containment.

The reactor configuration selected for testing the code, as well as the initial layout of the Lagrangian grids, is shown for time zero in Fig. V.D.1; axial symmetry permits only half the cross section to be shown. The core is assumed to have oxide fuels contained in stainless steel pins supported in stainless steel grid plates (not included in the analysis) and to be cooled by liquid sodium. The sodium is covered by argon gas and is held in a steel pot within a concrete primary containment that has a rotatable shield plug in the platform at the top of the primary cavity.

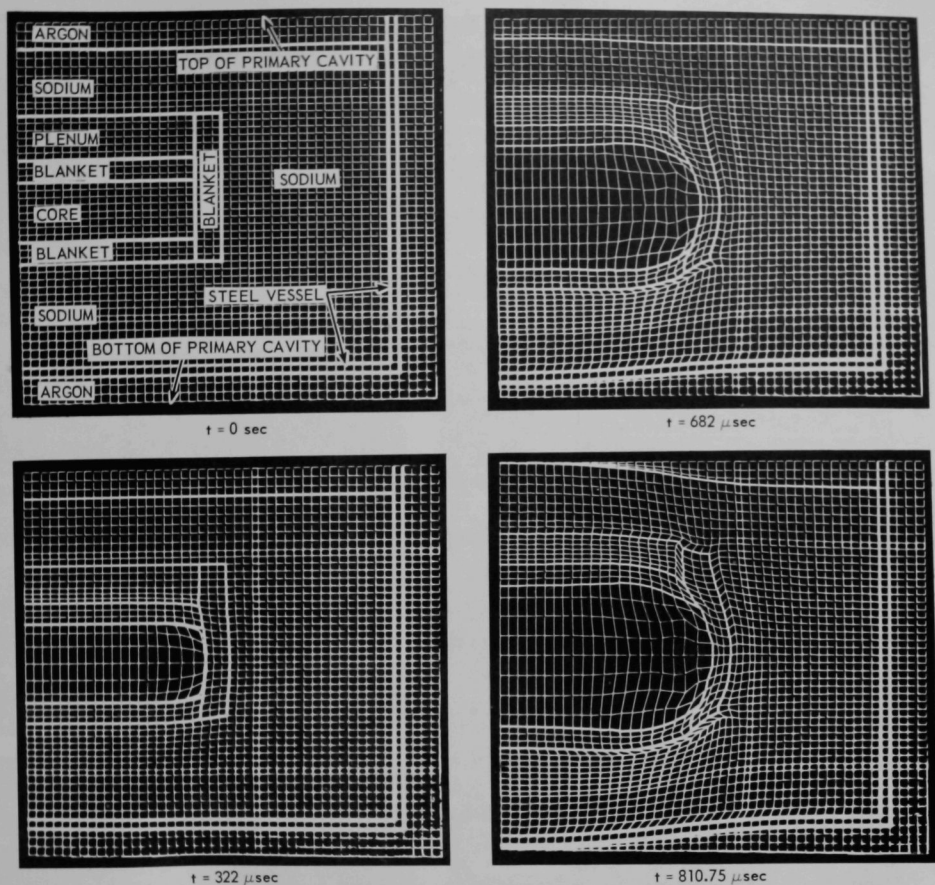


Fig. V.D.1. Deformations of Lagrangian Grids at Various Times after Start of a Power Excursion in a "Pancake" Core Configuration

For the excursion model, it is assumed that at the start of the power excursion the core is molten, and the sodium has already been vaporized and expelled from the core region. However, the blankets are assumed to be intact. The energy is released so rapidly in the excursion that the molten oxide fuels are assumed to be vaporized and superheated to high temperature and pressure. Therefore, at the end of the power excursion, the core consists of only high-pressure oxide vapor.

Figure V.D.1 shows the time sequence of deformations of the Lagrangian grids. Figure V.D.2 shows the pressure profiles along the vertical centerline at various times. Figure V.D.3 shows the pressure profiles along

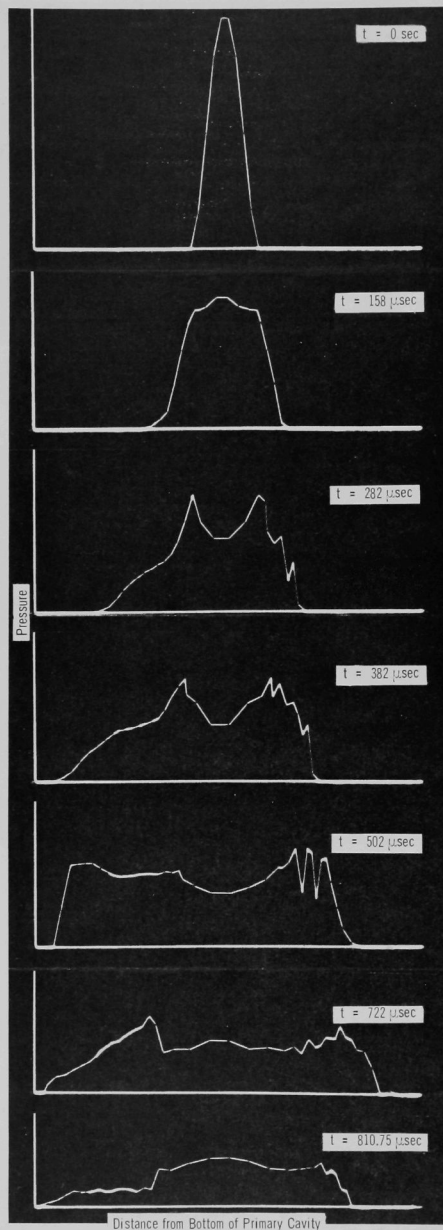


Fig. V.D.2. Pressure Profiles along Vertical Centerline of Core at Various Times

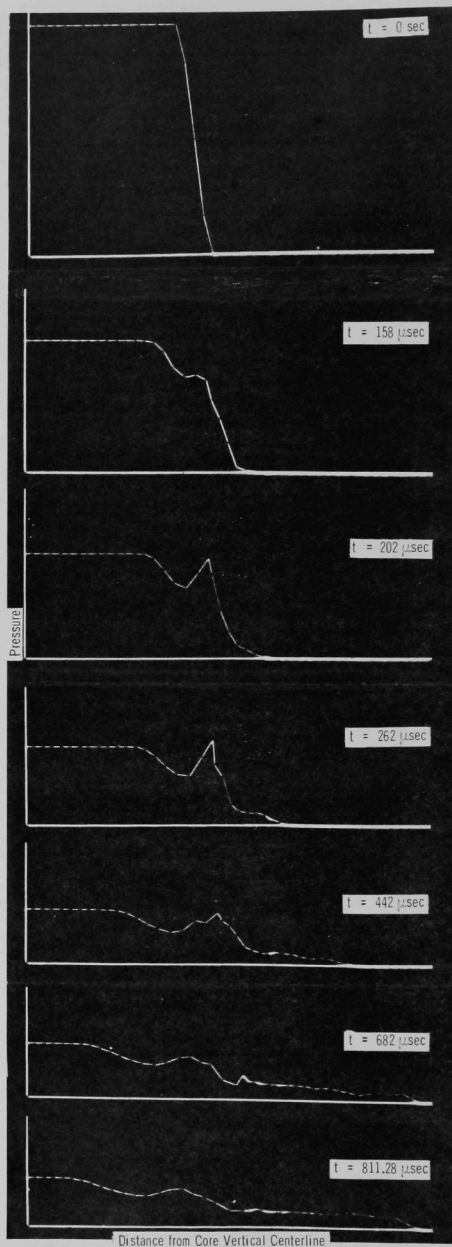


Fig. V.D.3. Pressure Profiles along Horizontal Axis of Core at Various Times

the horizontal axis of the core at various times. The computation was terminated at $t = 811.28 \mu\text{sec}$ because at that time the force acting on the plug exceeded the strength of the plug-holddown device. The total computer time for this sample problem was about 68 min.

A code to calculate the automatic rezoning is being developed.

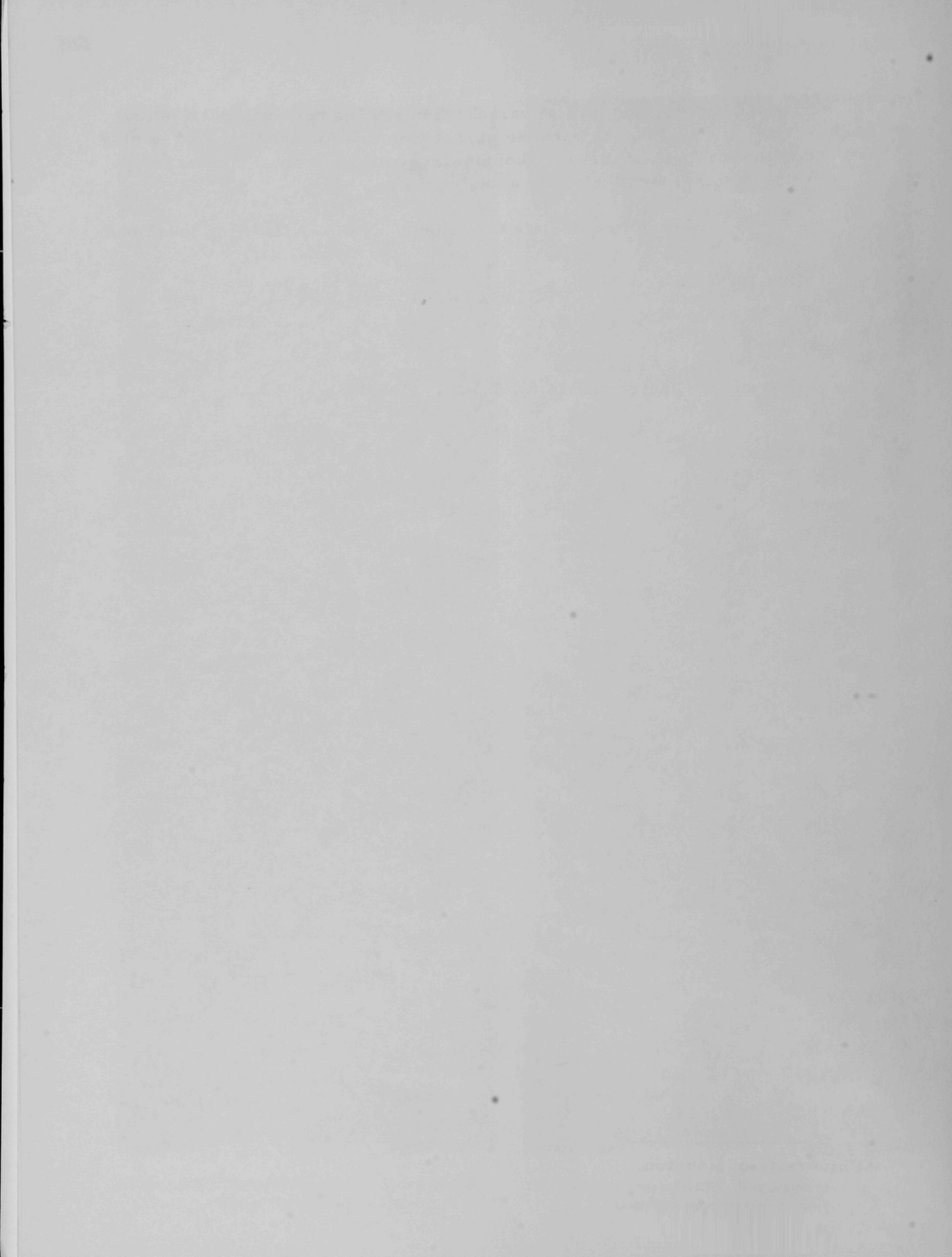
PUBLICATIONS

An Identifier

C. F. Chen* and A. E. Knox

Intern. J. Electronics 24(6), 521-533 (1968)

*University of Houston.



ARGONNE NATIONAL LAB WEST



3 4444 00007946 7

X

